Evaluating the performance of different machine types to operate a Flywheel energy storage system

by

Khaled Raouf Tawfik Mohamed Rafaat

Khaledraouf13@gmail.com

Submitted to the Department of Electrical Engineering, Electronics, Computers and Systems
in partial fulfillment of the requirements for the degree of
Erasmus Mundus Master Course in Sustainable Transportation and Electrical Power Systems
at the
UNIVERSIDAD DE OVIEDO
September 2017

Author…….

Certified by…….

Dr. Christian Klumpner

Associate Professor

Thesis supervisor

Evaluating the performance of different machine types to operate a Flywheel energy storage system

by

Khaled Raouf Tawfik Mohamed Rafaat

Submitted to the Department of Electrical Engineering, Electronics, Computers and Systems
on August 31, 2017, in partial fulfillment of the
requirements for the degree of
Erasmus Mundus Master Course in Sustainable Transportation and Electrical Power Systems

Abstract

In this thesis, the performance of 3 different drives to operate the flywheel energy storage system (FESS) were analysed. These machines are the permanent magnet synchronous machine (PMSM), the squirrel cage induction machine (SCIM) and the doubly fed induction machine (DFIM) (also referred to as slip ring/wound rotor induction machine). The vector control model for the 3 systems were built using PSIM.9 in order to prove the functionality of the 3 machines for the flywheel application as different vector control topologies as well as different methods for speed control of the machines were used. For PMSM and SCIM, field weakening is required to reach higher speed above rated speed while keeping the back emf voltage and the power constant, while for DFIM a slip range of +/- 0.3 (+/- 30 % of rated speed) can be used. The speed ranges of the 3 machines as well as their voltage and current rating while operating in the constant power region was examined to determine the energy storage capability as well as the converter rating, cost and losses. Some improvements for reducing the converter rating and thus the losses and cost for the DFIM were proposed by reducing the full speed range used to be -20% to 30% of the rated speed. Also, another improvement for the PMSM design was proposed for reducing the amount of injected magnetizing current required for the field weakening approach. This was done by using smaller magnets, and this will reduce the overall current so smaller current rating for the converter can be used and thus also reducing the losses and the size of the converter.

Thesis Supervisor: Dr. Christian Klumpner
Title: Associate Professor

Acknowledgement

This research project was carried out at the department of Electrical and Electronics Engineering at the University of Nottingham, United Kingdom as part of the Erasmus Mundus program in sustainable transportation and electrical power system (STEPS).

First, I would like to thank god for giving me the power to carry on my master degree with success and for his guidance and blessing. I would like to thank the Erasmus Mundus committee for the financial support by providing a full scholarship offered for a period of 2 years to conduct my Master degree in Electrical Engineering. I would like to thank my professors in the three universities where I attended my courses (Instituto Superior de Engenharia de Coimbra-Portugal, University of Nottingham- UK and Universidad de Oviedo) for their continuous effort in teaching us new subjects, their valuable follow up and encouragement. Special thanks to my master thesis supervisor Professor Christian Klumpner for his effort in teaching me new concepts and his guidance and help during the period of my master thesis. I would like to thank my family for being of great support and encouragement during my two years masters and being abroad and for believing in me and pushing me forward to be a better person in my life.

Finally, many thanks to my colleagues in the Erasmus Mundus program for being a second family for me and make the master degree period more interesting and beneficial as well as my house mates in Nottingham for their kind support and encouragement.

TABLE OF CONTENTS

Chapter 1 1

Literature review of the flywheel energy storage technology 1

1.1. Background and Operation concept 1

1.2. The main components of the FESS structure 3

1.2.1. Spinning rotor 3

1.2.2. Motor/Generator 5

1.2.3. Magnetically levitated bearings 6

1.2.4. Power electronics/converters 6

1.2.5. Vacuumed housing 8

1.3. Different energy storage technologies 8

1.3.1. Batteries 9

1.3.2. Super capacitors and super conductive magnetic energy storage (SMES): 10

1.4. FESS application fields 12

Chapter 2 15

Estimating the Performance of the doubly fed induction machine used in the Flywheel Energy storage system 15

2.1. Introduction 15

2.2. The Topology of a DFIM and previous researches on DFIM based FESS 18

2.3. System calculation for the full speed range and its simulations discussion 20

2.4. The optimized speed range operation and its related impacts 28

2.5. Discussion on the findings 31

Chapter 3 32

Analyzing the performance of the permanent magnet synchronous machine in the field weakening region (constant power region) for the flywheel energy storage application 32

3.1. Background 32

3.1.1. Previous work done on field weakening application for various synchronous machines 34

3.2. The design of PMSM vector controlled simulation model for flywheel energy storage applications 37

3.3. The analysis of the PMSM vector control model in the constant power region 41

3.4. The proposed improvements to the field weakening for PMSM used in FESS to reduce the peak value of the required injected $\mathbf{I}\boldsymbol{d}$current 44

3.5. Conclusion 48

Chapter 4 49

Induction machines (DFIM and squirrel cage) vector control models 49

4.1. DFIM vector control model 49
4.1.1. DFIM vector control model design results and discussion 52
4.2. Squirrel cage induction machine (SCIM) vector control model 56
4.2.1. SCIM design results and discussion 59
Chapter 5 63
The comparison between DFIM, SCIM and PMSM in terms of converter sizes, converter and thermal stresses. 63
5.1. PMSM converter sizing, losses and cycle efficiency analysis using PSIM thermal module. 65
5.2. SCIM converter sizing, losses and efficiency analysis using PSIM thermal module. 70
5.3. DFIM converter sizing, losses and efficiency analysis using PSIM thermal module. 74
5.4. Discussion on findings: 78
Chapter 6 79
Conclusion and future development 79
6.1. Conclusion 79
6.2. Future development 81
Quality report 82
References 84

List of figures

Figure 1.1.The two-dimensional representations of the FESS rotating mass 2

Figure 1.2. A general structure and main component of a FESS beside a cross section from Beacon power 450 FESS 3

Figure 1.3.The power converter connection with the FESS 7

Figure 2.1.The topology of the doubly fed induction machine based FESS with the grid connection……..18

Figure 2.2.The DFIM mechanical power, Torque, Speed (rpm) and rotor current curves vs time. 22

Figure 2.3.The DFIM rotor phase voltage vs time.....23

Figure 2.4.The DFIM stator power vs time 23

Figure 2.5.The DFIM rotor power vs time 24

Figure 2.6.The DFIM stator power, rotor power and mechanical power vs time.....24

Figure 2.7.The rotor converter power vs time 26

Figure 2.8.The energy extracted from the FESS vs time.....27

Figure 2.9.The percentage of the rotor current vs the percentage of energy extracted.....27

Figure 2.10.The rotor current for the new speed range vs time.....28

Figure 2.11.The energy extracted from the FESS over the new speed range vs time 29

Figure 2.12.The stator power and the DFIM rating over then new speed range vs time.....29

Figure 2.13.The rotor converter rating over then new speed range vs time 30

Figure 3.1.Comparison of different types of machines that can be used for higher speed ranges by field weakening 32

Figure 3.2.The direct rotor flux vector control of PMSM with d axis oriented on the rotor flux 33

Figure 3.3. Torque, Flux, Back emf voltage and Power vs speed showing the field weakening implementation 34

Figure 3.4.The PMSM vector control model used for FESS during the constant power region 38

Figure 3.5.The field weakening equation phasor diagram representation 39

Figure 3.6. The Id, Iq and their references values vs time at constant speed of 1200 rpm.....41

Figure 3.7.The constant power and speed change during charging and discharging vs time..42

Figure 3.8.The flux weakening implementation using negative Id to maintain constant power and back Emf 42

Figure 3.9.The speed, emf and Id ,Iqresultant curves and their references vs time during the field weakening implementation for a PMSM based FESS.....43

Figure 3.10.The emf increasing slopes and the required Id currents for the new proposed flux and within the same speed range 45

Figure 3.11.The speed, power, emf and Id , Iqresultant curves with their references vs time during the field weakening implementation for a PMSM based FESS for the new model 46

Figure 3.12.The speed, Id , Iqresultant curves with their references and flux vs time during the field weakening implementation for a PMSM based FESS for the Ld=3 mH and PM flux of 0.9728 Wb 47

Figure 4.1.Phasor diagram representation of the rotor current in the stationary axes αβ and their Ird, Irq projections using $\lambda\Psi s$and θr 50

Figure 4.2.The AC voltage signals together with the high frequency triangular signal (carrier signal) to generate the PWM signal used by the IGBT 51

Figure 4.3.DFIM vector control model representation 53

Figure 4.4.The PSIM vector control model for the DFIM used in FESS operation 54

Figure 4.5.The speed curve, dq axis rotor currents **Ird** and **Irq** aligned with their reference signals, during a constant power cycling of 30 kW for a DFIM used in FESS vs time 55

Figure 4.6.A SCIM requires a full-scale power converter to interact with the utility grid (reprinted from [47]).....56

Figure 4.7.The phasor diagram representation of the stator currents Isq and Isd with respect to the αβ stationary axes together with the angle λ used for the transformation 57

Figure 4.8.SCIM indirect rotor flux orientation vector control model representation (reprinted from [49]) 58

Figure 4.9.The PSIM vector control model for the DFIM used in FESS operation 59

Figure 4.10.The speed range, constant power, stator currents Isd and Isqaligned with their reference signals during charging and discharging within the selected speed range for a SCIM used in FESS vs time 60

Figure 4.11.The flux reduction with increasing speed for keeping the power and the back emf constant above the rated speed (field weakening approach) vs time 61

Figure 5.1.IGBT module thermal resistance model with the heat sink and case relevant components [50] 64

Figure 5.2.The PSIM vector controlled model with the SKM200GB125D (dual module) representing 1 leg of the converter 66

Figure 5.3.The simple circuit used to measure the heat sink temperature as well as the junction (diode and transistor) temperature by setting the ambient temperature to 40 o C 66

Figure 5.4.The thermal module conduction and switching losses for both the IGBT and diode during charging and discharging cycles for 1 leg of SKM200GB125D (dual module). 67

Figure 5.5.Speed, power, heat sink, IGBT and diode temperature plots for the PMSM converter thermal module 69

Figure 5.6.The SCIM vector controlled model with the SKM200GB125D dual module (1200 V, 150A) 71

Figure 5.7.The speed range, processed power,IGBT and diode conduction and switching losses during charging and discharging of the SCIM vector controlled model 72

Figure 5.8.Speed, Processed power, heat sink, transistor and diode temperature plots for the SCIM converter thermal module 73

Figure 5.9.The DFIM vector controlled model with the Powerex 6-pack module (600 V, 100A) 75

Figure 5.10.The speed range, power, IGBT and diode conduction and switching losses during charging and discharging of the DFIM vector controlled model 76

Figure 5.11.The speed range, power, heat sink, transistor and diode temperature plots for the DFIM converter thermal module 77

List of Tables

Table 1.2.The comparison between different energy storage technologies 9

Table 1.3.FESS application and some of the FESS criteria for each application 13

Table.2.1. PMSM and DFIM comparison..... 16

Table 2.2.The VEM 30 kW slip ring machine specifications 19

Table 2.3.Ps, Pr, Temand Pmechcharacteristic through the sub-synchronous and super synchronous modes 25

Table 3.1.The PMSM parameters used for the field weakening analysis of the FESS application 37

Table 4.1.30 kW DFIM machine parameters used for the vector controlled PSIM model..... 52

Table 4.2. 30 kW SCIM parameters used for the vector control model of the SCIM based FESS 58

Table 5.1.Converter losses (transistor and diode conduction and switching losses) during both charging and discharging cycles for the PMSM system 68

Table 5.2. The Heat sink, transistor, diode and junction peak temperature of the PMSM module during charging and discharging 69

Table 5.3.Converter losses (IGBT and diode conduction and switching losses) during both charging and discharging cycles for the SCIM system..... 72

Table 5.4. The Heat sink, transistor, diode and junction temperature of the SCIM module during charging and discharging 73

Table 5.5.Full (3phase) rotor inverter losses (transistor and diode conduction and switching losses) during both charging and discharging cycles for the DFIM system 76

Table 5.6.The Heat sink, transistor, diode and junction peak temperature of the DFIM module during charging and discharging 77

Table 6.1.A comparison between the 3 machines that can be used for the FESS application..... 81

Chapter 1

Literature review of the flywheel energy storage technology

1.1. Background and Operation concept

Nowadays with an increased demand of energy supply quality and especially with the introduction of renewable sources of generation which normally have unpredictable nature and experience many interruptions/disturbances. Different types of Energy Storage Systems (ESS) can be used to compensate this issue. These ESSs basically aim at balancing the electrical energy supply and demand and thus improving the electrical systems reliability/availability besides improving the quality and stability of the system for steady supply operation. The principle of the ESS is based on storing and recovering one available source of energy (chemical, thermal, magmatic or mechanical) into electrical power/energy [1]. When the power demand is high, the ESS provides the extra power needed and when generation exceeds demand, this extra power/energy will be stored. This makes ESS more important as storage is needed during high generation periods or for sources which has unpredictable nature (e.g. wind energy sometime generates more energy than needed if the wind speed is quite high) [2] [3]. On the other hand, during low generation problem/failures or when not enough power source from renewable energy systems is available, the stored energy can be used.

Flywheel energy storage system (FESS) is one form of energy storage which was used from long time ago but introduced to the industry lately as an alternative to the existing energy storage systems. The FESS operation concept is using electrical energy input from the network when the generation is more than the demand and convert it into kinetic energy. The flywheel has a spinning mass called a rotor which will use this kinetic energy form to keep spinning and storing the energy using the basic kinetic energy equations:

$$E = \frac{1}{2}mv^2 = \frac{1}{2}m(r\omega)^2 = \frac{1}{2}mr^2\omega^2 \quad (1.1)$$

Where E is the energy stored in the FESS, m is the mass of the rotating body, r is the radius of the cylinder through which the mass rotates and ω is the angular speed of its rotation. The term mr^2 is referred to as the moment of inertia.

This rotor/spinning body as presented in Figure 1.1 is rotating in a vacuum (frictionless) enclosure to reduce the drag effect and thus provide low discharge. In case of power system failure, a backup supply is required for a short time, the inertia will keep the rotor spinning as it slows down and the stored kinetic energy is converted in electrical energy. The current flywheels consist of a large rotating cylinder, magnetic bearing, motor/generator, power electronics and vacuumed enclosure. The flywheel is connected to an electrical machine which acts either as a generator or motor depending on the state of operation (charging/discharging) and this machine is the mean of interaction with the utility grid via advanced power converters [4].The Power electronics (normally a back to back converters is used) consists of two stages: a machine side converter (MSC) and grid side converter (GSC). The MSC will control the power between the machine and the grid by controlling the active and reactive power and the torque via the rectifier stage. Also, the GSC and the DC link control the grid frequency and voltage in order to keep it within a desired range by controlling the DC link voltage. This will provide a reliable system and reduce the disturbances that may cause an unstable grid to fail.

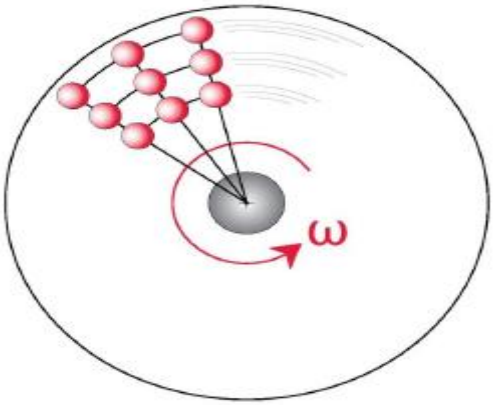

Figure 1.1.The two-dimensional representations of the FESS rotating mass (reprinted from [5])

1.2. The main components of the FESS structure

In this section, a brief description of the main components of the FESS structure will be discussed. These components can also be seen in Figure 1.2.

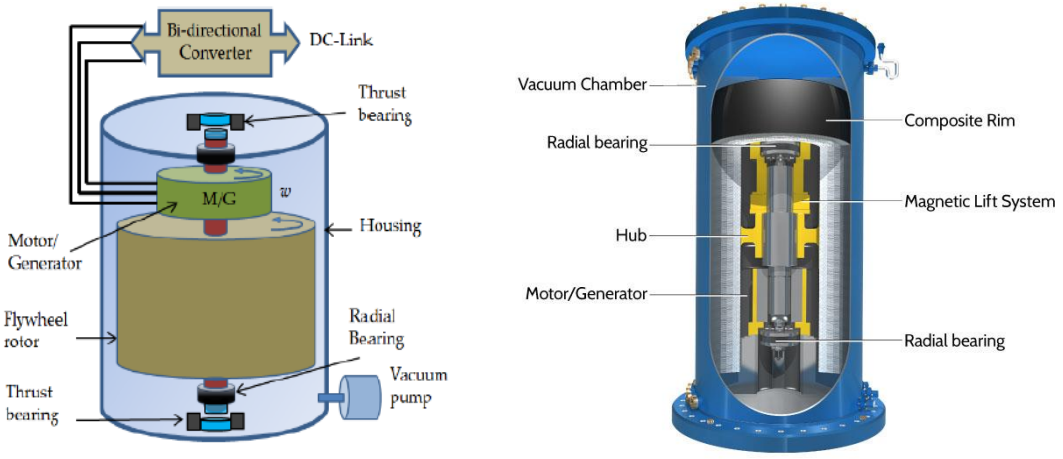

Figure 1.2. A general structure and main component of a FESS beside a cross section from Beacon power 450 FESS (reprinted from [6])

1.2.1. Spinning rotor

This component determines the amount of energy that can be stored by the flywheel in terms of its material, speed limit and shape. This energy is directly proportional to the moment of inertia J and angular velocity squared Ω^2 [7] [8] according to the following equation:

$$E=\frac{1}{2}J\Omega^2 \tag{1.2}$$

Since the FESS are electrically driven by a motor/generator, normally it operates within the speed limits of the machine (between $\Omega_{max}$and Ω_{min}). This is done to avoid high voltage that may increase the rating/stresses and to limit the maximum torque that the machine needs to produce and thus the associated currents for a certain power rating and the energy stored in equation 1.2 can be rewritten as following:

$$\Delta E=\frac{1}{2}J\,(\Omega_{max}{}^2-\Omega_{min}{}^2) \tag{1.3}$$

Also, the structure of the FESS will affect the amount of the energy stored as the moment of inertia used in equations (1.2) and (1.3) is based on the mass of the rotor as well as the rotor

diameter as can be seen in equation (1.4) and (1.5). For this, the structure of the flywheel is built from hollow or solid cylinders with a shape that can vary from a long drum shaped to a short disc shaped rotor [9].

$$J=\frac{1}{2}mr^2 \tag{1.4}$$

$$J=\frac{1}{2}\rho\pi r^4 h \tag{1.5}$$

Where m is the mass of the rotor, r is the hollow/average diameter, h is the length of the flywheel and ρ is the mass density.

The strength of the rotor material also influences the maximum speed limit of the flywheel, where this strength is referred to as a tensile strength σ [10]. For safety reasons, a margin should be kept between the stress on rotor and the rotor strength and this maximum stress can be calculated as following:

$$\sigma_{max} = \rho r^2 {\Omega_{max}}^2 \tag{1.6}$$

Lastly another factor affects the speed limit and hence the energy stored is the rotor geometry shape factor K. This shape factor in a relation with the energy per mass unit can be seen in the following equation:

$$\frac{E}{m} = K\frac{\sigma_{max}}{\rho} \tag{1.7}$$

From the previous mentioned equations, the amount of stored energy by the FESS can be optimized either by increasing the moment of inertia (increasing mass or radius) or by increasing the rotating speed and managing the geometry and material used. Based on the application, the speed range of the flywheel can be decided to be a low speed flywheel (10,000 rpm or below) or high-speed ones (above 10,000 rpm). So, upon the choice of speed, the flywheel material can be chosen to be either heavy metallic material with magnetic or mechanical bearing for low speed FESS or light but composite materials with magnetic bearings for high speed FESS. FESS offers a good choice for applications which require very quick response time (5-10 ms) with a short discharge period (few sec to 1 hour) and they are suitable for medium power rating application requiring a constant power supply during their discharging. Despite of the relatively high costs, they have very low maintenance cost and long-life cycle. This life cycle can be of about 20 years (some flywheels have the ability to perform 100,000 full depth of discharge cycles and some modern designs are capable of about 200,000

cycles) with a very low environmental impact (as no chemicals are used mainly) compared to the other energy storage systems.

1.2.2. Motor/Generator

The electrical machine is connected to the FESS which enables the conversion of mechanical energy to electrical energy and vice versa as well as enabling the charging and discharging of the flywheel. This machine will act as a motor to charge the flywheel in case of excess power on the grid allowing it to withdraw this excess power and accelerating the rotating mass. The stored kinetic energy will be converted back to electrical energy by the machine in terms of energy deficit as the machine will act as a generator drawing the stored mechanical energy from the FESS by discharging it (deceleration). Flywheel operating machines are normally either Induction machines, permanent magnet synchronous machines and switched reluctance machines.

1.2.2.1. Permanent magnet synchronous machine

The permanent magnet synchronous machine (PMSM) are the most commonly used for the FESS in market due to its high-power density and high efficiency and low rotor losses. It is mainly used for applications where high speeds are needed or for having a smaller gearbox with the high speed of flywheel as it offers a high-speed range [11]. The drawback of the PMSM is that it has high eddy currents (high standby losses), its price is higher than other machine types and it has a low tensile strength.

1.2.2.2. Induction machine

Induction machines (IM) are mainly used for high power application and are characterized by lower cost compared to the PMSM... Two types of IM can be used: Squirrel cage (SC) which can be normally be used for low response application and the wound rotor/slip ring induction machine which is also referred to as doubly fed induction machine (DFIM) which offers a good alternative to the squirrel cage in terms of speed control. The DFIM have direct access to the rotor winding through which all the power processing control is done. For this, a smaller power converter can be used (for a normal slip (s) of 0.3 a power converter of only s* stator power which means only 30 % of the stator power flow will require a smaller converter to be

processed while the rest of the power will be directly connected to the utility grid via the stator. The drawbacks of using wound rotor induction machines is that they have a speed limit by the slip (normally it is within +/- 30% the rated speed) beside the control complexity and the higher maintenance requirement [12].

1.2.2.3. Reluctance machines

Lastly, for reluctance machine, they are very robust with a high-speed range, low idling losses and less complex control. Yet, it has a low power factor and power density compared to the other 2 machines besides a high torque ripple [12] [13]. Two types of reluctance machines can be used for high speed FESS applications which are: synchronous reluctance (synchronous AC machine) and switched reluctance (DC machine)

1.2.3. Magnetically levitated bearings

Bearings are used to maintain the position of the rotor and they can either mechanical or magnetic according to the required life cycle, weight and speed. For long time, the mechanical bearings have been used but for the higher speeds, the magnetic bearings are used as they provide almost no friction losses without the need for any lubrication as the mechanical ones [14]. For the magnetic bearings used, it requires to be energized by some energy as long as it is active then it can stabilize the FESS by providing support to its weight using permanent magnets. Some of the commonly used magnetic bearings are: active magnet permeant bearings, passive magnet permeant bearings and super conducting magnetic bearings [12].

1.2.4. Power electronics/converters

As discussed earlier, the operation of the FESS is based on energy conversion mechanism where the interaction with the utility grid is provided by the machine and a bi-directional power converter as can be seen in Figure 1.3 to control the power flow beside voltage and frequency.

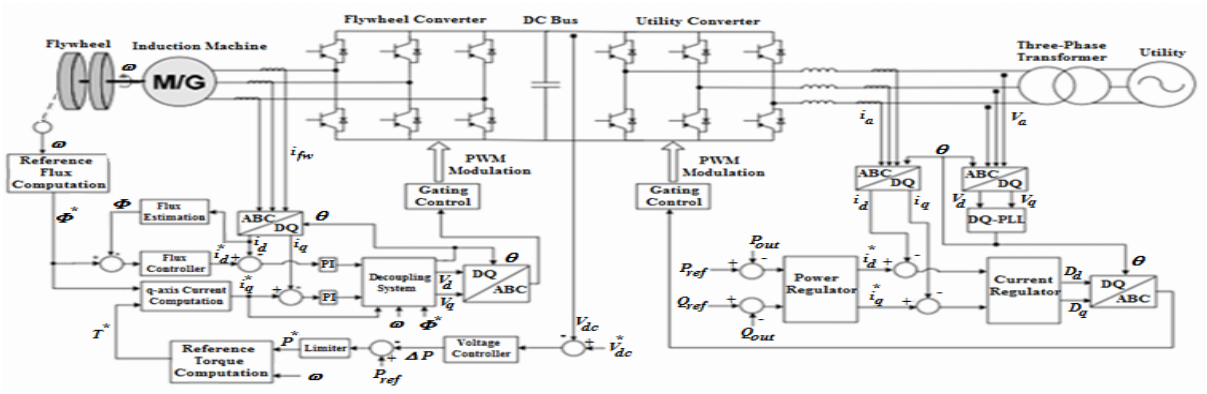

Figure 1.3.The power converter connection with the FESS (reprinted from [15])

Many types of power converters can be used in the FESS such as: DC/AC, AC/AC or AC/DC/AC. The components of the converter (switching components) are selected depending on the application and the power ratings and they include mainly insulated gate bipolar transistors (IGBTs), bipolar junction transistor (BJT), thyristors (GTO, MCT and SCR) and metal oxide semiconductor field effect transistor (MOSFETS) [16] . The most commonly used switching devices recently is the IGBTs due to its high switching frequencies and high-power ratings available. And the most commonly used power converter arrangement with the FESS is the back to back AC/DC/AC together with a DC link (a capacitor) in a form of a three phase bridges switching inverter. These devices are controlled via a pulse width modulation mechanism (PWM) which uses rectangular pulses whose widths are modulated to generate AC signals. These pulses are used in the converter to generate a sinusoidal AC voltage from a DC source. The converter can also be seen as consisting of two main parts: machine side converter (MSC) and grid side converter (GSC) which is mainly an inverter producing an AC signal with the required frequency and magnitude from the fixed/variable DC voltage of the DC link capacitor.

For both the machine side converter (MSC) and the grid side converter (GSC), higher switching frequencies are used to lower the current ripple and increase the control range but on the opposite side this will cause an increase in the switching losses. Besides, the use of high switching frequencies can reduce the harmonics of high order and generate better quality sinusoidal signals and those harmonics can be further reduced if AC filters are used along with the AC sides of the converter which will hence reduce the ripples and the processed power losses [17].

1.2.5. Vacuumed housing

The vacuumed housing is used to contain the spinning rotor and the other components in an environment of low gas drag as this aerodynamic drag losses is proportional with the rotational speed cubed so more losses are caused if it is operated in atmospheric pressure. This housing /enclosure is the static part of the FESS and is normally built from either heavy steel or materials with high strength (such as composite materials). To ensure that the enclosure is vacuumed, a vacuum pump (with a mixture of air and helium) is used to maintain a low pressure which works better with an efficient cooling system to process the heat generated from the motor/generator and the other part of the FESS [18]. Since the power that goes into or outside the FESS is done through the motor/generator without rotary seals, this means that there will be a very little leakage in this case. For this reason, the pump is not required to operate continuously and can be used once then removed if a proper sealing of the housing is done. In case of the rotor failure, if it is made of composite materials then it will break down into small fragments. This will cause a pressure to exist inside the housing and its end plates as those fragments will cause energy to be dissipated by friction as the rotor keep rotating. For single piece rotor made of steel, if failure occurs, it will break down into bigger fragments and make it difficult for the housing to withstand the impact. For this a large containment is used beside trying to make the rotor from thinner discs. Finally, for high speed FESS, this containment represents almost half the weight of the whole FESS.

1.3. Different energy storage technologies

Energy storage systems as discussed in section 1.1 are used for maintaining the quality of the electrical systems by solving the misbalance that may occur either on short term or long term. Table 1.1 summarize different types of energy storage and for this section the focus will be on the ESS which have quick response times (batteries, super conductors, super conductor magnetic energy storage) to be compared to the FESS.

Table 1.1.The comparison between different energy storage technologies (reprinted from [19])

Technology		Typical Nominal Power	Discharge time	Respones Time	Efficiency	Lifetime
Pumped Hydroelectric Energy Storage		100-4000 MW	6-24 h	10s -3 min	65-85%	30-75 years
Compressed air energy storage		25-30000 MW	4- 24 h	3-15 min	50-85%	20-40 years
Battery	Flow Batteries	25 kW-10 MW	1-8 h	30 - 100 ms	65-85%	2-10 years
	Lithium Ion	10 kW - 10 MW	10 min - 1 h		85-90%	
	Lead Acid	50 kW - 30 MW	15 min – 4 h		70-80%	
	Sodium Sulphur	50 kW - 30 MW	1-8 h		75-90%	
Supercapacitors		10 kW - 1 MW	1s - 1min	5-10 ms	85-95%	40 years
Superconduction Magnetic energy storage		1 MW - 100 MW	1s - 1min	5-10 ms	85-95%	30-40 years
Flywheels		10 kW - 20 MW	1s - 1 h	5-10 ms	85-95%	20 years

1.3.1. Batteries

Batteries have been used as a form of energy storage for long time, they store energy in chemical form and during discharge of the battery (which can take a short time of about 30-100 ms to respond and from 10 minutes up to 8 hours to discharge all the stored energy), electrical energy is released using the redox reaction. Batteries are built from negative and positive electrodes referred to as anode and cathode. Those electrodes are connected externally to a circuit which manage the charging/discharging of the battery. Batteries can be connected in a form of battery bank either in parallel or series according to the desired voltage and current for the application. There are different batteries technologies where the oldest among them is the lead acid battery and the new alternatives are sodium sulphur and lithium ions which will be explained briefly as following:

1.3.1.1. Lead acid batteries

They are the oldest form of batteries used and they are made of a lead cathode and lead dioxide anode and the electrolyte is made of sulphuric acid which is used during the discharging process of the battery. Normally those batteries have an efficiency of 70-80 % and are normally used for small and medium scale energy storage yet they have the disadvantages of short life cycle,

high cost and high maintenance, low energy density and environmental risks due to the use of lead and sulphuric acid [20].

1.3.1.2.Sodium Sulphur batteries

One alternative to the traditional lead acid batteries which consist of a negative sodium electrode and a positive sulphur solution electrode with an electrolyte of alumina ceramic. They operate at high temperature of 300 ˚C to maintain the electrodes in molten state and have an efficiency of up to 80% [21]. The typical application is for high power energy systems of up to 30 MW and they can provide energy for up to 6 hours.

1.3.1.3. Lithium ion batteries

A high efficiency battery (90-95 %) [21] consist of lithium oxide cathode and graphite carbon anode separated by a lithium salt electrolyte. The typical energy storage system can be for power ratings from 1-10 MW in a form of battery banks.

1.3.1.4. Redox flow batteries

They are made of two electrolyte sets that flow through separate loops and those loops are joined in a cell yet separated by a membrane that prevents the mixing of the two electrolytes yet allow the ions to be exchanged. The advantage of these batteries is that since the electrolytes are contained outside the battery cell, this allows an energy storage extension by expanding the volume of the electrolyte containment [22]. There are different types of flow batteries such as Vanadium, ZnBr and Polysulphide bromide and the typical efficiency is about 75%. They are normally used for large scale energy storage systems with a high life cycle expectancy and high-power capacity but high cost and lower power densities.

1.3.2. Super capacitors and super conductive magnetic energy storage (SMES):

Super capacitors are used to store energy in the same way the normal capacitor operate using the following equation

$$E = \frac{1}{2} C v^2 \tag{1.8}$$

Normally a double layer capacitor is used with a very high electrostatic capacitance than the electromechanical pseudo capacitance which act to separate charges in Helmholtz double layer. This double layer exists between the electrolyte and the conductive electrode surface. It consists of 2 electrodes, electrolyte, 2 current collectors and a separator all contained in a housing. They are used for high power systems with a very quick response time, a very long-life cycle (up to 40 years) and high efficiency of about 85-95%. Their main disadvantages are the low energy density and high self-discharges besides their high cost [22].

The SMES uses a magnetic field to store the processed energy where this field is generated using a DC current passing through a superconducting coil. This system requires a power converter interface between the SMES and the utility grid. The resistive losses of this system can be eliminated by operating a very low temperature (77 K-4 K). They offer a very quick response time in order of milliseconds and a high efficiency of 90% but to keep the system temperature low there will be energy consumed by the cryogenic cooling system. The main disadvantage of this system is that they have huge electromagnetic fields, a complex structure due to the cryogenically cooling system and high costs [23].

1.4. FESS application fields

FESS can be used in many applications especially those which require a very quick response such as microgrids and renewable technologies. They are used to resolve the mismatch between the generated and demanded energy in order to handle peak loads or to store the excess energy during low loading periods. This is essential in fulfilling the gap occurred due to power outages especially for critical loads in industrial and commercial areas.

Some of the other applications where the FESS is used includes:

1. Electric vehicles (peak power buffer in the vehicle), the use of the FESS can extend the battery life and also increase the regenerative braking capability
2. Transportation: where pulsed power applications are needed
3. Hybrid electric combat system
4. Utility grid application and distribution systems support: this includes
    - Uninterrupted power supply (UPS)
    - Voltage sag compensation
    - Harmonic compensation
    - Frequency regulation
    - Flexible power conditioner (FACTs)
5. Renewable technologies: to overcome the intermittency of the source
6. Aerospace application: Satellites and international space stations (ISS)

A summary of the FESS applications and the type of FESS material, power ratings, speed range for each application is shown in Table 1.2

Table 1.2.FESS application and some of the FESS criteria for each application (reprinted from [24])

Application-Specific Flywheel Battery Designs

	Peak power	Stored energy, MJ (kWh)	Maximum rotational velocity, rpm	Rim speed, m/s	Rotor material	Rotor mass, kg
Satellite	2 kW	1.4 (0.4)	53 000	900	Composite	30
Power quality	400 kW	4.7 (1.3)	10 000	400	Steel	1400
Hybrid bus	150 kW	7 (2)	40 000	900	Composite	60
Space station	3.6 kW	13 (3.7)	53 000			75
Hybrid combat vehicle	11 MW pulsed; 350 kW continuous	25 (14)	18 000	540	Composite/ metallic	280
Electromagnetic launcher	5–10 GW	50–150 (14–42)	10 000	450	Composite	4000
Train	2 MW	470 (130)	15 000	950		2500

Source: University of Texas

As discussed earlier, the amount of energy stored by FESS is calculated from equation 1.3, so it can be seen that the speed range as well as the moment of inertia are the main factors for calculating the amount of energy to be stored by the flywheel. The speed range is obtained from the machine used for interaction between the FESS and the utility grid for a given constant power rating decided by the application.

Project aims and objectives

In this project, different electrical drive types will be analyzed in terms of the speed range that they can operate with the FESS as well as how to optimize this speed range and the installed power in the converter in order to achieve better efficiency, lower losses and cost as well as obtaining a good percentage of energy stored.

For this analysis, doubly fed induction machine (DFIM), Permeant magnet synchronous machine(PMSM) and squirrel cage induction machine will be analyzed in the following chapters. Chapter 2 will discuss the operation of the DFIM for the FESS operating on a full speed range of +/-30% of the rated speed (as a function of the slip). A proposed improvement in terms of reducing the converter size and thus its cost and losses will be discussed by reducing the speed range partially. This should yield in reducing the machine torque and thus the rotor current which is directly proportional to the torque. And since the converter is processing the rotor power, reducing the rotor current will reduce the converter size and losses which will cause a small compromise in terms of reducing the amount of energy that can be stored by the FESS.

In chapter 3, the PMSM will be discussed in detail beside the vector control topology that is used with it and a simulation model for the whole system will be built using PSIM.9. Since we are interested in the constant power application for the FESS, only speeds above the rated machine speed will be analyzed. For this reason, the field weakening approach will be applied to maintain constant back emf voltage and thus constant power. This is done by reducing the flux with the increasing speed (above the rated speed). The speed range that can be achieved by the PMSM will be analyzed as well as the functionality of the system in the field weakening region for the FESS application. A proposed technique for reducing the amount of the flux current that needs to be injected during the field weakening application in order to achieve a smaller overall current and thus a smaller converter rating and losses.

In chapter 4, The 2 induction machines (DFIM and squirrel cage) vector control models will be analyzed using PSIM together with a detail discussion of the different vector control topologies used for each machine. Also, the squirrel cage operation above rated speed will require the application of field weakening to operate at higher speeds above the rated speed. This is done to ensure its operation in the constant power region required for the FESS application. The functionality of the 2 systems will be discussed and the speed ranges as well as the current and voltage rating to be compared with the PMSM vector control model in the last chapter in terms of converter sizing and losses.

In chapter 5, the 3 vector controlled systems of the 3 drives will be compared in terms of the machine side converter ratings, losses, cost and temperature limits experienced by the IGBTs and diodes of the converter. The thermal modules in PSIM.9 will be used in the analysis in order to obtain those results which will give a proper comparison of the 3 systems in the conclusion chapter.

Chapter 2

Estimating the Performance of the doubly fed induction machine used in the Flywheel Energy storage system

2.1. Introduction

This chapter discusses how the doubly fed induction machine can be exploited in terms of speed range and rotor current limits in order to reduces the losses (to be discussed in later chapter) of the machine during motoring/generating mode, the size of the used converter and the machine as well as the relation between the energy extraction in case of an imposed speed range +/- 30 % around the synchronous speed with the new proposed speed range.

The doubly fed induction machine (DFIM) when used in a flywheel storage system (FESS) offers an opportunity to substitute the permanent magnet synchronous based machines (PMSM) as used in commercial FESS. This can help in reducing converter and machine cost and improve efficiency at top speed, as the bulk of the power is fed directly in the AC grid via the stator rather than being processed via an AC/DC and DC/AC power conversions. The PMSM performs well with the FESS based on the fact that they have high power density and a compact design together with a high round trip efficiency (The efficiency of storing the energy during the charging and discharging process [25], [26], [27]; yet the self-discharge losses are high due to mechanical friction and generator core losses. In addition, it needs to use a full-scale AC/DC/AC converter [26],through which all the power has to pass from the machine to the grid and vice versa. This process increases the price of the system (also the maintenance costs). The power losses during the processing of the full power passing through the converter lowers the top efficiency by the need to process the full power through two conversion stages. Also, the PMSM experiences high self-discharge losses due to the magnetism which can be reduced slightly by some mechanisms but still will remain high [27]

As a proposed solution for this, DFIM specifically the wound rotor type can be used which has a direct access to the rotor winding via slip rings. This enables the stator power to be routed directly to the grid [28], [29]without the need for a transformer while a smaller portion of the mechanical power will be processed by the rotor as shown in Fig.1. This rotor processed power

represents 30% of the total machine rating according to the relation Pr = Smax*Ps. For this case, the slip range of the DFIM is normally between +0.3 to -0.3 [28] depending on the mode of operation either super synchronous or sub synchronous mode. The DFIM offers a significant solution for the high self-discharge losses of the PMSM at light loading and/ or when operating at high speed. On the opposite side, the maximum speed that can be achieved is 3900 rpm (using a 2-pole machine on a 50Hz network while operating at super synchronous mode of 30% above the synchronous speed). This can be considered as a disadvantage as for smaller power rating machines below 100 kW normally the lower poles machines available are 4 (ns=1500 rpm) which means a gearbox needs to be used between the FESS and the DFIM. The flywheel can operate at high speeds up to 16000 rpm (for this analysis, a smaller speed will be used- 4000 rpm) which means a gear box of a 3.8:1 ratio (ratio between 4000 rpm of the FESS and the lowest speed of the DFIM reached at sub synchronous mode 0.3*1500= 1050 rpm) will be needed, and thus the cost and losses of this gearbox will be discussed later.

For this case, a quick comparison between DFIM and PMSM is presented in table 1 in order to get an idea of how they can be used for FESS application.

Table.2.1 provides a general comparison between the PMSM and DFIM as a potential machine to operate the FESS.

Table.2.1. PMSM and DFIM comparison

PMSM advantages	**DFIM advantages**
No need for excitation	Demagnetization is impossible to happen as long as the machine is connected to the grid/supply.
No components are subject to wear out as no need for electrical winding.	Possibility to control excitation field (by disconnecting the stator from the grid otherwise the field stays constant) , so no electromagnetic spinning losses
High overall efficiency	Can be built be low cost high strength material
Highest power density	Normally lower cost than PMSM as no permanent magnet is needed (high cost)

PMSM disadvantages	DFIM disadvantages
Risk of demagnetization	Low overload capability
Electromagnetic spinning losses at zero torque	High maintenance costs
Low strength of the Permeant magnet material which requires structural support against the centrifugal forces	Complex rotor design due to the need of electrical windings and slip rings.
Sensitive to heating	High losses during excitation
	Lower power density, power factor and efficiency compared to PMSM

2.2. The Topology of a DFIM and previous researches on DFIM based FESS

It can be seen in Figure 2.1 that the reduced sized converter used in the DFIM set up consists of two stages: AC/DC Rotor side converter (RSC) and a DC/AC grid side converter (GSC). The back to back converters (normally PWM based) enable the control of the machine power via the field-oriented (vector) control [30]. The RSC enables the control of the torque and the active and reactive power of the machine (providing the reference active and reactive power by controlling the rotor current through a synchronously rotating frame using linear feedback loops with feed forward terms. The GSC together with the DC link between the 2 converter stages will allow the control of the grid voltage and frequency via controlling the DC link voltage within the desired limits [31], [32], [33] and the vector control of the DFIM will be discussed in next chapters when analyzing the performance of the system as a whole.

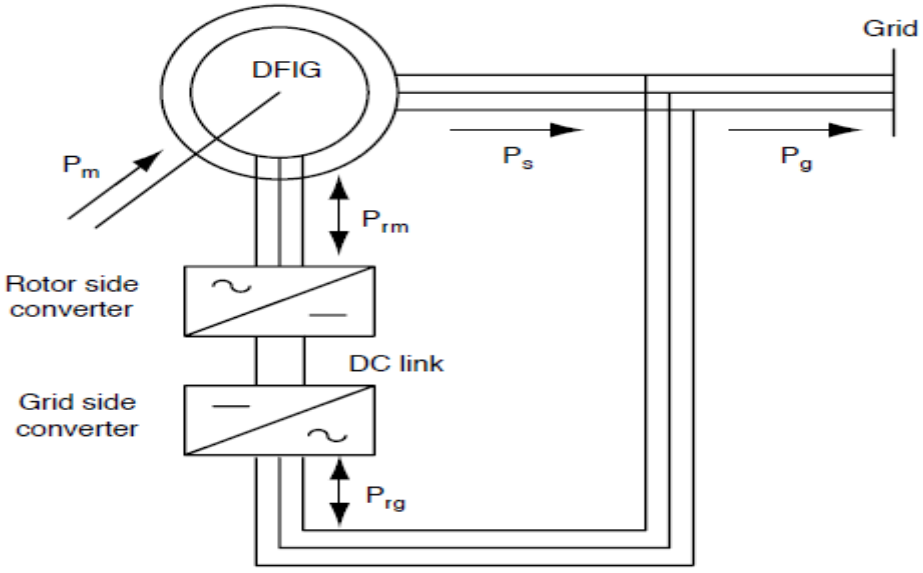

Figure 2.1.The topology of the doubly fed induction machine based FESS with the grid connection (reprinted from [32])

Some researchers have been done on the use of DFIG to operate the FESS. It was proposed in [34] a new arrangement for using a DFIG based flywheel together with a battery for a micro grid application using wind turbines. It was proven that the flywheel performs well in terms of reducing the wind fluctuations as well as controlling frequency and the voltage of the micro

grid in islanded condition. Another paper [35] discussed the use of a DFIG based FESS to overcome the grid voltage sags when they occurred. As seen in fig. the maximum time for a voltage sag to occur is about 3 sec which make the FESS an ideal solution as it can provide the required voltage to compensate the voltage sag for short period until the problem is resolved. For this analysis, a 2.2 KW DFIG with a full speed range was used (+/-30% of the synchronous speed) and the control of the system was implemented to prove the functionality of the proposal. No previous researches were done to analyse the impact of altering the speed range of the DFIG on the amount of the stored energy percentage by the FESS and how a reduction or increment of this speed range (either in sub or super synchronous mode) can affect the converter and system size.

In this chapter, the focus will be on how to determine the performance of the DFIM based FESS in terms of evaluating the speed range within the machine can operate and the relation between that and the energy extraction, the losses and the converter costs. For this purpose, a 30 kW VEM slip ring doubly fed induction machine was used for the analysis which has the characteristic presented in Table 2.2 and a MATLAB script for the associated calculations and for plotting the results using the data of the machine mentioned before was used.

Table 2.2.The VEM 30 kW slip ring machine specifications

Constant Power rating: 30 kW	**Rotor current:**88 A
Stator-Rotor configuration: star-delta	**Rotor Voltage (L-L):** 210 V
Stator voltage: 400 V	**Rotor resistance:** 0.02235Ω
Stator current at full load: 54.5 A	**Number of poles:** 4
Rated speed: 1455 rpm	**Moment of inertia:** 0.476Kg.m^2
Efficiency: 91%	**Weight:** 330 kg
Power factor: 0.87	**Locked rotor voltage**: 500 V

2.3. System calculation for the full speed range and its simulations discussion

The system which will be tested is assumed to be an ideal system and the DFIM rotor circuit is considered lossless (ideal), so no power losses between the FESS and the DFIM (either through the shaft or the gearbox) as well as the mechanical torque of the shaft will be equal the electromagnetic torque of the machine as in the equation:

$$T_{em} = T_m. \tag{2.1}$$

Since the discussion was performed for a constant power mode (a constant power of 30 KW should be maintained while charging (generating) or discharging (motoring)), so the torque and speed are inversely proportional according to the equation:

$$T_m = \frac{Pmech}{\Omega} \tag{2.2}$$

Where omega (Ω) is the rotor rotational speed in rad/s and Tm is the mechanical torque in N.m and it is the same as the electromagnetic torque of the machine. Since the torque and speed will be inversely proportional so it can be concluded that as the speed decreases faster (especially towards the edge of the sub synchronous speed 1050 rpm) the torque curve increases in faster scale than the super synchronous mode due to the following equations:

$$T_m = \text{J} * \frac{d\Omega}{dt} \text{ but } T_m = P_{mech} * \Omega \tag{2.3}$$

Where J is the moment of inertia in Kg.$m^2$and $\frac{d\Omega}{dt}$ is the acceleration/ deceleration of the machine in rad/ s^2. So, using a time step (dt) of 0.001s (1 ms) and Pmech to be constant and a given moment of inertia, the change in rotor speed per time step can be obtained and thus the rotor speed over the speed range chosen can be plotted and the equivalent torque can be calculated and plotted from the following equations using a for loop in the MATLAB script:

$$T_{em}(\text{x}) = \frac{Pmech}{\Omega(x)} \tag{2.4}$$

$$d\Omega\ (\text{x}) = \frac{T_{em}\ (\text{x}) * dt}{J} \tag{2.5}$$

$$\Omega\ (\text{x+1}) = \Omega\ (\text{x}) + d\Omega\ (\text{x}) \tag{2.6}$$

The rotor rotational speed range which will be used in the analysis is considered to be +/- 30 % of the synchronous speed which is 1500 rpm, which means from 1950 rpm to 1050 rpm or 204.2035 rad/s to 109.9557 rad/s.

The torque of a three-phase induction motor is proportional to the flux per stator pole, rotor current and the power factor of the rotor as following.

$$T = \mathbf{k}\ \phi\ I_2 \cos\phi_2 \tag{2.7}$$

Where, ϕ is the stator flux, I2 is the rotor current, ϕ2 is the phase angle between rotor emf and rotor current and K is a constant = 3/(2π*ns/60), ns is the machine synchronous speed and divided by 60 to have its rps value.

But the rotor emf (E20) is directly proportional to flux per stator pole, i.e. E2 ∝ ϕ, so the equation can be rewritten as: T ∝ E20* I2 cosϕ2 or T =k1 E20*I2 cosϕ2. And the rotor current in terms of Torque can be rewritten as:

$$I2 = \frac{T}{E20 * \cos\phi 2 * \frac{3}{2\pi * \frac{ns}{60}}} \tag{2.8}$$

So, by substituting the machine equivalents in the equation:

$$E20 * \cos\phi 2 * \frac{3}{2\pi * \frac{ns}{60}} = \frac{210}{\sqrt{3}} * 0.87 * \frac{3}{2\pi * \frac{1500}{60}} = 2.00067 \tag{2.9}$$

And dividing that by the efficiency of 0.91; the Torque and rotor current relation can be expressed as:

$$I_r = \frac{Tem}{2.213} \tag{2.10}$$

Note: During the selection of the DFIM required to supply/store the required mechanical constant power of the FESS, it is important to compare several machine manufacturers for the same power ratings in terms of:

1. The Power factor and efficiency
2. The Moment of inertia
3. The overall weight of the machine and the design dimensions.

The relation between the mechanical power, rotor speed, toque and the rotor current as a function of time can be seen in Figure 2.2.

Note that the at lowest operating speed, the torque is maximum and since the rotor current is directly proportional to the torque, then maximum rotor current occurs at 0.3*rated speed (1050 rpm which is the lowest speed at the sub synchronous mode) and it is equal to **123.2 A**. This means that the maximum rotor power losses at that point can be calculated as following: 3* $(I_r)^2 * R_r$ = 3* $(123.2)^2$*0.0223 = **1 KW**

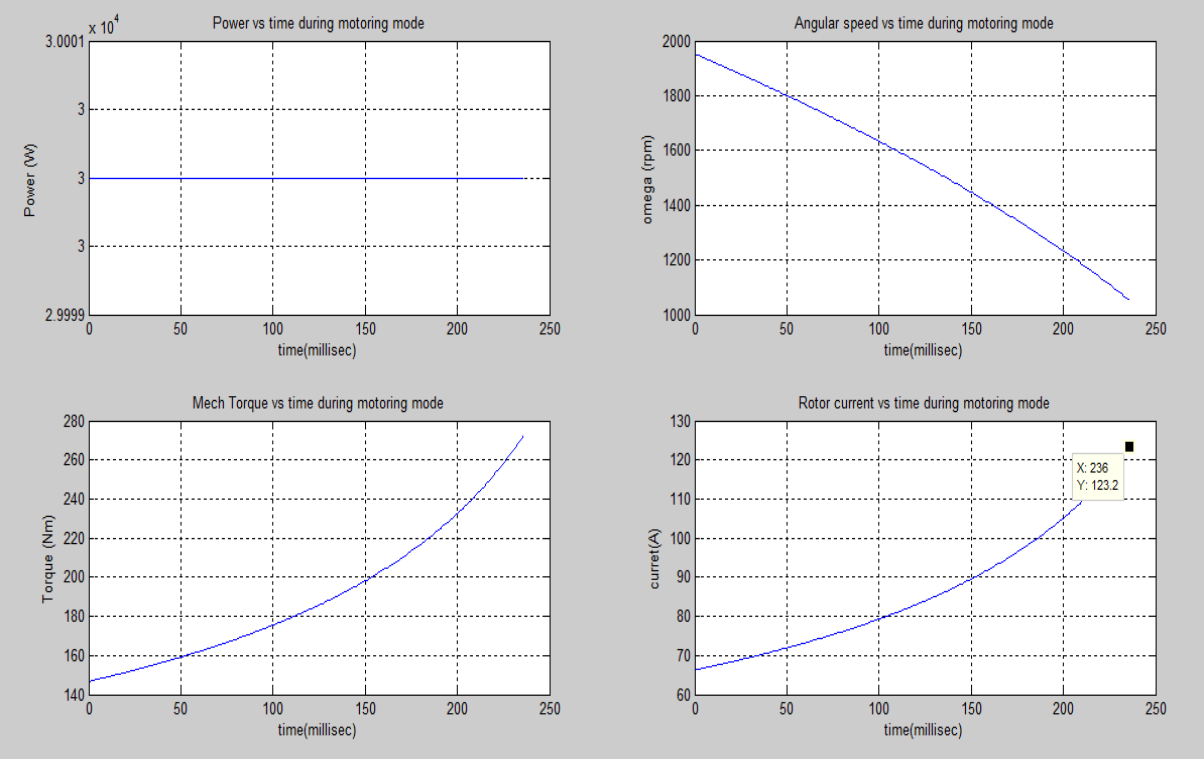

Figure 2.2.The DFIM mechanical power, Torque, Speed (rpm) and rotor current curves vs time.

The rotor voltage can be calculated using the given open circuit rotor voltage (line voltage converted to phase voltage) and the calculated slip (s) as following:

$$V_r = s * \frac{V20_{L-L}}{\sqrt{3}} \quad (2.11)$$

Where s is the slip (s = $\frac{\Omega_{s-\Omega_r}}{\Omega_s}$ where $\Omega_s = 1500\ rpm\ and\ \Omega_r$ is varying from 1950 rpm to 1050 rpm and s is varying from -0.3 to 0.3) and the V20 is the open circuit rotor line voltage. The V_r values with the changing slip against time can be seen in Figure 2.3.

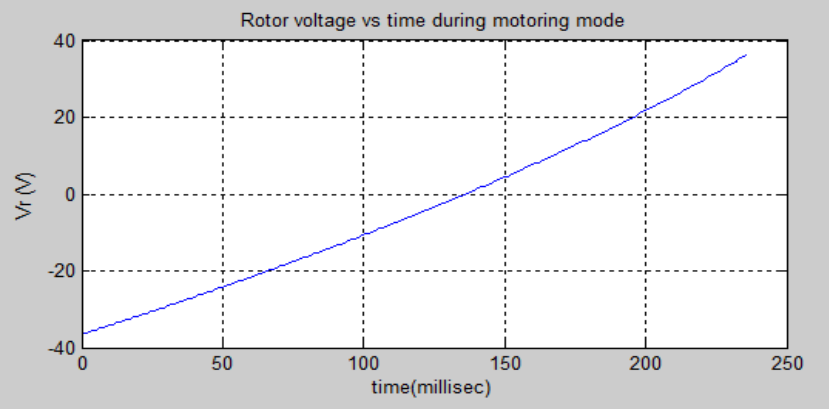

Figure 2.3.The DFIM rotor phase voltage vs time

In order to calculate the stator power (Ps) and hence the rotor Power (Pr); the rotor current referred to the stator side (I2ref) is calculated as following:

$$I_{2ref} = (N_r/N_s) * I_r \tag{2.12}$$

where the N_r/N_s is the rotor to stator turns ratio, which is obtained from V_r/V_s (both should be phase voltages and they have the value 121.24355 V and 400 V respectively). Having the I2ref and the stator voltage; the stator power and thus the rotor power can be calculated and plotted as seen in Figure 2.4 and Figure 2.5 (Figure 2.6 shows the stator power, rotor power and the mechanical power in the same plot) using the following equations:

$$P_s = 3*I_{2ref}*V_s \tag{2.13}$$

$$P_r = -s*P_s \tag{2.14}$$

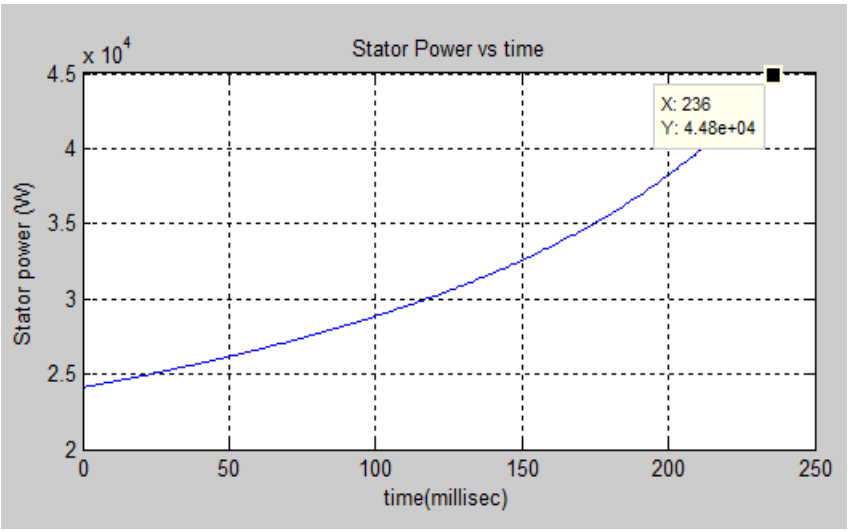

Figure 2.4.The DFIM stator power vs time

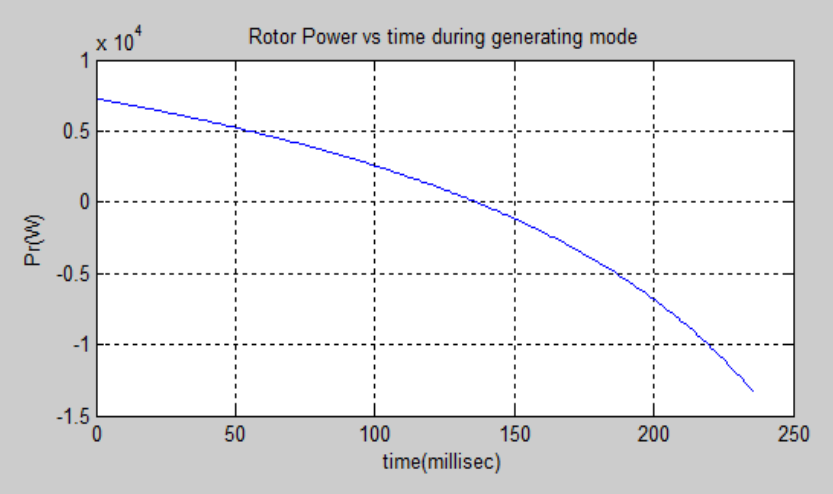

Figure 2.5.The DFIM rotor power vs time

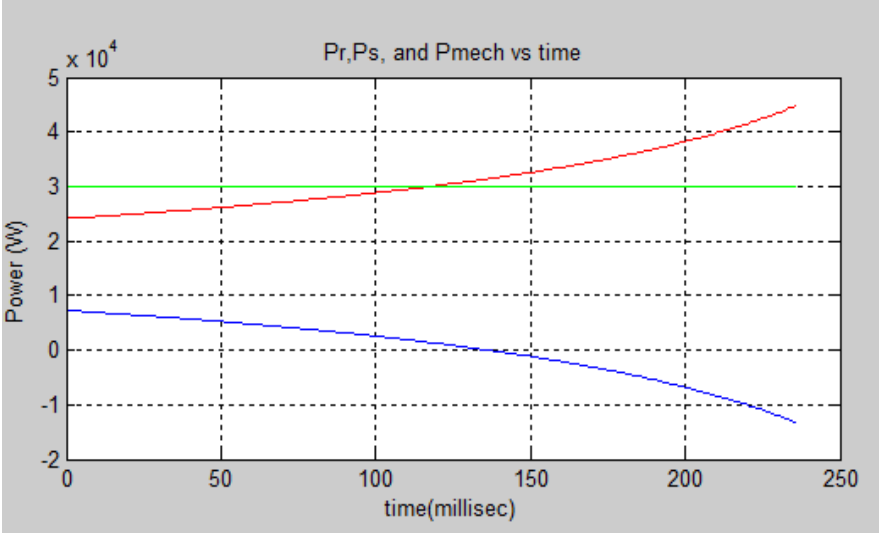

Figure 2.6.The DFIM stator power, rotor power and mechanical power vs time

In order to understand the behavior of the stator and rotor power during a constant mechanical power mode, Table 2.3 summarize the direction of the P_s and P_r (and the signs of the torque and the slip) in both the sub synchronous mode and the super synchronous mode during motoring (discharging).

Table 2.3.Ps, Pr, $T_{em}$and P_{mech}characteristic through the sub-synchronous and super synchronous modes

Mode (Motoring)	**Slip and speed**	**Stator power**	**Rotor power**	**Mechanical power**	**Torque**
Super synchronous	s<0, ωr>ωs	>0 (grid receives power via stator)	>0 (grid receives power via rotor)	Constant	(Tem>0)
Sub synchronous	s>0, ωr<ωs	>0 (excess power above the mechanical power rotates through the rotor back to the stator	<0 (machine delivers power via rotor and stator power is circulating via the rotor)	Constant	(Tem>0)

From Figure 2.6 it can be seen that during the sub synchronous mode, the stator power will keep on increasing and will be rotating through the rotor; so, by using the full speed range in order to deliver/store the constant mechanical power of 30 KW, **a 44.6 KW DFIM must be used instead (Ps=44.6kW; Pr = 0.3*44.6kW=13.4kW; Pm = 44.6kW-13.4kW=30kW)**.

In order to analyze the rotor converter (RSC+GSC) rating, the rotor power will be plotted using the absolute value of either the slip or the rotor voltage so that the maximum rotor power can be evaluated using a positive value and also the influence of the fast increase in the rotor current in the lowest speeds (especially approaching the edge of the sub synchronous mode) can be clearly examined. The difference between the rotor power in the sub and super synchronous regions can be seen in Figure 2.7 and was calculated using the following equations:

$$P_{converter} = 3* \text{abs}\,(V_r) * I_r \text{ or } P_{converter} = \text{abs}\,(s) * P_s \qquad (2.15)$$

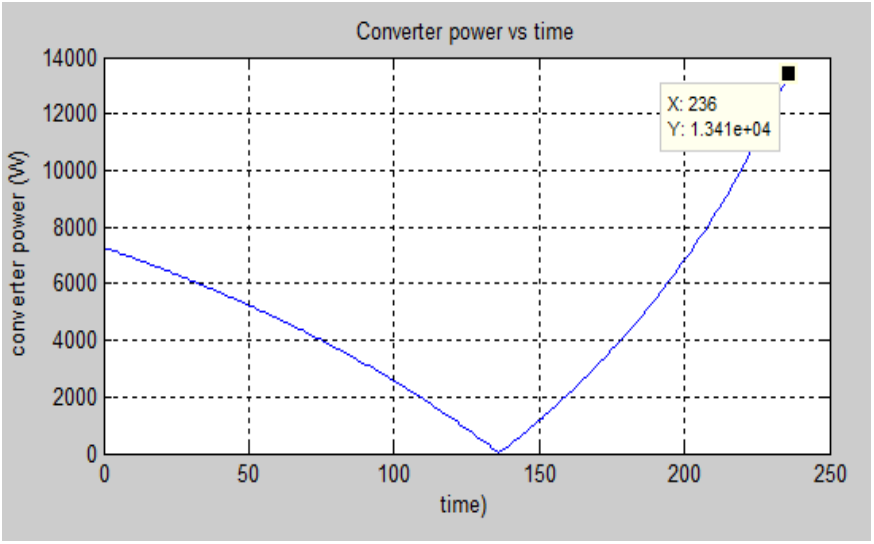

Figure 2.7.The rotor converter power vs time

It can be seen clearly in Figure 2.7 that by reaching the lower edge of the sub synchronous speed region, the rotor power which is used to decide the converter power rating is almost **double (13.41013 KW)** compared to the maximum rotor power in the super synchronous mode **(7.244 KW).**

Lastly, in order to calculate the amount of energy that can be stored in the FESS or to be delivered to the grid when required and the rating of the FESS system the following equations can be used:

$$E_{FESS} = 0.5*J*\Omega max^2 \quad (2.16)$$

$$E_{stored/extracted} = 0.5*J*(\Omega max^2 - \Omega min^2) \quad (2.17)$$

Substituting J=0.476Kg.m^2, Ω max $= 204.2\frac{rad}{s}$ and Ωmin = $109.95\frac{rad}{s}$, E_{FESS} is found to be 9924.038 joules and $E_{stored/extracted}$ =7046.855 Joules. From these 2 values, the percentage of energy extraction can be calculated as following:

$$\boldsymbol{E_{stored/extracted}\% = \frac{E_{stored/extracted}}{E_{FESS}} * 100 = \frac{7046.855}{9924.038} = 71\%} \ (2.18)$$

The Energy extracted from the FESS across the speed range changing from the super synchronous mode to the sub synchronous mode is presented in Figure 2.8 and the relation between the percentage of the rotor current and the percentage of energy extracted in seen in Figure 2.9

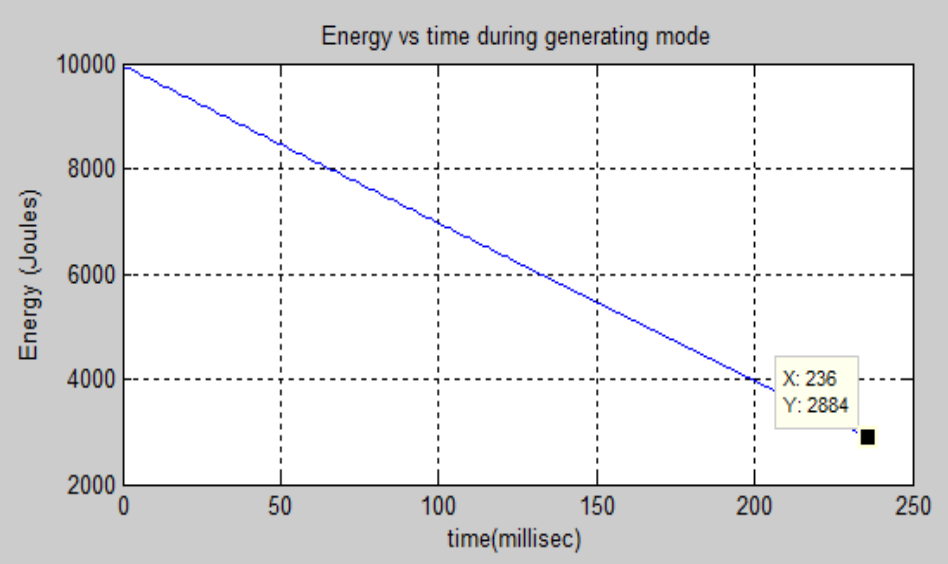

Figure 2.8.The energy extracted from the FESS vs time

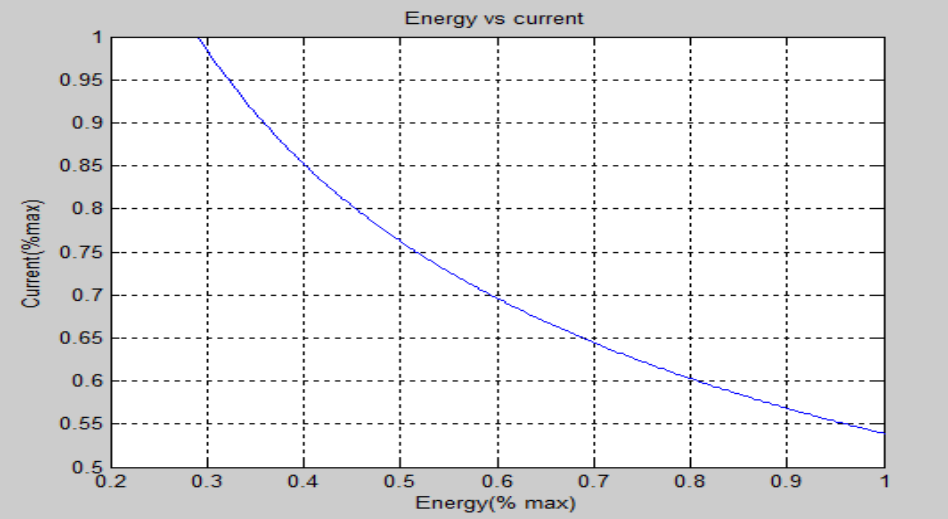

Figure 2.9.The percentage of the rotor current vs the percentage of energy extracted

From Figure 2.9, it can be concluded that if the reduction of the percentage of energy extraction by 9% (from 71 % to 60 %) is acceptable, the rotor current can by reduced by about 15% and thus the converter rating and the associated cost, the rotor power losses and the DFIM stator winding rating can be reduced as well and this what will be discussed in the next section.

2.4. The optimized speed range operation and its related impacts

A proposed way to optimize the system performance in terms of losses, rotor converter rating, DFIM rating and the system losses with maintaining a good percentage of the energy extraction; is using a narrower speed range and this new speed range proposed was from 30% above synchronous speed to 20% below the synchronous speed (from 130% of 1500 rpm to 80 % of 1500 rpm which means from 1950 rpm = 204.203 rad/s to 1200 rpm =125.6637 rad/s).

Since the speed reduces faster in the sub synchronous region where the torque and the rotor current increase significantly, this 10 % reduction in the speed range will have the following impacts:

1. Regarding the rotor current, the maximum rotor current that was achieved at minimum speed will be reduced from 123.2 A (at 0.7*ns) to 108 A (at 0.8*ns), which is a 12 % reduction in the maximum rotor current as can be seen in Figure 2.10.

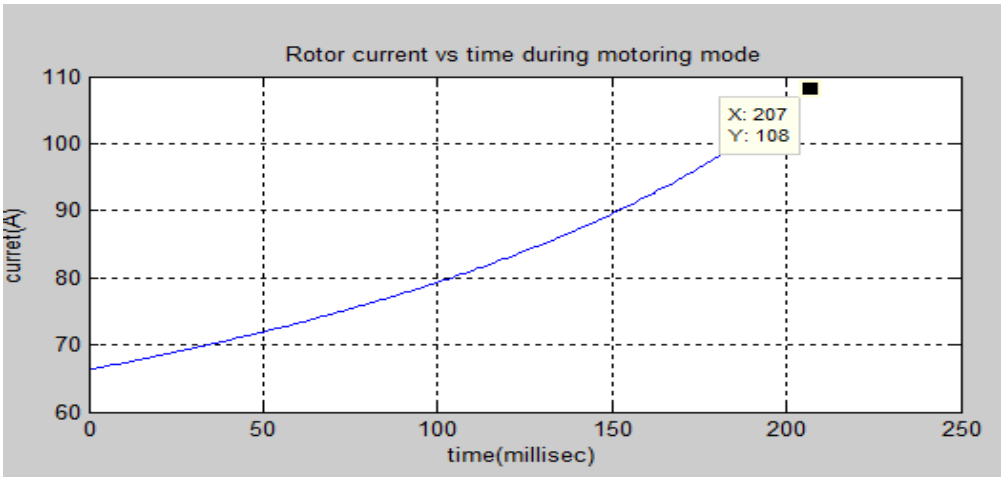

Figure 2.10.The rotor current for the new speed range vs time

2. The rotor power losses in case of a full speed range was about **1 KW**, but using the new speed range with a maximum rotor power of 108 A, the new rotor power losses will be = 3* $(Ir)^2$*Rr = 3* $(108)^2$*0.0223 = **780 W** which is almost (22% reduction in the rotor power losses).
3. The amount of reduction in energy extraction percentage with the new speed range is **8.8 %,** so the new energy extraction percentage is 62.1975 **%** instead of 71% which means there is still a good percentage of energy extracted/stored and this can be seen in Figure 2.11

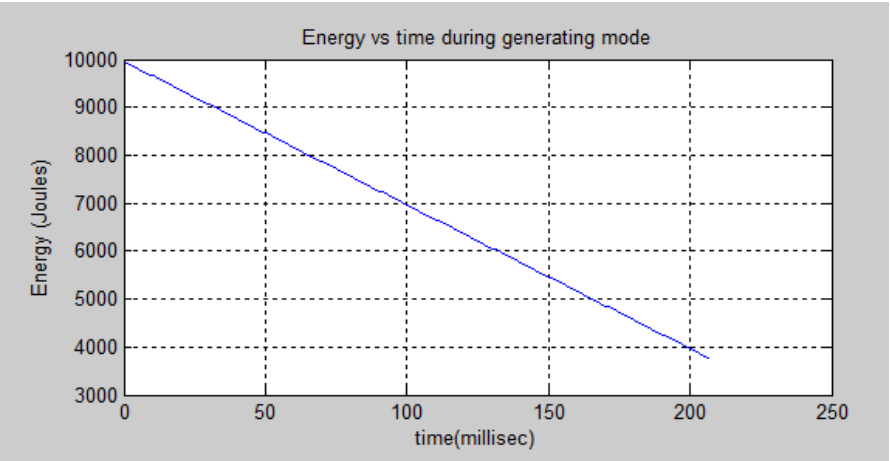

Figure 2.11.The energy extracted from the FESS over the new speed range vs time

4. The 12 % reduction in the rotor current discussed in point 1 will have a big impact on the DFIM rating reduction, as the maximum rotor current decreases towards the lowest speed edge, the I2ref will be reduced and since it is used to calculate the stator power and thus the stator power/DFIM rating this means that a smaller machine can be used as well. In can be seen in Figure 2.12 that the new DFIM rating is 39.2 KW instead of 44.8 KW (which is equivalent to 12.5 % reduction in the machine size). Thus, by using the new rating machine which will be cheaper, the related stator and rotor power losses will also be reduced for obtaining the same stored or extracted constant power by the FESS.

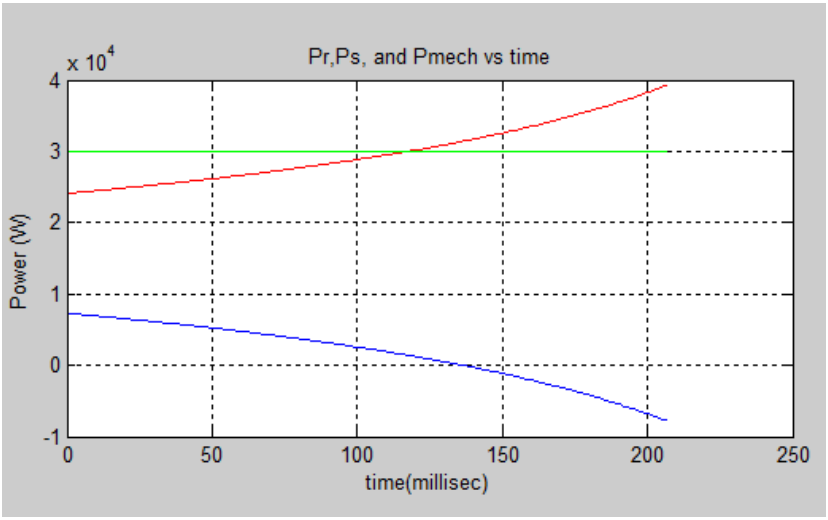

Figure 2.12.The stator power and the DFIM rating over then new speed range vs time

5. The same 12 % reduction in the rotor current will have a significant reduction in the rotor converter rating. In the full speed range, it was seen that a converter of a rating **13.410 KW** will be needed, but in the case of the new speed range, it can be seen from Figure 2.13 that the converter rating become only **7.883 KW**: which is about **41.2 % less than the first case** so **7.883 KW** will be the converter power rating needed.

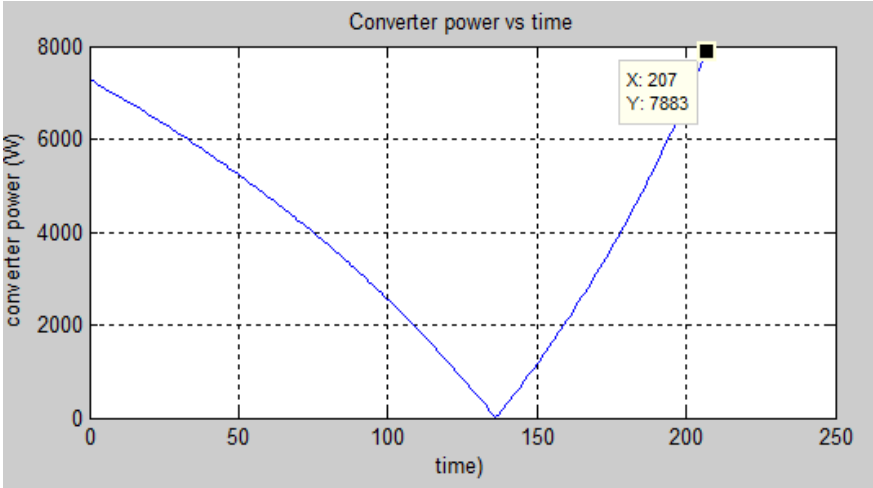

Figure 2.13.The rotor converter rating over then new speed range vs time

2.5. Discussion on the findings

1. The main reason behind choosing the speed range to be from **130 % of the ns to 80 %** of the ns is that at the maximum rotor speed the converter power rating can be seen to be **7.244 KW** so reducing the speed limit in terms of the lowers rotor speed beyond **80 % of the synchronous speed** will have no impact on reducing the converter rating nor the losses accompanied with it any further.
2. The savings in the converter size as well as the DFIM size can be considered as costs savings, or this saving can be used to purchase a bigger FESS capacity for storing or extracting more energy.
3. According to the equation P_{mech}= P_r+P_s and P_r= s*P_s, so for using a maximum slip of 0.3m this means that the maximum peak mechanical power that can be achieved for an instant of time at maximum speed can be Ps + 0.3*Ps (38.810 KW + 0.3* 38.810 KW = 50.45 KW), so this can be considered for some applications such as the super capacitors where a peak power need to be captured and used instantaneously.
4. It has been discussed earlier that the reduction of the speed range from (130 % to 70 % of synchronous speed) to (130%- 80%), the stator winding power rating can be dropped significantly. The new DFIM rating will be 39.2 KW instead of 44.8 KW (which is equivalent to 12.5 % reduction in the machine size). Thus, by using the new rating machine which will be cheaper, the related stator and rotor power losses will also be reduced for obtaining the same stored or extracted constant power by the FESS

Chapter 3

Analyzing the performance of the permanent magnet synchronous machine in the field weakening region (constant power region) for the flywheel energy storage application

3.1. Background

As discussed earlier, PMSM is widely used as a high efficiency and high performance variable frequency machine drive with high-power density and a compact design together with a high round trip efficiency [36]. There are several arrangements for placing the PMSM magnets, the interior or buried permanent magnet motors (IPMSM), the surface mounted magnet machines (SPMSM) [37]. The IPMSM has high speed ratio (3-6 :1), so higher speeds can be reached above the rated speed. The SPMSM has limited capabilities in terms of field weakening and thus a smaller speed range (2-4 :1) and this can be seen in Figure 3.1.

Machine	Torque Density Nm/m³	Speed ratio	noise	Cost
AC Surface Mount PM	28,000	2-4	✓	✓✓
AC IPM	25,000	3-6	✓	✓✓
Induction	15,000	3	✓	✓
Switched Reluctance	12,000	6	×	✓

Figure 3.1.Comparison of different types of machines that can be used for higher speed ranges by field weakening (reprinted from [38])

The vector control algorithm that can be used with the PMSM is a direct rotor flux vector control. The d axis is aligned/oriented on the rotor flux which is also the direction of the magnet (the flux angle is the same as the rotor position) as can be seen in Figure 3.2.

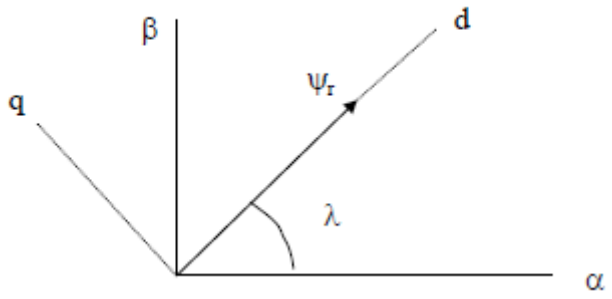

Figure 3.2.The direct rotor flux vector control of PMSM with d axis oriented on the rotor flux (reprinted from [38])

The machine 3 phase currents are transformed into the dq axis (which is rotating at the instantaneous speed ω_e using the rotor flux angle λ that is calculated from the following equation:

$$\lambda = \int(\omega_e)\, dt \tag{3.1}$$

The saliency ratio is also to be considered, this is the ratio between the direct and quadrature inductances (L_q and L_d). The machines which have equal d&q inductances (saliency ratio=1) are referred to as non-salient machines while those with non-equal dq axis inductances are called salient machines. Normally the PMSM are designed to operate at maximum torque and thus use maximum magnetizing flux from the permanent magnets until the machine reach its rated speed as this is required for a fast start/speed dynamic of the machine (this is the maximum torque and maximum rated back emf voltage). But if higher speeds are required above base speed, field weakening approach much be implemented to achieve these higher speeds as the maximum rated voltage of the converter is reached so it must be kept constant above 1500 rpm. The concept of the field weakening is to decrease the machine flux which will reduce the torque with the increase in speed in order to keep the back emf voltage constant at rated value and thus a constant rated power can be maintained without exceeding the current rating [39] and the operation of the PMSM before and after the base speed can be seen in Figure 3.3.

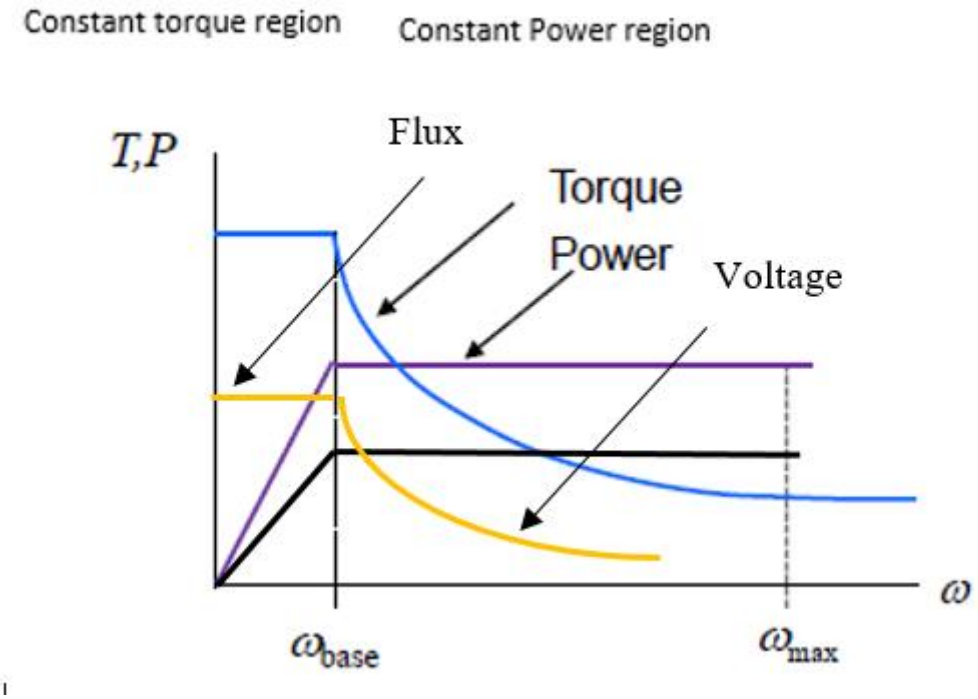

Figure 3.3. Torque, Flux, Back emf voltage and Power vs speed showing the field weakening implementation

Below the base speed, the back emf of the machine keeps on increasing linearly with the speed until it reaches the maximum rated value assuming a maximum/constant magnetic flux during this region (constant torque region) according to the following equation:

$$EMF = k\psi_m\Omega \tag{3.2}$$

Where ψm is the magnetic flux of the machine in weber and the Ω is the machine speed in rad/sec

But above the base speed, the emf is required to be kept constant as limited by the semiconductor voltage ratings, so the magnetic flux from equation 2.1 and thus the torque will be reduced to keep the back emf and the power constant within this region with the increasing speeds (constant power region).

3.1.1. Previous work done on field weakening application for various synchronous machines

Many papers studied the field weakening implementation for the PMSM mostly for the electric vehicles traction drives as they are required to operate with constant power with the ability to achieve higher speeds while keeping the efficiency high.

3.1.1.1. Field weakening application for IPMSM and synchronous reluctance machines

In [40], the field weakening performance was analysed for IPMSM and synchronous reluctance under rated and over load conditions, and it was proven that IPMSM with multiple-barrier interior permanent magnets offer higher constant power speed range (CPSR = $\frac{\Omega \max}{\Omega \text{ base}}$) of about 3 to 4 :1 above the base speed compared to the synchronous reluctance machine whose performance was similar to the induction machine operation with only a CPSR of 2:1 ratio.

3.1.1.2. Field weakening application of synchronous reluctance with axially laminated rotor

The design of a synchronous reluctance with axially laminated rotor was discussed in [41]. The focus of the design was to produce a high saliency ratio machine in order to achieve a high torque capacity, power factor and a reasonable CPSR of about 2.25:1 and also to reduce the machine losses by using a narrow circumferential rotor slots to split the axial eddy currents.

3.1.1.3. Field weakening application comparison for self-mounted permanent magnet machine (SMPMSM), inset surface magnet (I-PMSM), v-shaped internal magnets (VIPMSM) and rotor with radial internal magnet arrangement (RI-PMSM)

Different permanent magnet machines were studied in [42] in terms of their applicability in the field of electric vehicles and their CPSR that can be achieved. The machines used in the study were: SMPMSM, inset surface magnet (I-PMSM), v-shaped internal magnets (VIPMSM) and rotor with radial internal magnet arrangement (RI-PMSM) with both 4 and 8 poles and distributed and concentrated winding configurations. The maximum torque, power density, losses and field weakening capability of the different machine were compared and presented to be used for different electric vehicle power rating requirements.

3.1.1.4. Field weakening application of axially laminated interior permanent magnet machine

Another paper [43] focused on the design of an axially laminated interior permanent magnet machine aiming at achieving a very high CPSR of 7.5:1 for a 7.5 kW rated power. They studied the effect of different pole number, the magnet material selection, the lamination material as well as the demagnetization behaviour of the magnet in the field weakening region.

None of the previous papers discussed the implementation of the field weakening approach for PMSM to be used in the energy storage systems. So, in this chapter, the field weakening

approach will be studied for the flywheel application which is required to operate at high speeds within the constant power region. The vector control of the machine (field oriented configuration) will be modelled to verify the capability of PMSM to operate the FESS.

3.2. The design of PMSM vector controlled simulation model for flywheel energy storage applications

For a flywheel application, the PMSM operation is based on charging and discharging (storing energy or releasing energy) in a short period of time while processing a constant power irrespective of the state of charge, as demanded by the application. The field weakening approach for a FESS will be examined since we are interested in studying the CPSR that can be achieved by the PMSM above the base speed (constant power region) and a vector control for the system will be designed to analyse the overall performance of the model. For this study, a non-salient machine with equal d and q axes inductances and 4 poles (to be compared with DFIG and squirrel cage of same number of poles later) is used and its parameters are shown in Table 3.1. The simulation model is built using PSIM 9. The torque current is referred to as I_q while the magnetising current is referred to as I_d.

Table 3.1.The PMSM parameters used for the field weakening analysis of the FESS application

Rated Power	30 kW
Rated speed	1470 rpm
Rated torque	190 N.m
Rated flux	1.4 Wb
Number of poles	4
Rated back emf voltage	220 V
Stator resistance	0.027Ω
$L_q = L_d$	2 mH

The PSIM vector controlled simulation model is shown in Figure 3.4. The model uses a constant torque mechanical load as a rotating body and the inverter has a DC link of +/-300 V.

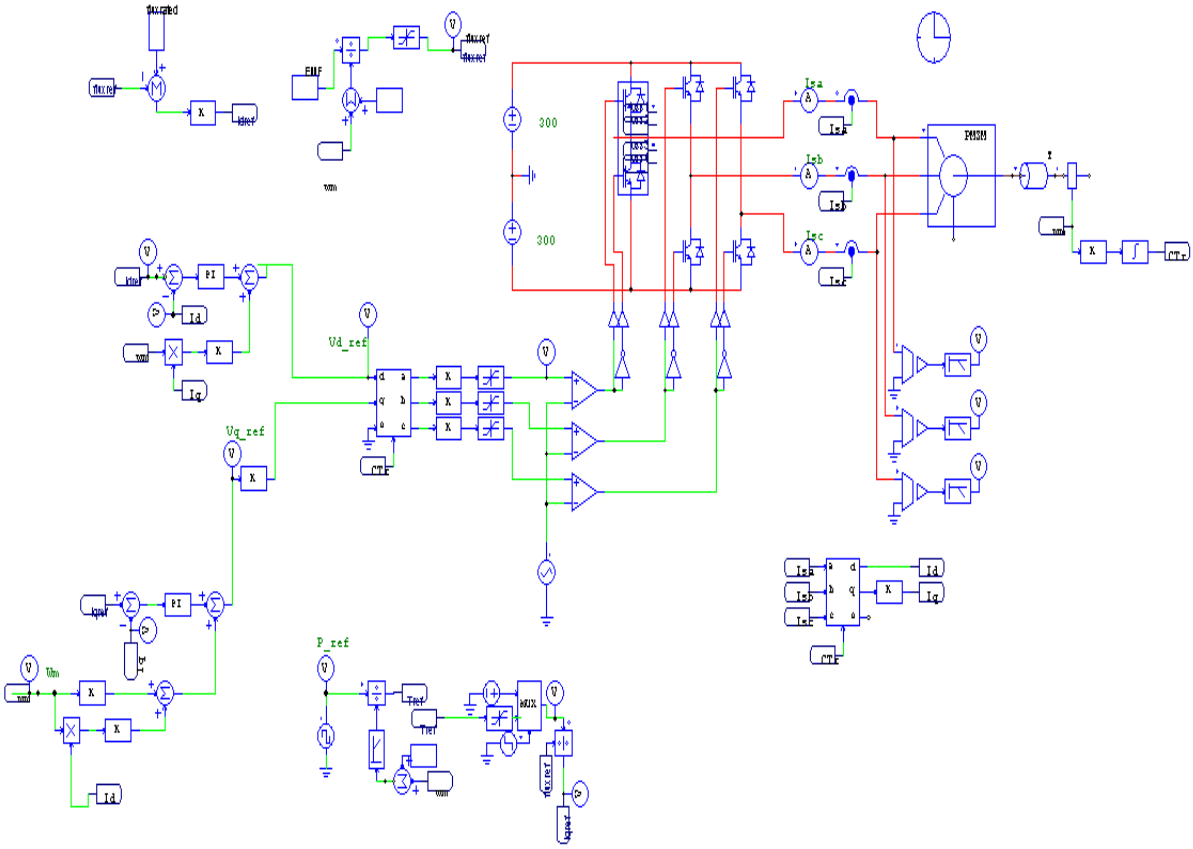

Figure 3.4.The PMSM vector control model used for FESS during the constant power region

Using abc/dq transformation block I_d and I_q currents are obtained from the stator current. For obtaining the reference currents I_{dref} and I_{qref} , first the flux (Ψd) above the base speed (1500 rpm) for obtaining a constant back emf voltage of 220 V is calculated from equation 3.2 to be 1.4 Wb and then it is used in the following equation:

$$\psi_{ref} = \psi_m + I_{dref} * L_d \tag{3.3}$$

For I_{qref} , it is calculated using the following equation:

$$T_{ref} = k * I_{qref} * \psi_{ref} \tag{3.4}$$

Having I_{qref} and I_{dref} , The PI controllers that were manually tuned were used to eliminate the error and V_{dref} and V_{qref} were calculated using the following equations:

$$V_{dref} = I_d * R + L_d * \frac{dI_d}{dt} - \Omega_r * L_q * I_q \tag{3.5}$$

$$V_{qref} = I_q * R + L_q * \frac{dI_q}{dt} + \Omega_r * L_d * I_d + \Omega_r * \psi_m \quad (3.6)$$

Please note that (- $\Omega_r * L_q * I_q$) and ($\Omega_r * L_d * I_d + \Omega_r * \psi_m$) are referred to as feed-forward (FF) terms of the rotational emf. The feedforward terms are used to ensure that the current transients for each channel are independent of the speed and the field weakening equation can be represented by the phasor diagram shown in Figure 3.5.

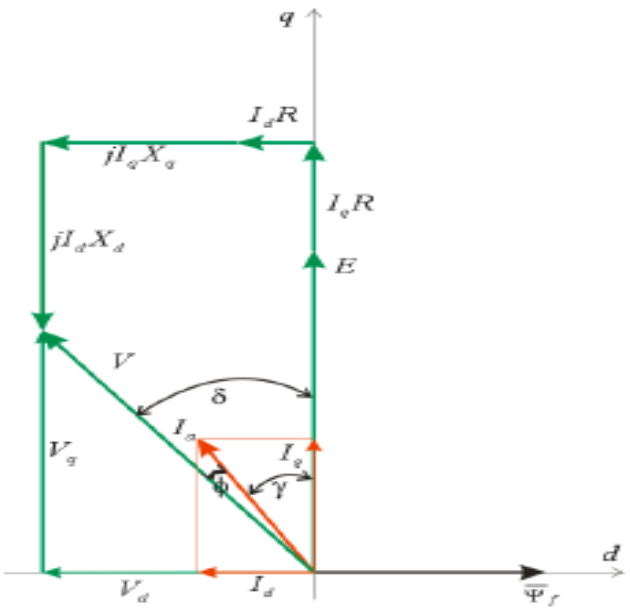

Figure 3.5.The field weakening equation phasor diagram representation (reprinted from [38])

For obtaining the required angle for the abc/dq transformation, first the mechanical speed is recorded from the rotating body in rad/sec and then the electrical speed is calculated as following:

$$\Omega_e = \frac{P}{2} * \Omega_m \quad (3.7)$$

Where p is the number of poles and both Ω_e and Ω_m are calculated in rad/sec. The angle theta needed for the transformation block is simply the integration of the rotational electrical angle.

For obtaining the I_{qref} which is the torque current, a constant power supply of 30 kW (positive for charging and negative for discharging) is divided by the mechanical speed of the machine in rad/s. The torque is then divided by a constant (was found to be 1.266) and the reference torque current I_{qref} can be calculated.

I_{dref} can be calculated first by obtaining the reference flux, this can be calculated by dividing the maximum rated back rms of 220 V by the speed in rad/s and limiting the resultant flux to 1.4 Wb (maximum flux at rated speed 1500 rpm) using a limiter. The flux reference is then subtracted from the rated flux 1.4 Wb and since we operate only above rated speed then the flux will always be lower than 1.4 Wb. The difference is then divided by the $-L_d$ to obtain the I_{dref}

3.3. The analysis of the PMSM vector control model in the constant power region

There are 2 aspects that need to be analysed in this section:

1. The CPSR that the PMSM can operate beyond the base speed during changing and discharging and if this range is reasonable in terms of energy storage capability.
2. Since the aim of the model is to verify the feasibility of the field weakening approach to be working with the complete vector controlled PMSM model for the FESS application, it is to be noticed that the machine is not optimized in terms of the converter currents and voltages and this can be optimized later.

To start with, a constant speed model as in Figure 3.6 was used to obtain the system parameters, to tune the PI controllers and to know the current value before/at the base speed (only I_q since I_d will be zero) and the resultant current can be calculated as following:

$$I_{rated} = \sqrt{{I_d}^2 + {I_q}^2} = \sqrt{0^2 + 122^2} \quad = 122 \text{ A} \tag{3.8}$$

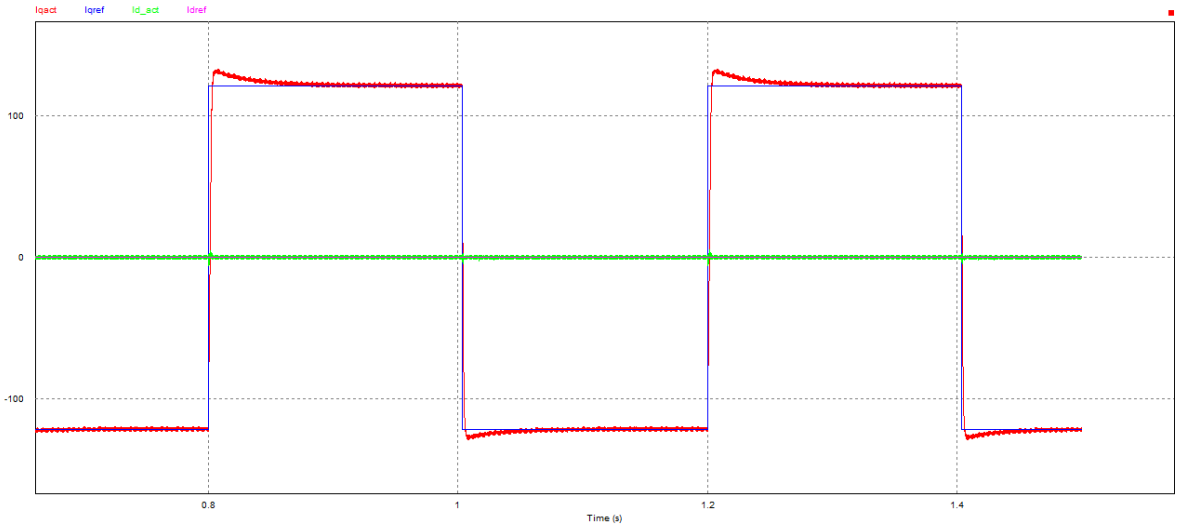

Figure 3.6. The I_d, I_q and their references values vs time at constant speed of 1200 rpm

Following that the model will be adjusted to operate only in the constant power region (FESS requirement) and the speed range that was achieved by the model can be seen in Figure 3.7 to be from 1500 rpm to 3850 rpm (CPSR: 1:2.56) which is a reasonable wide range for storing sufficient energy = $\frac{{\Omega_{max}}^2 - {\Omega_{min}}^2}{{\Omega_{max}}^2} = \frac{3850^2 - 1500^2}{3850^2}$ = 84.8% of the rated energy that can be stored

.

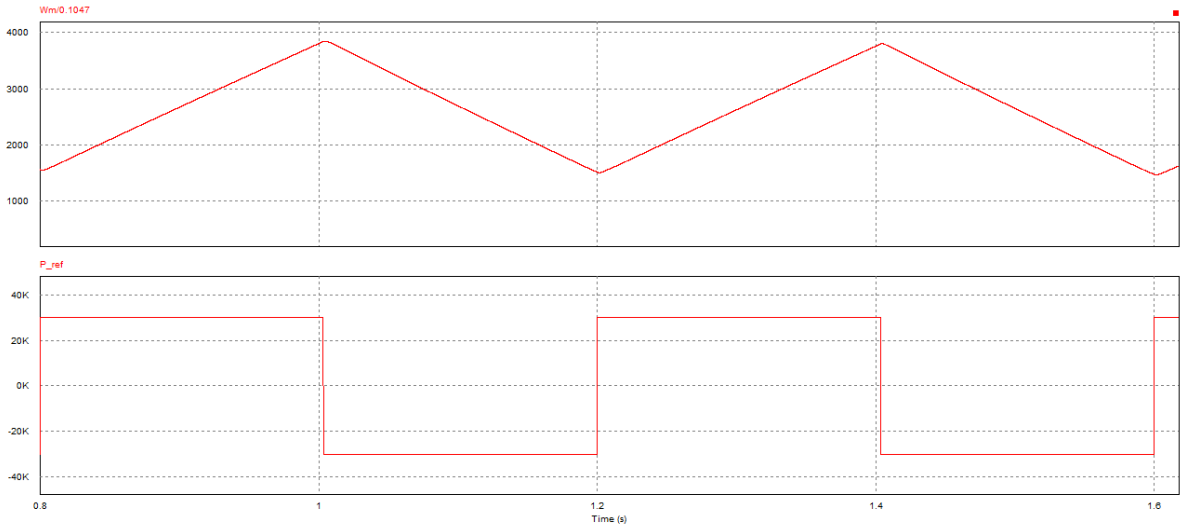

Figure 3.7.The constant power and speed change during charging and discharging vs time

The concept of the field weakening is to inject negative I_d in order to demagnetize the machine above the base speed using equation 3.2 (as maximum flux is achieved and cannot increase further). Doing this the flux and thus the torque will start decreasing as speed increases keeping the emf voltage and the power constant as seen in Figure 3.8. In this analysis, the maximum negative Id that was injected in order to maintain the constant converter voltage (using equation 2.2 and which can be seen in Figure 3.9 is relatively large. It should be noted that the scope of this chapter not to optimize the model rather than proving its functionality.

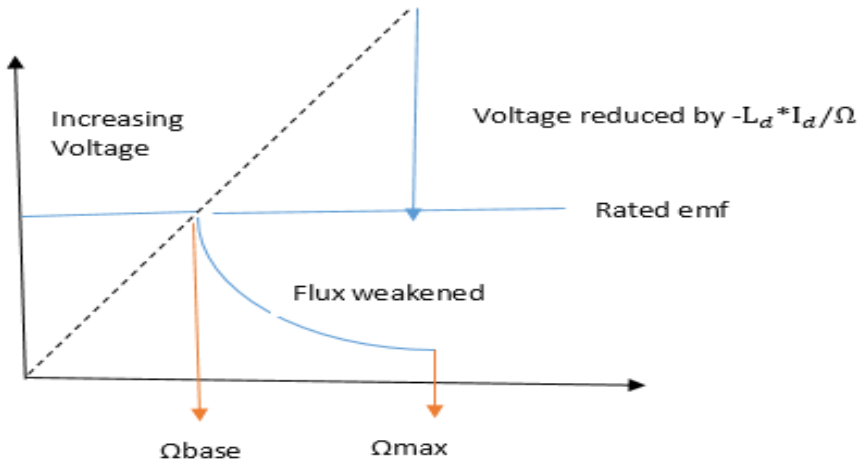

Figure 3.8.The flux weakening implementation using negative I_d to maintain constant power and back Emf

So, using equation 3.3 by injecting negative I_d, the resulting flux will be reduced and from equation 3.2), as speed increases, the flux will keep on decreasing by injecting more negative I_d and thus the emf can remain constant as well as the power. The I_d and I_q resultant curves during the charging/discharging of the FESS in the field weakening region can be seen in Figure 3.9. It can be seen that at the maximum speed, the negative I_d reaches a very high value (-175 A) compared to the rated I_q and a total current calculated from equation 3.8 is equal 213.3 A which is almost 1.75 times the current I_{rated} before the base speed. Two approaches will be discussed in the next section in order to reduce the amount of negative $I_d$that needs to be injected to obtained the constant emf and power and without affecting the energy percentage that can be stored and it can be seen that the back emf voltage is kept constant.

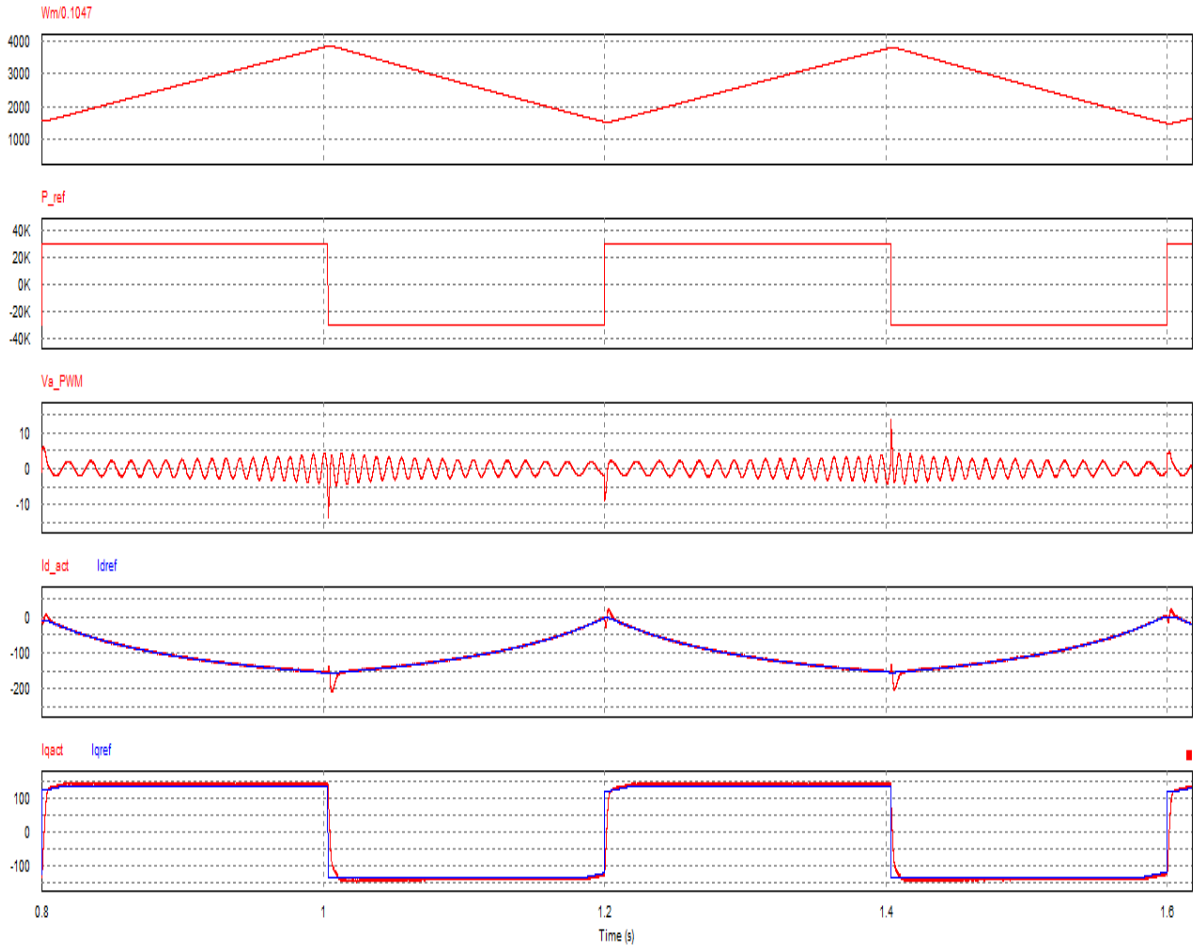

Figure 3.9.The speed, emf and I_d ,$I_q$resultant curves and their references vs time during the field weakening implementation for a PMSM based FESS

3.4. The proposed improvements to the field weakening for PMSM used in FESS to reduce the peak value of the required injected $I_d$current

The proposed approach of reducing the negative I_d current beyond the base speed in order to maintain the constant emf and power is to design a new machine with the same parameters but with less magnets which will result in a reduced flux produced by PM. By reducing the flux this means that emf according to equation 3.2 will be increasing with a lower gradient and thus reaching a smaller rated emf (at previous base speed) or reaching the rated value of emf at higher speed than the previous base speed. According to Figure 3.10, the emf reaches its rated value at a point above the base speed, thus a positive I_d needs to be injected to magnetize the machine further to the full rated flux to keep the emf constant, starting from 1500 rpm. The speed point at which the emf reaches its rated value above the base speed is to be decided so that an equal I_d peak can be injected (positively or negatively) between the base speed and the maximum speed and this will ensure a lower overall maximum current needed from the converter. In order to calculate this, PM fluxe needs to be set to the mean value between base speed and maximum speed, so at the base speed (1500 rpm) the overall flux is 1.4 Wb and at the maximum (3850 rpm) the flux should be 0.5456 Wb, so the average value is **0.9728 Wb**. At this point the speed needs to be calculated using equation 2.1 for maintaining a constant back emf of 220 V and thus the speed where Id=0 and magnetisation is provided only by the PMs is calculated to be **2159 rpm.** This was an interesting finding because knowing that the full speed range is between 1500 rpm to 3850 rpm and the point at which an equal I_d peak can be injected (positively or negatively) between them is at 2159 rpm means it is not mid-point of the speed range. For this an equation that can enable finding this point for any speed range is based on the following rule:

For a given speed range K, the speed point which achieves equal $\frac{L_d * I_d}{\Omega}$ is not the mid speed between the base and maximum speed but it is at a point which is equal to $\frac{1}{1+K}$ from the base speed and $\frac{K}{1+K}$ from the maximum speed. (This was proved using different speed ranges). So in our case the speed range was 1:2.56 (2350 rpm), so the point of equal $\frac{L_d * I_d}{\Omega}$ is $\frac{1}{1+2.56}$ = 0.2809 from the base speed which gives the point at 0.2809*2350 =660.115 rpm above the base speed which is 1500+660=2160 rpm and between that point and the maximum speed is $\frac{2.56}{1+2.56}$=0.72 from the whole range which

is equal 0.72*2350= 1692 rpm so adding this to the found point (1692+2160) gives the correct maximum speed 3852 rpm.

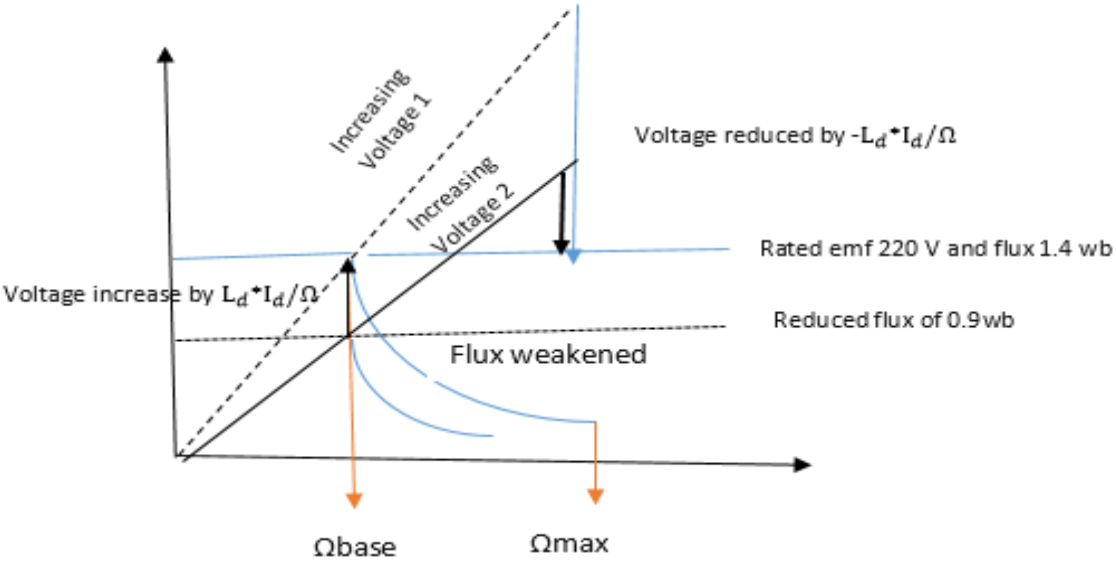

Figure 3.10.The emf increasing slopes and the required I_d currents for the new proposed flux and within the same speed range

The new approach was implemented on the PSIM model to verify the results and the I_d value that needs to be injected negatively and positively is shown in Figure 3.11 to be +/- 87.5 A and the I_q value at that point is 135 A. This means that the new total rated current reached by this approach from equation 3.8 is calculated to be: $\sqrt{87.5^2 + 135^2}$ = 160.83 A which is 1.3 times the rated current below the base speed (122 A) compared to the first model where the rated current reached was 1.75 times the rated current while keeping both the power and the emf constant. This approach will provide lower losses as well as lower converter current rating and stresses over the full speed range.

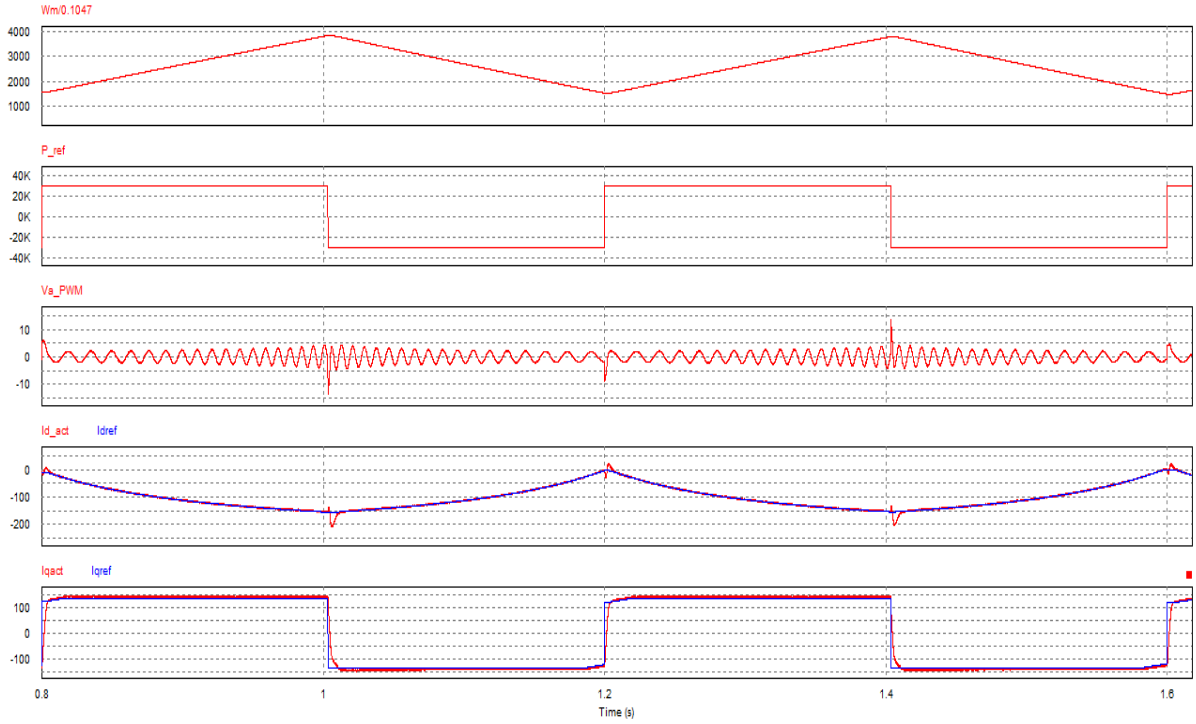

Figure 3.11.The speed, power, emf and I_d , $I_q$resultant curves with their references vs time during the field weakening implementation for a PMSM based FESS for the new model

The further improvement to reduce the I_d peak and thus the converter current rating is to use bigger d axis inductance L_d as the amount of flux ($\frac{\mathbf{L_d * I_d}}{\Omega}$) that needs to be injected positively or negatively is the same. This means that if the same approach of reduced PM flux of 0.9728 Wb is used since the same flux change is to be constant it means that using bigger L_d (1.4 times) will result in **$\mathbf{I_d}$ reduced by the same factor** so instead of using L_d =2mH, L_d=3 mH will be used and it can be seen from Figure 3.12 that I_d value is 62 A compared to the previous model where I_d was 87.5 A.

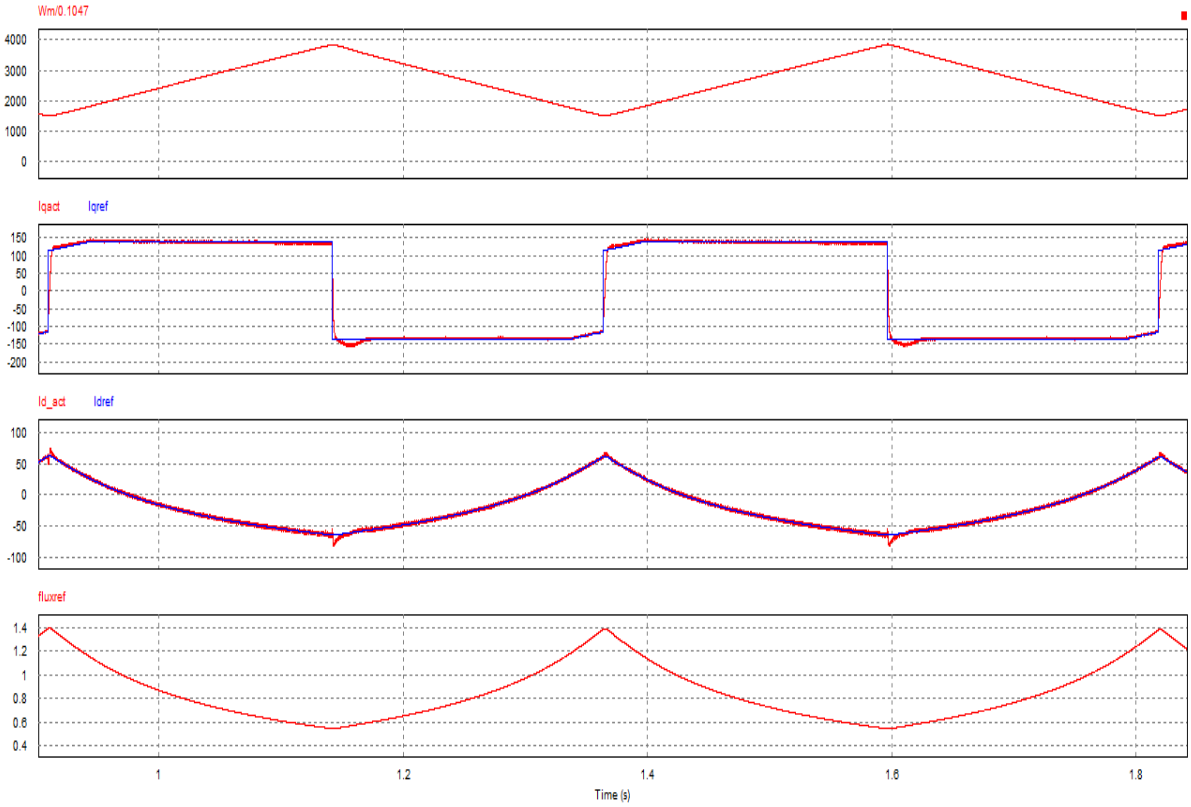

Figure 3.12.The speed, I_d , $I_q$resultant curves with their references and flux vs time during the field weakening implementation for a PMSM based FESS for the L_d=3 mH and PM flux of 0.9728 Wb

3.5. Conclusion:

1. From the analysis, it was proven that the field weakening approach is functional with the FESS using PMSM and the model was adjusted and tuned for the operation of the FESS only above the base speed (1500 rpm) until the maximum speed for the proper analysis.
2. It was found that a CPSR of 1:2.56 can be achieved for the used model which provide a good percentage of energy extraction of about 84.8% of the rated flywheel value.
3. It was proved that instead of injecting a very large negative I_d at maximum speed (above the base speed) in order to keep the emf and power constant within a large speed range, a machine with smaller magnets (smaller flux) can be used so that emf will reach the rated value at higher speed and in order to keep the emf constant above the base speed, positive I_d is injected below that speed until the rated emf is reached, then above this speed level, a negative I_d is used. This will help in reducing the converter current rating and stresses as the I_d maximum that was used in the first approach is now divided into half.
4. An equation was derived which can help finding the speed point at which the rated emf is reached and it was proved to be $\frac{1}{1+k}$ between the base speed and this point and $\frac{k}{1+k}$ between this point and the maximum speed (it is not a mid-point).
5. Knowing the point at which equal flux change is obtained from $\frac{L_d * I_d}{\Omega}$, Id can be reduced further by increasing the inductance current and thus reducing the current rating more.

Chapter 4

Induction machines (DFIM and squirrel cage) vector control models

This chapter will analyze the design of the vector control models for both induction machines Doubly fed induction machine (DFIM) and squirrel cage induction machine (SCIM). This is done to verify their operation and to be used for a performance comparison in the next chapters with permanent magnet synchronous machine (PMSM) in terms of speed range, converter losses, converter sizes, machine size and gear box ratio needed.

4.1. DFIM vector control model

As discussed in chapter 2, DFIM can be used to operate the FESS having the advantage that the rotor windings are separated (can be accessed using the slip rings) from the stator winding and the control of the Power, frequency and voltage can be done only on the rotor winding. This is advantageous compared to SCIM and PMSM as it is possible to connect external resistances to the rotor circuit which makes it possible to increase the torque. This is done by increasing series resistance and it is used to adjust the starting torque. Also, the additional resistance to the rotor circuit allow the speed control which is not possible for the PMSM and SCIM. Since the control is done on the rotor windings, for a DFIM with a +/-30% slip range, only 30 % of the stator power is processed and controlled through the converter so a smaller converter can be used while the rest of the power is directly fed to the utility grid via the stator. For this purpose, vector control (Stator flux oriented) can be used to control the voltage and the currents of the rotor side converter (RSC). In the stator flux oriented methodology, the d axis is fixed to the stator flux and Ψ_{sq} is equal to zero. The rotor 3 phase currents (I_{ra}, I_{rb}, I_{rc}) as well as the rotor voltages (V_{ra}, V_{rb}, V_{rc}) must be transformed into 2 axes αβ. These 2 moving axes are synchronized with the rotor winding rotational speed (slip frequency) and rotates at ω_r .These 2 moving axes αβ equations rewritten again to the synchronous dq frame which is synchronized with the stator flux vector

rotating with ω_e. To perform the vector control algorithm, the transformation equations requires, a stator flux angle λ to be calculated using the following equations:

$$\Psi_{s\alpha} = \int (V_{s\alpha} - R_s\, I_{s\alpha})\, dt \tag{4.1}$$

$$\Psi_{s\beta} = \int (V_{s\beta} - R_s\, I_{s\beta})\, dt \tag{4.2}$$

$$\lambda_{\Psi_s} = tan^{-1}\left(\frac{\Psi_{s\alpha}}{\Psi_{s\beta}}\right) \tag{4.3}$$

The stator flux angle λ_{Ψ_s} together with the rotor angle θ_r obtained by an encoder (speed sensor) are used by the transformation blocks to obtain the rotating torque and flux currents (I_{rd} and I_{rq} and they are orthogonal to each other) which can be represented by the phasor diagram seen in Figure 4.1

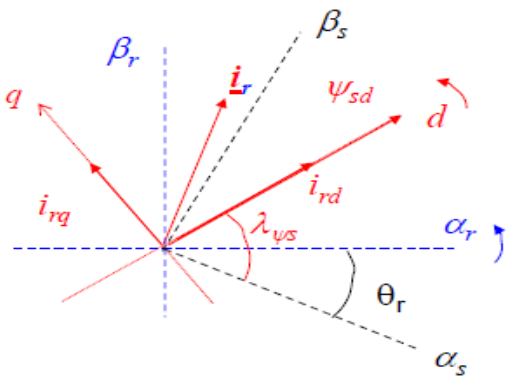

Figure 4.1.Phasor diagram representation of the rotor current in the stationary axes αβ and their I_{rd}, I_{rq} projections using $\lambda_{\Psi_s}$and θ_r (reprinted from [44])

The I_{rd} and I_{rq} are then compared to their reference currents and the corresponding errors are controlled using PI controllers (to keep them almost equal to the reference values). The output of the controllers provides V_{rd} and V_{rq} which will be retransformed into 3 phase voltages. A triangular signal which is referred to as a carrier signal and normally has a high frequency is used with the 3 phase stator AC voltages references output of the controllers.to obtain the PWM signals as seen in Figure 4.2 required for the IGBT operation. This PWM signals will define the IGBTs switching frequency.

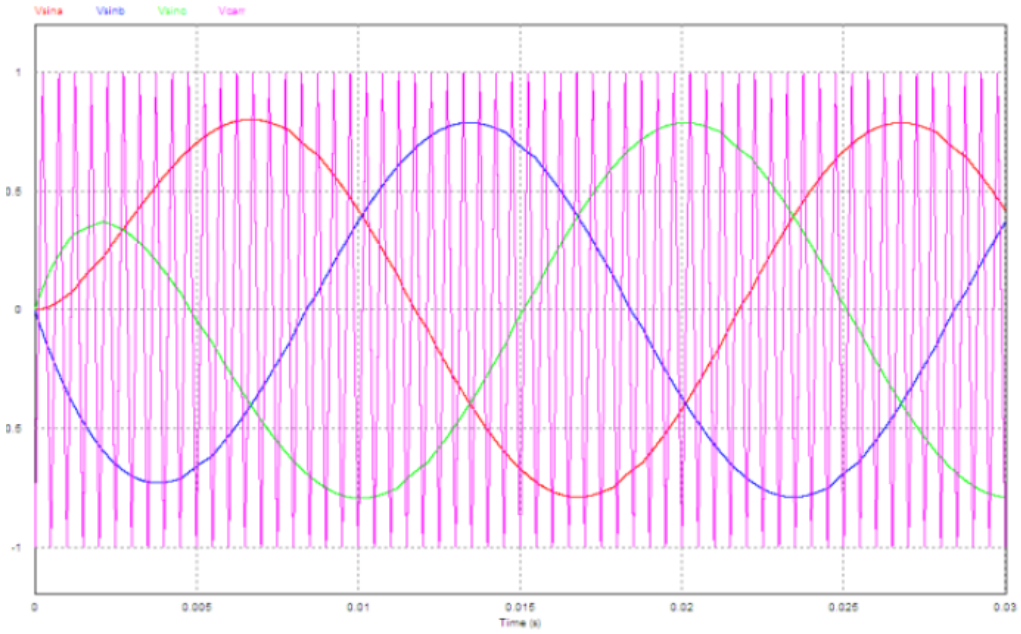

Figure 4.2.The AC voltage signals together with the high frequency triangular signal (carrier signal) to generate the PWM signal used by the IGBT (reprinted from *[45]*)

The DFIM model together with the vector control for the system was designed using PSIM.9 and a 30 kW DFIM was used which has the parameters shown in Table 4.1 used in [45].

The locked rotor voltage of the machine is 400 V (L-L) = 700 V (peak), so the maximum peak voltage achieved at the maximum slip of 0.3 is 210 V. So, in order to use a DC link of 300 V, the rotor voltage must be increased. This can be done by decreasing the stator to rotor turns ratio by a factor of 1.4285 (300/210) and the ratio reduced from the one used for 210 V which was 1.7 to 1.2. Having this, a converter of double this DC link voltage can be used and the converter voltage rating will be fully utilized. This will result in a reduction of the rotor current by the same factor as the power is constant which will result in reduced converter current rating as well and current was reduced (135.7 A to 95 A). For this analysis I_{rd} is referred to as the flux current while I_{rq} is the torque current.

Table 4.1. 30 kW DFIM machine parameters used for the vector controlled PSIM model

Rated power	P_{rated}	**30 kW**
Rated torque	T_{rated}	**241 N.m**
Stator resistance	R_s	**0.19 Ω**
Rotor resistance	R_r	**0.28 Ω**
Stator inductance	L_s	**2 mH**
Rotor inductance	L_r	**7.1 mH**
Magnetizing inductance	L_m	**117.1 mH**
Stator to rotor windings ratio	$(\frac{N_s}{N_s})$	**1.2**
Inertia	**J**	**0.485 Kg.m^2**
Number of poles	**P**	**4**

4.1.1. DFIM vector control model design results and discussion

The DFIM with the parameters shown in Table 4.1 was built using PSIM.9 and the vector control of the system was implemented to monitor the performance of the system as a whole. This was done to test the functionality of the DFIM as a FESS operating machine in terms of changing speed and torque during charging and discharging cycles within the speed range required. Some key points were considered during the design which include:

1. The DFIM speed range as discussed in chapter 2 should be normally within +/- 30% of the synchronous speed of the machine. Choosing a 4-pole machine means that the synchronous speed is 1500 rpm. The speed range applicable in this case is from 1050 rpm to 1950 rpm. As discussed and proved in chapter 2, the speed range can be modified in terms of using a smaller range. This is because at the lowest speed, the torque is the highest and thus the rotor current. And since the rotor current has a direct proportional relation with the torque, so at lowest speed it will be at the highest value as well. For this, by changing the lower speed from 30% below the synchronous speed to 20%, it means a lower torque and thus a smaller rotor current can be achieved and thus a lower converter rating and losses. The speed range discussed in chapter 2 of 1.62:1 (1200 rpm to 1950 rpm) was used in this design.

2. I_{rd} in this model is used as the flux current and $I_{rq}$is referred to as the torque current. I_{rd} is set to zero during the analysis which means that the magnetization is performed by the stator current I_{sq} and thus all the rotor current is in the form of torque current I_{rq}.

3. The complete vector control model representation of the DFIM is shown in Figure 4.3, where the speed reference in our case can be calculated by providing a constant power source (FESS operation requirement) and dividing that by the changing speed of the machine. This will obtain the changing torque and thus the rotor current reference which is proportional to the torque. The machine inertia as well as the torque injection algorithm used to adjust the speed until it reaches the minimum required speed within the speed range can be modified to obtained the required speed range mentioned in point 1.

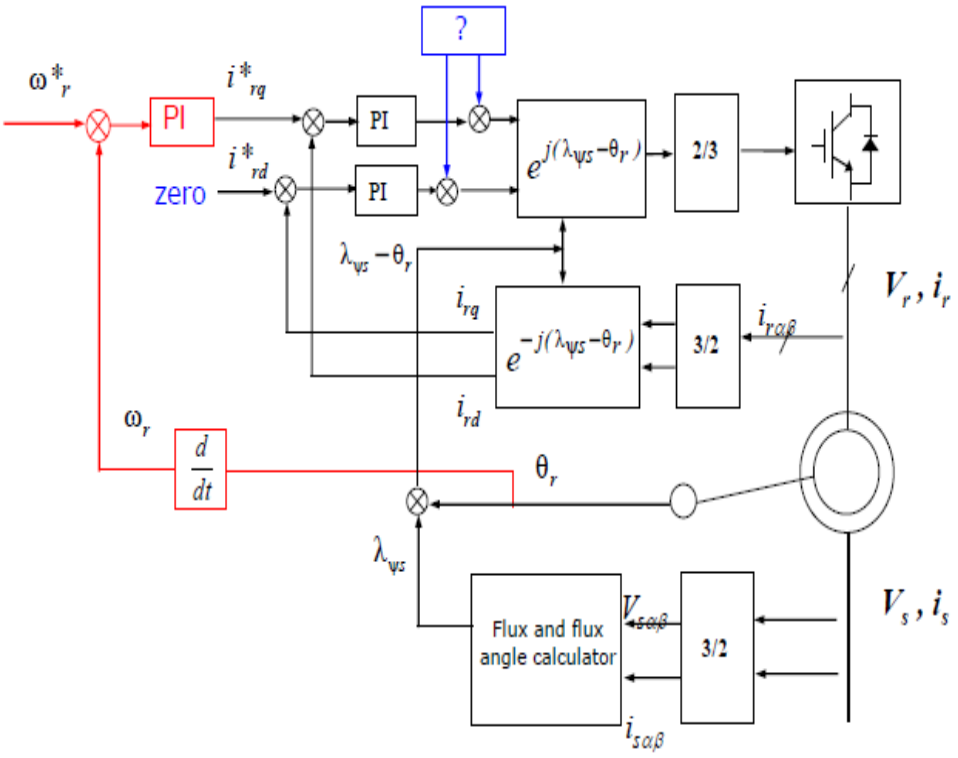

Figure 4.3.DFIM vector control model representation (reprinted from [44])

The operational designed PSIM vector controlled model of the chosen DFIM for the FESS application is represented in Figure 4.4

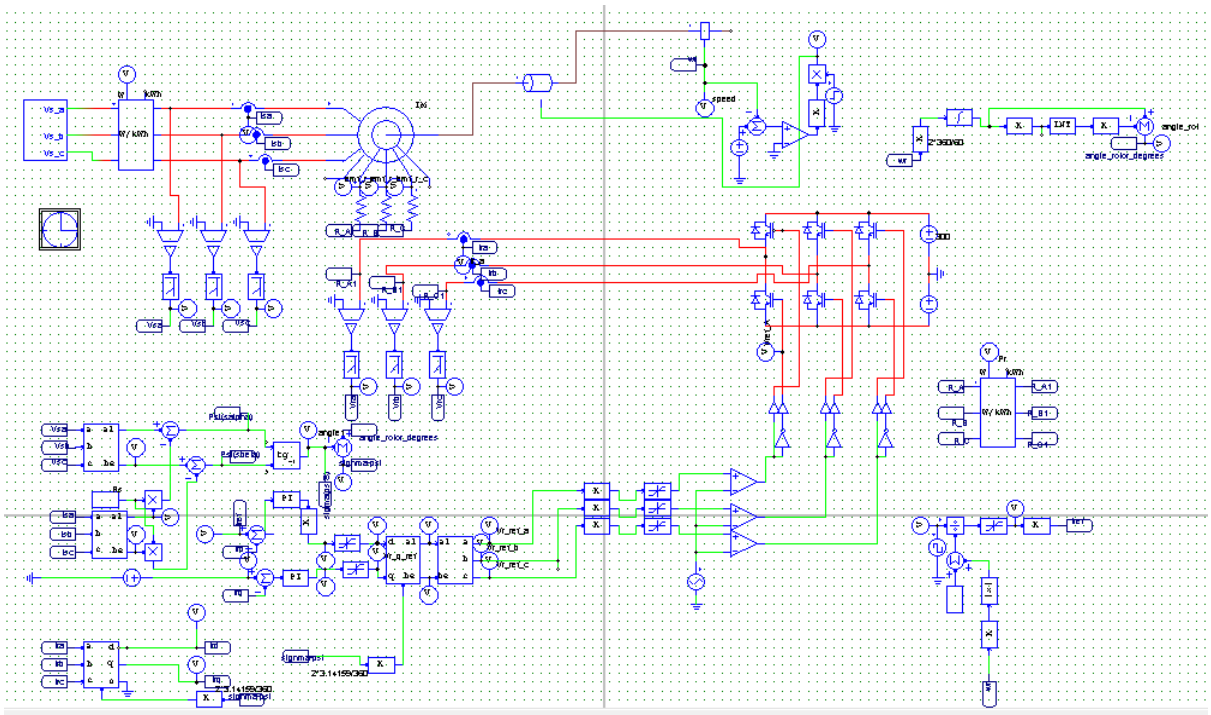

Figure 4.4.The PSIM vector control model for the DFIM used in FESS operation

The model is operational and some of the key results discussion are:

1. The speed range was adjusted as can be seen in Figure 4.5 to be 1.625:1 within the desired range of 1200 rpm to 1950 rpm.
2. The percentage of energy that can be stored/ released within this speed range can be calculated from equation 2.18 to be 62% of the rated energy that can be stored in the flywheel
3. The I_{rd} which is the torque current is proportional to the torque curve so during constant power charging as speed increases, torque decreases as well which means that the rotor current represented by I_{rd} decreases to keep the power constant at 30 kW. The opposite happens during discharging as can be seen Figure 4.5.
4. The PI controllers were tuned manually to make the reference currents/voltages aligned as much as possible with the dq axis currents and voltages with the least error.
5. No field weakening is necessary for the DFIM operation as in the case with the squirrel cage induction machine and the PMSM because the stator frequency is constant

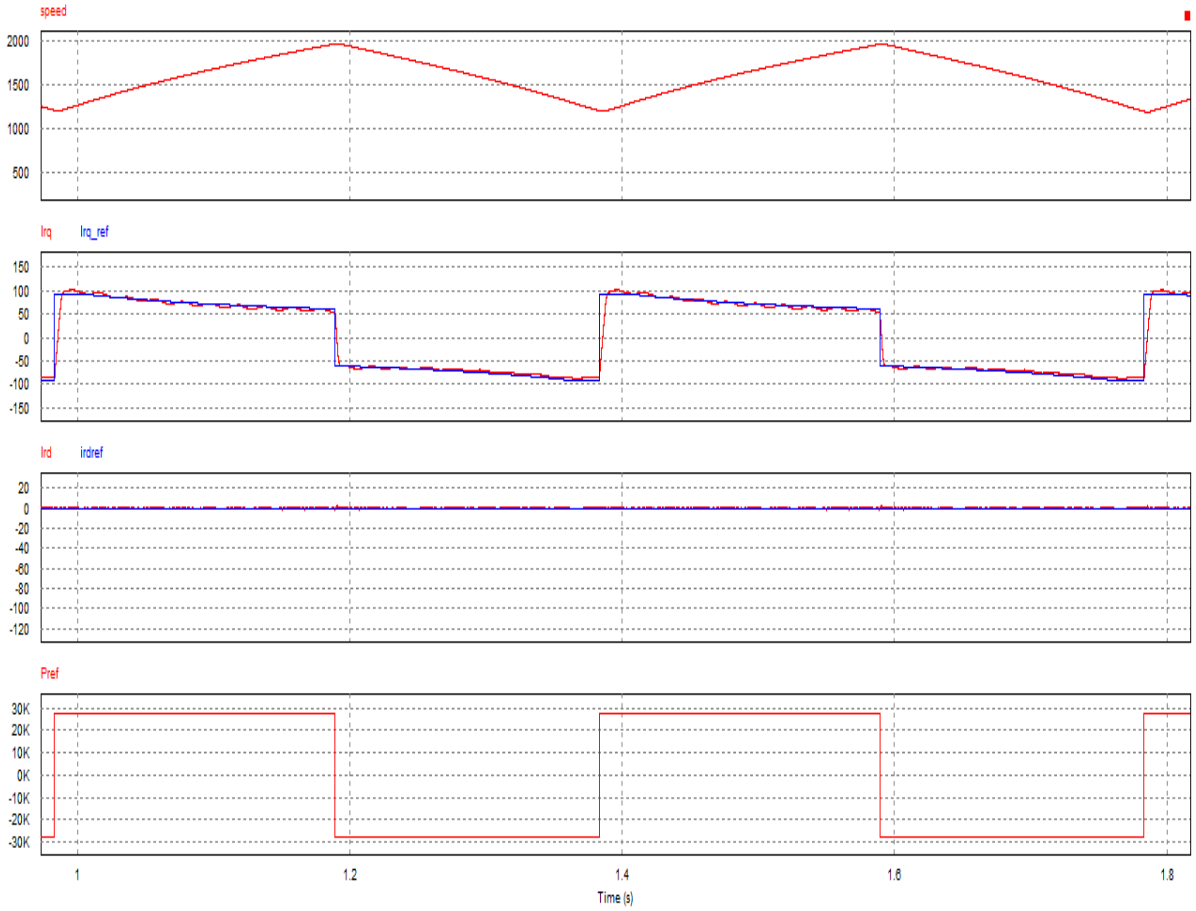

Figure 4.5.The speed curve, dq axis rotor currents $\mathbf{I_{rd}}$ and $\mathbf{I_{rq}}$ aligned with their reference signals, during a constant power cycling of 30 kW for a DFIM used in FESS vs time

4.2. Squirrel cage induction machine (SCIM) vector control model

As another form of induction machines, in this section the squirrel cage induction machine (SCIM) will also be analyzed and its vector control model will be built using PSIM.9 to demonstrate its functionality with the FESS as well as to use the model later for the comparison with the DFIM and PSIM in terms of performance, converter sizing, stresses and losses. The differences between the SCIM and DFIM is that for SCIM, the rotor structure is simple and rigid in the form of cylindrical laminated rotor core with conductive bars made of aluminum or cupper alloys and embedded in the lamination slots along the length of the rotor. Thus, those bars have no electrical connection with the motor terminals and the rotor current cannot be measured and it is only a function of the machine slip while in the case of the DFIM the rotor current can be controlled by accessing the rotor winding via the slip rings. Since the SCIM rotor currents and hence the speed cannot be controlled via the rotors as in the case of the DFIM, the SCIM uses a full-scale converter to process the bulk of energy between the grid and the machine as seen in Figure 4.6

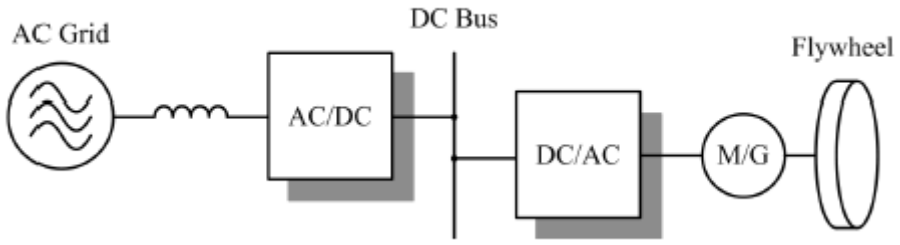

Figure 4.6.A SCIM requires a full-scale power converter to interact with the utility grid (reprinted from [46])

The vector control algorithm that is used in this section is the indirect rotor flux oriented vector control (IRFO). The concept of the IRFO is that the controller calculates the stator current reference values $I_{sd}*$ and $I_{sq}*$ to control the torque, flux and the transformation blocks angle. For PMSM, a direct rotor flux oriented vector control was used which measures the flux to define the rotor flux vector magnitude and the position (also referred to as flux feedback control and the required rotor flux information can be obtained either by measurement or by estimated calculation) [47].

The IRFO requires having the stator current dq components and machine parameters (resistance and inductance) and the slip to calculate the slip speed ω_{sl} and the rotor flux current I_{mrd} needed to calculate the transformation angle λ from 3 phases to dq axes by using the following equations (where I_{sd} is referred to as the flux current while I_{sq} is the torque current):

D axis equation:

$$\frac{L_r}{R_r}\frac{d\, I_{mrd}}{dt} + I_{mrd} = I_{sd} \tag{4.4}$$

$$\tau_r s\, I_{mrd} + I_{mrd} = I_{sd} \tag{4.5}$$

$$I_{mrd} = \frac{I_{sd}}{1+\tau_r s} \tag{4.6}$$

Q axis equation:

$$\omega_{sl} = \frac{R_r}{L_r\, I_{mrd}}\, I_{sq} = \frac{1}{\tau_r\, I_{mrd}}\, I_{sq} \tag{4.7}$$

Using equations (4.6) and (4.7), the transformation angle λ shown in Figure 4.7 which is needed to transform the 3 phase AC current to the 2 rotating axes dq and vice versa can be calculated as following:

$$\lambda = \int \omega_e\, dt = \int (\omega_r + \omega_{sl})\, dt = \int (\omega_r + \frac{1}{\tau_r\, I_{mrd}}\, I_{sq})\, dt \tag{4.8}$$

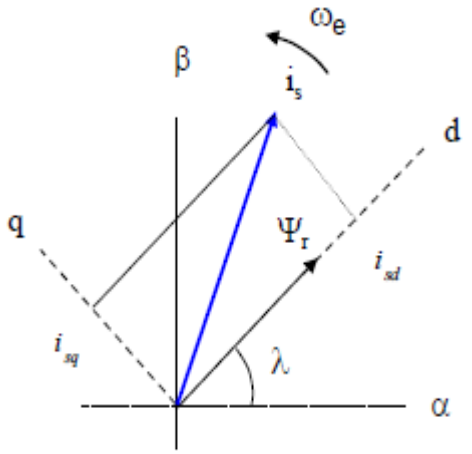

Figure 4.7.The phasor diagram representation of the stator currents I_{sq} and I_{sd} with respect to the αβ stationary axes together with the angle λ used for the transformation (reprinted from [48])

The SCIM model together with the vector control for the system which is represented in Figure 4.8 was designed using PSIM.9 and a 30 KW SCIM with the parameters shown in Table 4.2 which was used in [46] . A DC link of 600 V (+/- 300 V) was chosen and I_{sd} is referred to as the flux current while I_{sq} is the torque current.

Table 4.2. 30 kW SCIM parameters used for the vector control model of the SCIM based FESS

Rated Power	30 KW
Number of poles	4
Rated speed	1420 rpm
Stator resistance	0.087
Stator inductance	0.8 mH
Rotor resistance	0.087
Rotor inductance	0.8 mH
Magnetization inductance	37 mH

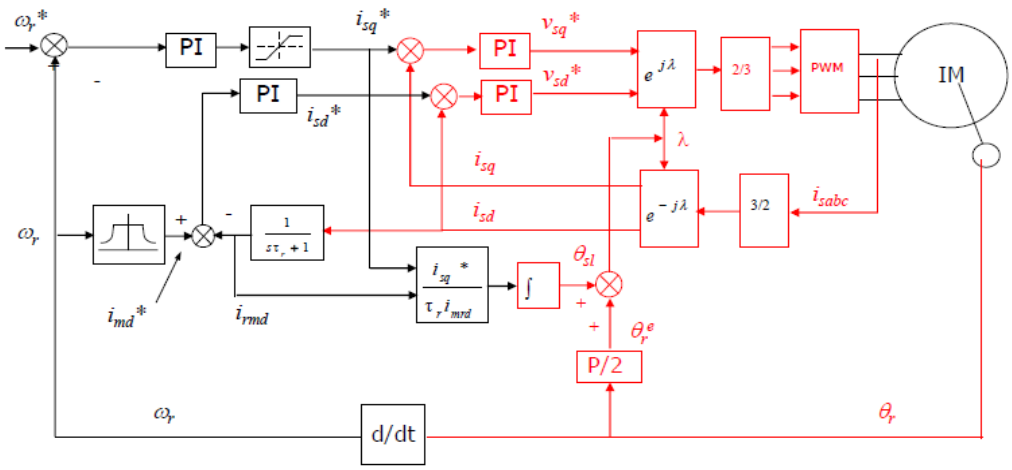

Figure 4.8.SCIM indirect rotor flux orientation vector control model representation (reprinted from [48])

It can be seen in Figure 4.8 that the SCIM requires the application of field weakening above the rated speed (base speed) of 1500 rpm as in the case of the PMSM. The field weakening will allow the machine to achieve the required constant power and constant emf voltage during charging or discharging when speeds higher than the rated speed need to be reached.

4.2.1. SCIM design results and discussion

The SCIM IRFO vector control model was designed in PSIM.9 as seen in Figure 4.9 to test the functionality of the SCIM as a FESS operating machine and its ability to change its speed and torque to keep the power constant during charging and discharging cycles within the speed range required.

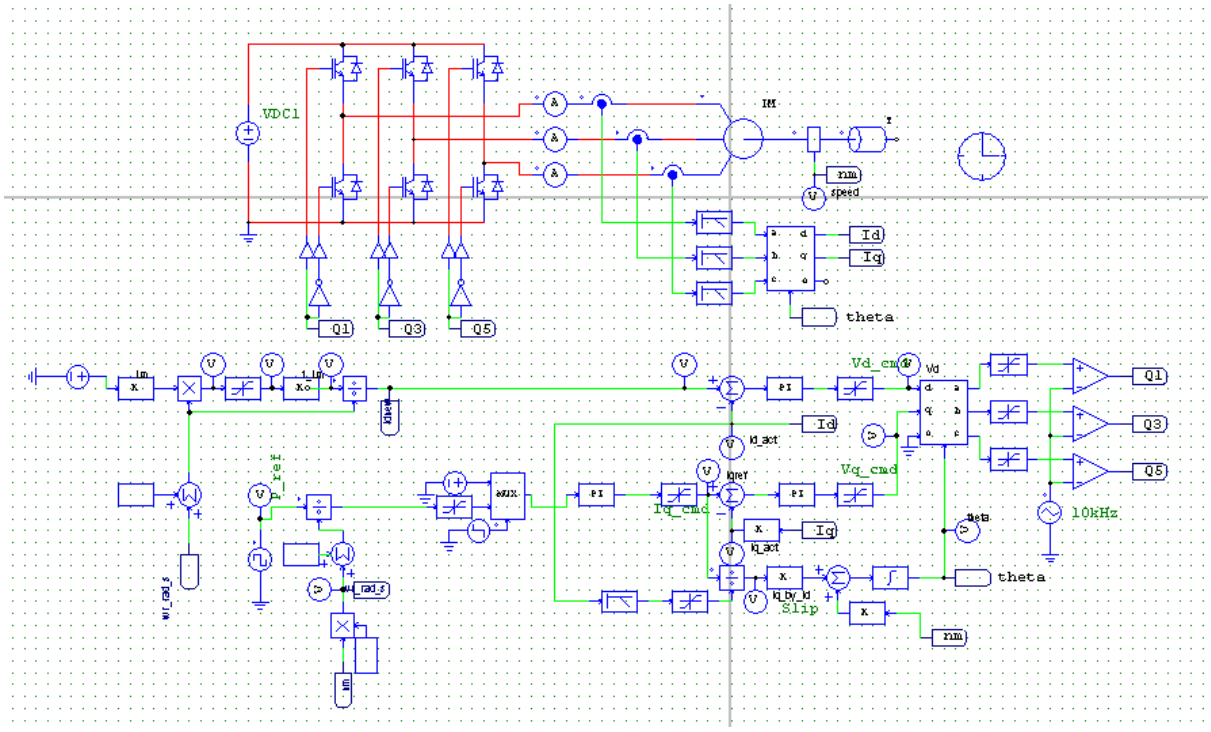

Figure 4.9.The PSIM vector control model for the DFIM used in FESS operation

Some key points were considered during the design which include:

1. The SCIM act in the same way as the PMSM so below the rated speed, it operates in constant torque/flux region and above the rated speed it operates in constant power mode. Since the FESS application is based on a constant power operation, only the region above the rated speed will be analyzed. Choosing a 4-pole machine means that the synchronous speed is around 1500 rpm and the speed range that can be reached above this synchronous speed is about 1:2 so from (1500 rpm until 3000 rpm). In case of the DFIM, as the speed decreases the torque and thus the rotor current kept on increasing to higher values, but for the SCIM, below the base/rated speed the machine operates at constant torque and constant flux. So, for SCIM, speeds above the rated speed will be achieved using a flux weakening approach., The torque will decrease with

the increasing speed keeping the back EMF and power constant. Therefore, a speed range from (1500 rpm to 3000 rpm) can be used to obtain a bigger range of 1:2 than that of the DFIM.

2. Since the speed range chosen was 1:2, this means that the percentage of energy that can be stored/released can be calculated from equation 2.18 is 75% of rated energy that can be stored in the flywheel
3. I_{sd} in this model is used as the flux current and I_{sq} is referred to as the torque current. Since the machine speed range is between (1500 rpm and 3000 rpm), this means that the machine needs to operate in the constant power/constant emf voltage region. Therefore, a flux weakening must be applied to maintain a constant back emf voltage of 220 V and constant power of 30 kW during charging and discharging. For this, a certain quantity need to be subtracted from the constant I_{sd} (25 A) to reduce the machine torque and flux above rated speed while the torque current remains constant.

The results of the SCIM vector controlled model in PSIM can be seen in Figure 4.10

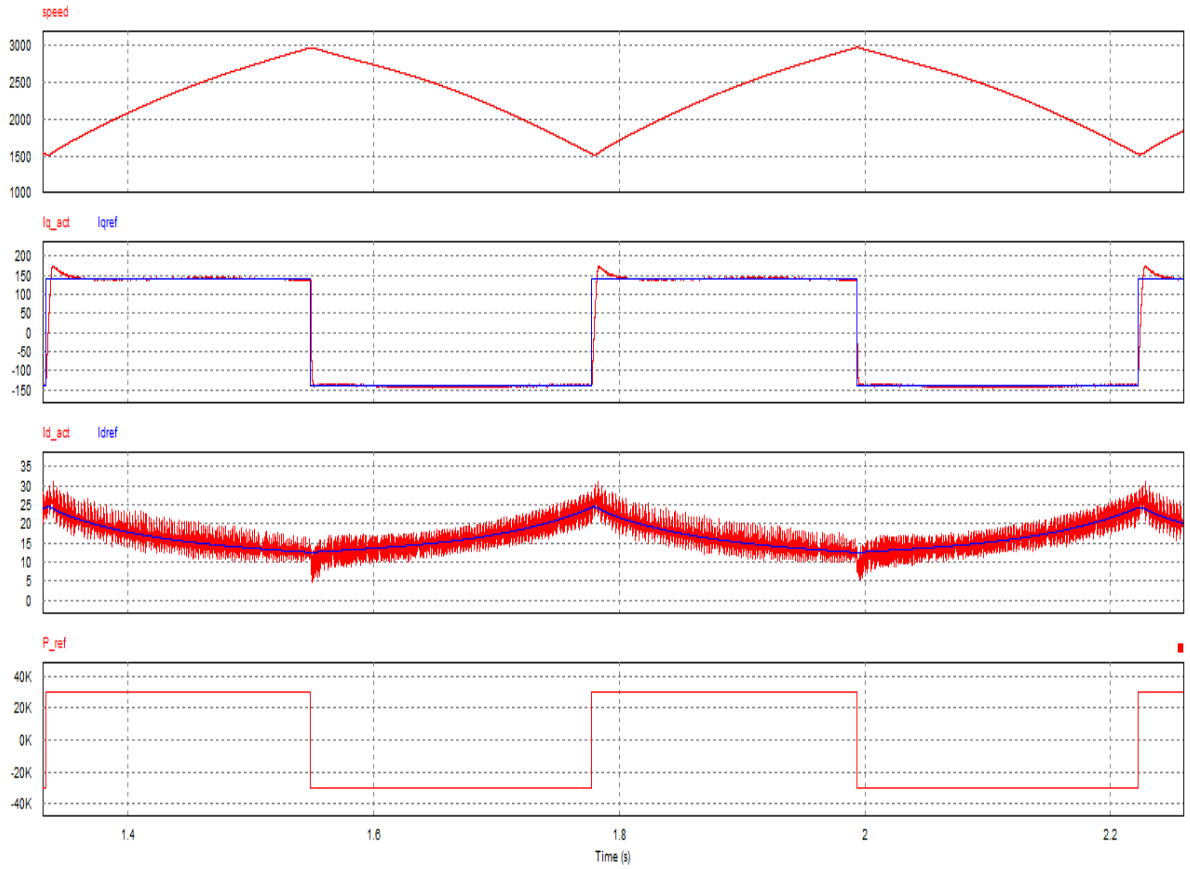

Figure 4.10.The speed range, constant power, stator currents I_{sd} and I_{sq} aligned with their reference signals during charging and discharging within the selected speed range for a SCIM used in FESS vs time

From Figure 4.10, it can be seen that the model is operational and some of the key results are:

1. The speed range that was applied in the design was 1:2 from (1500 rpm to 3000 rpm) which is similar to the speed range of the DFIM but using higher speed above the synchronous speed. A larger amount of energy extraction than the DFIM was achieved which is 75 % of the rated energy that can be stored by the FESS. A flux weakening approach is implemented above the rated speed, so that the flux below 1500 rpm will be kept constant at 1.4 Wb and above 1500 rpm, the flux as well as the torque will be reduced to achieve constant power of 30 kW and constant back emf voltage of 220 V until the maximum speed as seen in Figure 4.11. The maximum constant flux below the rated speed is calculated from equation 3.2 to be 1.4 wb. For speeds above 1500 rpm, the torque and the flux will reduce and the torque current I_{sq} will reduce in the same manner.

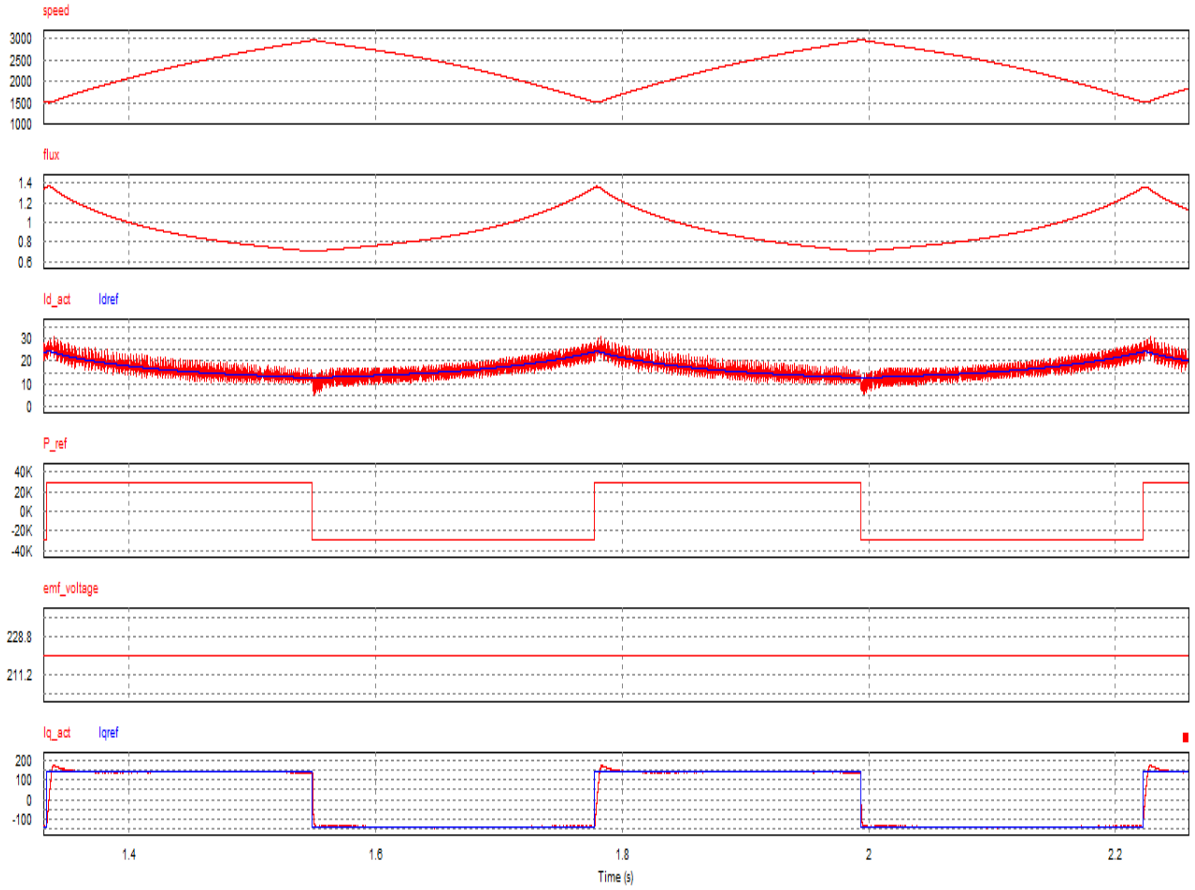

Figure 4.11.The flux reduction with increasing speed for keeping the power and the back emf constant above the rated speed (field weakening approach) vs time

2. The I_{sd} which is the flux current is constant below the rated machine speed 1500 rpm at 25 A, yet above the rated speed reduced I_{sd} will be imposed (flux weakening). The difference between the field weakening approach in SCIM and PMSM is that PMSM has a very wide speed range, so a very large negative I_{sd} must be imposed to maintain the constant power and voltage operation longer after the base speed unless the approach discussed in section 3.2 using smaller magnet and hence smaller flux can be implemented. While in case of SCIM since the speed range is limited, so the reduction of I_{sd} that needs to be injected will be smaller.
3. The PI controllers were tuned manually to make the reference current aligned as much as possible with the machine dq axes voltages and currents with least error.

Chapter 5

The comparison between DFIM, SCIM and PMSM in terms of converter sizes, converter and thermal stresses.

In this Chapter, the converter losses, charge discharge cycle efficiency and sizing of the electrical machine and the power converter will be analyzed for the three machines investigated in the previous chapters (PMSM, SCIM and DFIM) using the PSIM thermal module that estimates semiconductor losses (Note that only the machine side converter will be used in this analysis). This will give an overview of the performance of the three electrical drives in terms of the converter losses for the reduced current rating improvements proposed in the last chapters while ensuring a proper energy storage to be captured. The PSIM thermal modules offer the possibility to estimate semiconductor conduction and switching losses when using a particular type of semiconductor devices whose characteristics can be transferred from the datasheet in the PSIM thermal model with different ratings (voltage and current). Some are in the form of a discrete IGBT, so six modules will be needed for the analysis, others are dual modules which represent one converter leg, so three modules are needed and finally a six-pack module which includes the six IGBTs. The reason for using one form of those modules or another is that there are different fixed ratings so depending on the DC link voltage, peak current and the application needed, one can decide which module should be used. In this analysis two different modules (six-pack for DFIM and Dual module (x3) for the PMSM and SCIM) will be used. The six pack is from Powerex and its model is CM100TU-12H with rating (600V and 100A) and the dual modules are from the type Semikron and its model is SKM200GB125D with rating (1200 V and 150 A) and the selection of these ratings will be explained in next sections for each drive

Another important aspect that should be considered during the analysis is the temperature limits of the different semiconductor components within the layers of the power module to avoid exceeding the maximum device temperature by correctly choosing the heatsink. As can be seen in Figure 5.1, the main four temperatures that must be considered are: The ambient temperature, the heat sink temperature, the case temperature and the junction/device temperature (diode and Transistor temperature).

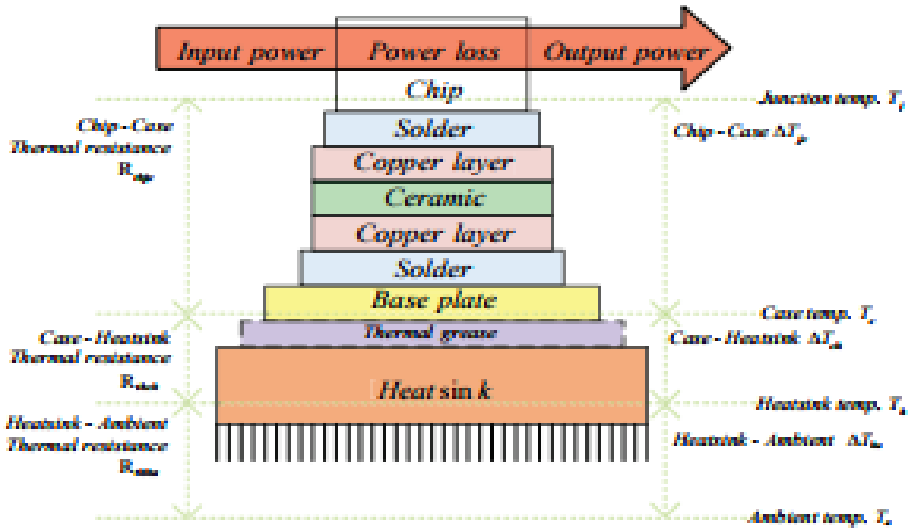

Figure 5.1.IGBT module thermal resistance model with the heat sink and case relevant components (reprinted from [49])

From the SKM200GB125D and CM100TU-12H datasheets, the case temperature limit T_c is set to 125^o C, but the junction temperature limit is 150^o C. The ambient operational temperature of 40^o C is used and the heat sink temperature should be in a range between the ambient and the case. These temperature limits will be considered during the analysis of the converter efficiency and losses to make sure that they are not exceeded which may cause the overheating and hence the malfunction of the converter later.

5.1. PMSM converter sizing, losses and cycle efficiency analysis using PSIM thermal module.

The PMSM vector controlled model was designed in chapter 3 and its functionality was proven in order to be used in this chapter to analyze the converter sizing and losses. The speed range that was achieved by the PMSM was 1: 2.67 (between 1500 and 4000 rpm) and the DC link of the VSI used in the simulation model was 600 V (peak of phase voltage) in order to match the required grid side inverter (not simulated) that would interface to an AC voltage of 415V L-L rms. Applying the field weakening approach for speeds above the base speed, torque current remains constant at 135A while the voltage and thus the power are kept constant for the FESS application purpose. A proposed model of using a smaller magnet and thus a smaller magnetic flux was proposed to have equal injections of flux current. I_d will be injected positively from the rated speed (1500 rpm) until the speed point where the rated back emf is reached at (2159 rpm) and I_d reaches zero. After that a negative I_d will be injected until the maximum speed so +/-87.5 A I_d was injected during the speed range. Using 1.4 times the inductance values used to obtain the +/-87.5 A, yields in the reduction of the Id that needs to be injected from (+/-87.5 A to +/-62 A). Thus, considering the I_d and I_q maximum current values achieved at lowest speed the overall current rating can be calculated to be $\sqrt{135^2 + 62^2}$=148 A (peak).

Using the information above, a converter with device voltage rating of twice the DC link voltage (1200 V) and a current rating 80 A can be used and the losses of this converter in terms of IGBT conduction and switching losses as well as the diode conduction and switching losses will be analyzed. This is done to estimate the losses of the converter and its impact on the overall efficiency of the system. For this analysis, the same 30 kW machine used in chapter 3 will be used together with the SKM200GB125D thermal module (dual) and the losses will be calculated for one inverter leg to represent and the results will then be multiplied by 3 to represent one converter.

5.1.1. The Converter losses for the PMSM based FESS

The SKM200GB125D dual module of 1200V/ 150A ratings will be used in order to analyze the transistor and diode conduction and switching losses during the charging and discharging cycle of the FESS.

Also, the thermal stresses on the converter in terms of heat sink temperature, and transistor and diode temperature will be analyzed to make sure they do not exceed the absolute temperature limits stated in the module datasheet.

The whole system with the dual thermal module attached to it is shown in Figure 5.2, it can be seen that there are 4 losses flags, and they are arranged as following:

1. Loss 1: Transistor conduction losses
2. Loss 2: Transistor switching losses
3. Loss 3: Diode conduction losses
4. Loss 4: Diode Switching losses

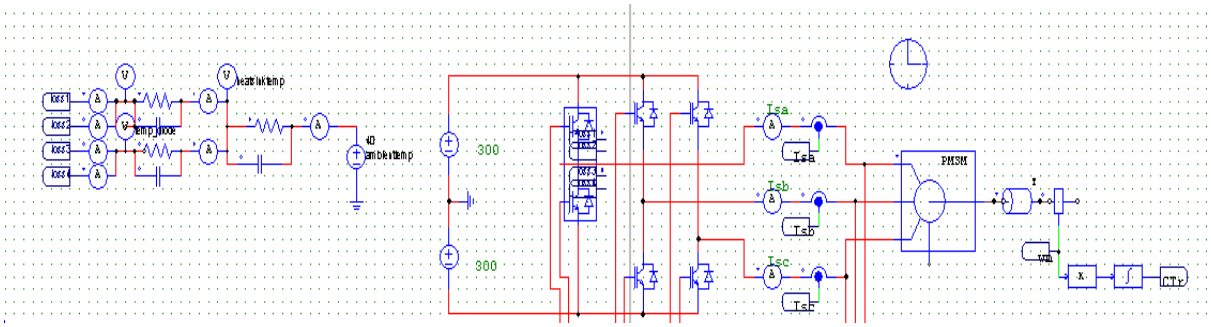

Figure 5.2.The PSIM vector controlled model with the SKM200GB125D (dual module) representing 1 leg of the converter

Also included in the model, the temperature measurement circuit which can be seen in Figure 5.3 and with an ambient temperature set to 40 ^{o} C, the heat sink temperature as well as the junction temperature (diode + transistor) will be measured.

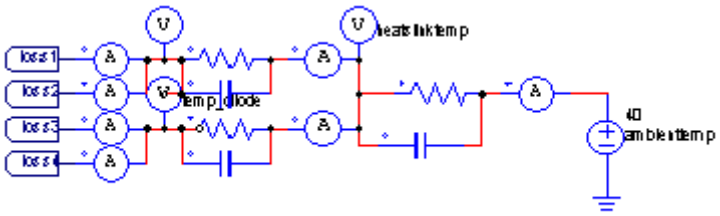

Figure 5.3.The simple circuit used to measure the heat sink temperature as well as the junction (diode and transistor) temperature by setting the ambient temperature to 40 ^{o} C

The conduction and switching losses for both the transistor as well as the diode can be seen in Figure 5.4

In order to calculate these losses, an average value for each of the 4 losses will be calculated for both the charging cycle as well as the discharging cycle and these values will be multiplied by 3 (since losses are measured for 1 leg only) and then the average values will be added together to get the total converter losses (machine side converter).

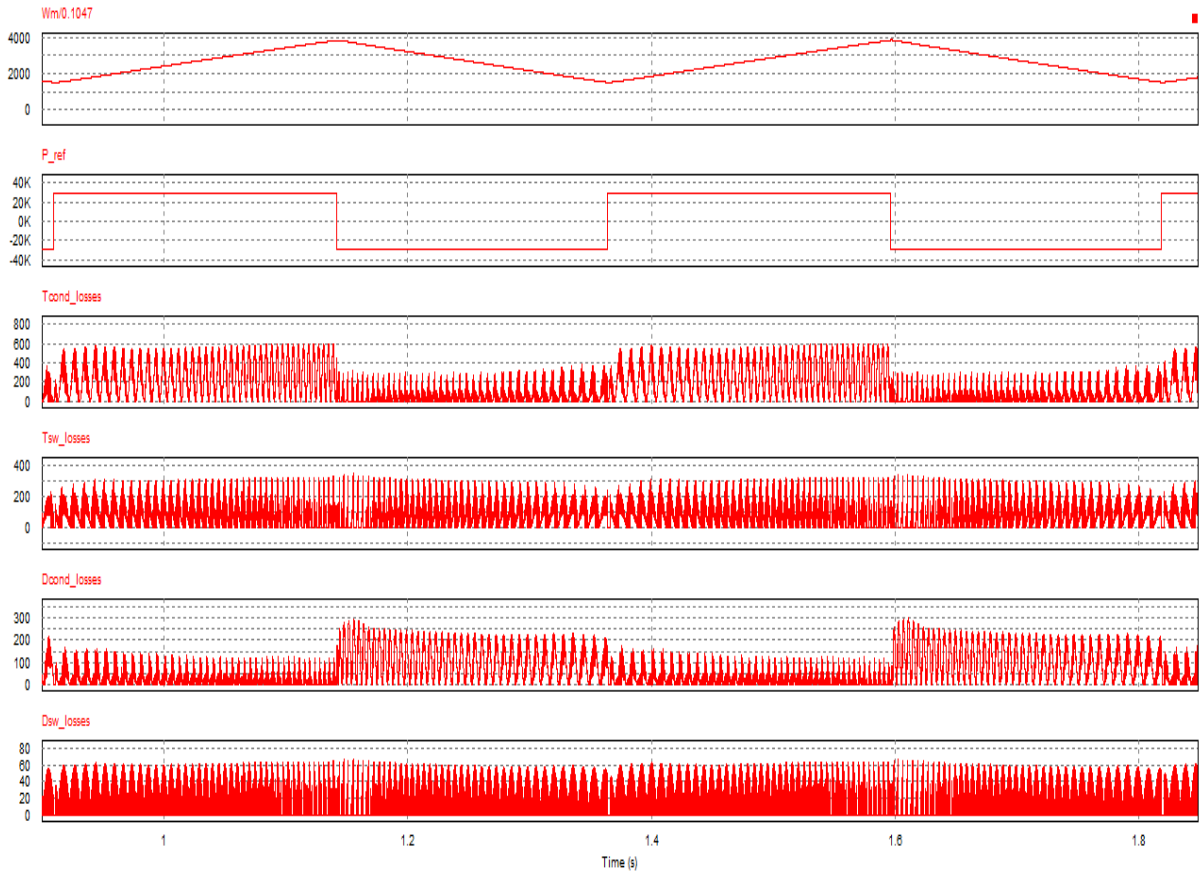

Figure 5.4.The speed, power and thermal module conduction and switching losses for both the IGBT and diode during charging and discharging cycles for 1 leg of SKM200GB125D (dual module).

5.1.1. Machine side converter losses and efficiency calculation method.

In order to calculate the losses, the measure conduction and switching losses for both the IGBT and diode are shown in Figure 5.4 are presented for both charging and discharging cycles. For charging cycle, the maximum and minimum losses were captured and their average were determined. Same procedure is followed for obtaining the averaged conduction and switching losses during discharging. Since one converter leg was used in

the analysis, the average values are summed up to represent the total losses of one converter leg and then multiplied by 3 to represent the total converter losses. These power losses will then be divided by the processed power (30 kW) to obtain the converter losses percentage. The converter efficiency is then to be calculated as 100- losses percentage. The round-trip efficiency of the converter will be calculated by subtracting the losses during charging and discharging from 100 %.

Those losses summery as well as the converter efficiency and its contribution to the overall losses of the system during the charging and discharging cycles are presented in Table 5.1

Table 5.1.Converter losses (transistor and diode conduction and switching losses) during both charging and discharging cycles for the PMSM system

Charging cycle	**Discharging cycle**
Transistor conduction losses averaged	**Transistor conduction losses averaged**
300 W	150 W
Transistor switching losses averaged	**Transistor switching losses averaged**
170 W	180 W
Diode conduction losses averaged	**Diode conduction losses averaged**
75 W	150W
Diode switching losses averaged	**Diode switching losses averaged**
32 W	35 W
Total losses (summed losses for 3 legs)	**Total losses (summed losses for 3 legs)**
577*3 = 1731 W	512*3 = 1536 W
Converter losses (percentage)	**Converter losses (percentage)**
$\frac{1731}{30000}$*100=5.77 %	$\frac{1536}{30000}$ = 5.21 %
Converter efficiency (percentage)	**Converter efficiency (percentage)**
100-5.77= 94.23 %	100-5.21= 94.79%
Round trip efficiency of the machine side converter	
100-5.77-5.21=89.02%	

It can be seen from the calculation that during charging, more conduction losses are occurring on the transistors where they are mainly used to process the power than during discharging. While during discharging, the diode conduction losses are higher as they direction is reversed.

5.1.2. The Converter thermal stresses for the PMSM based FESS

As mentioned before the temperatures experienced by the heat sink as well as the diode and transistor are important to make sure that the devices are not thermally stressed above the temperature limits set by the module data sheet. Those temperatures are shown in Figure 5.5, and it can be seen that for the heat sink temperature, it is within acceptable range (peak 51^{o} C) and the highest peak junction temperature (diode/ transistor) which is experienced by the IGBT during charging is about 110^{o} C and these temperatures summary is presented in Table 5.2. It can be seen also that higher temperature is experienced by the transistor during the charging than discharging and higher temperature is experienced by the diode during discharging. The junction temperature limit is set to 150 ^{o} C so this temperature was not exceeded neither during the charging nor thee discharging cycles.

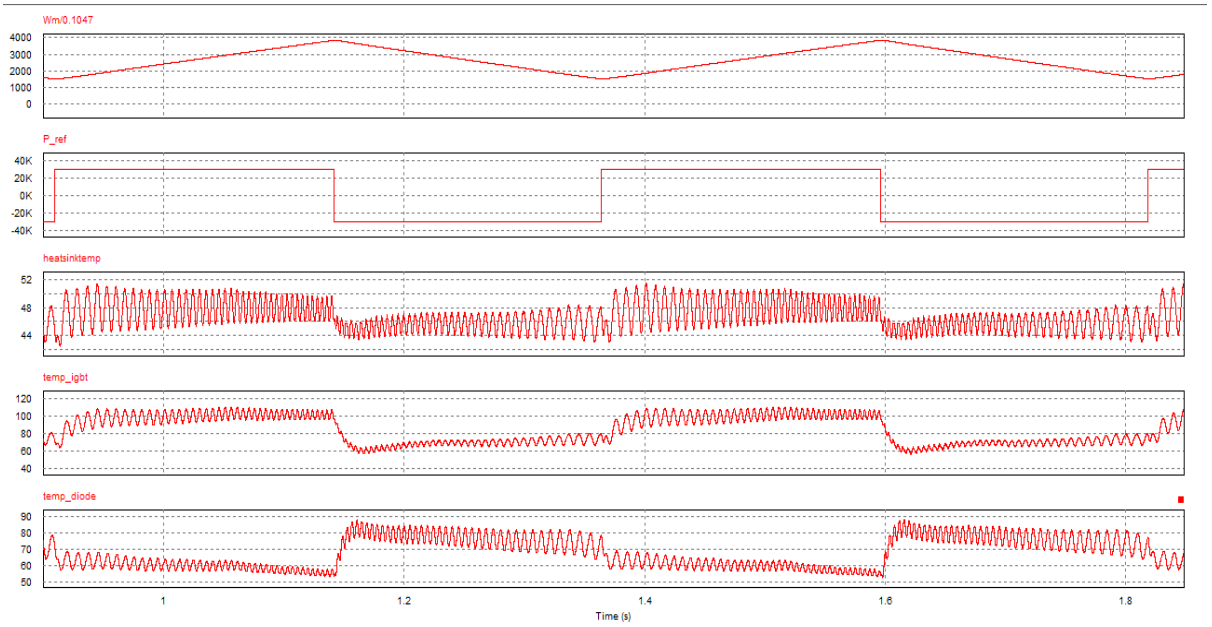

Figure 5.5.Speed, power, heat sink, IGBT and diode temperature plots for the PMSM converter thermal module

Table 5.2. The Heat sink, transistor, diode and junction peak temperature of the PMSM module during charging and discharging

Charging cycle	**Discharging cycle**
Heat sink Temperature (^{o} C)	**Heat sink Temperature (^{o} C)**
51	48
Transistor Temperature (^{o} C)	**Transistor Temperature (^{o} C)**
110	80
Diode Temperature (^{o} C)	**Diode Temperature (^{o} C)**
85	70

5.2. SCIM converter sizing, losses and efficiency analysis using PSIM thermal module.

The SCIM vector controlled model was designed in chapter 4 and its functionality was proven in order to be used in this chapter to analyze the converter sizing and losses. The speed range that was achieved by the SCIM was 1: 2 (between 1500 and 3000 rpm) and the DC link voltage of the VSI used for the analysis was 600 V (peak of phase voltage) in order to match the required grid inverter AC voltage of 415V L-L rms as a full-scale converter is used to process the power between the machine and the grid. The field weakening approach was applied for speeds above the base speed, and the torque current constant at 140 A with the decreasing flux. A certain amount of current will be reduced from the constant flux current of 25A and the minimum current at maximum speed is 14 A. This is done to keep the voltage and thus the power constant for the FESS application purpose. By considering the I_d and I_q maximum current values achieved at the lowest speed, the overall current rating can be calculated to be $\sqrt{140^2 + 25^2}$ =142.3A (peak). Using the information above, a converter of 1200 V voltage rating (twice the DC link voltage) and of current rating 150 A can be used and the losses of this converter in terms of Transistor conduction and switching losses as well as the diode conduction and switching losses will be analyzed. For this analysis, the same 30 kW machine used in chapter 4 will be used together with the SEMiX 151GD066HDs thermal module (dual) and the losses will be adjusted to account for all three modules used in the machine side inverter.

5.2.1. The Converter losses for the SCIM based FESS

The same SKM200GB125D dual module of 1200V/150A rating will be used in this analysis and the whole system with the dual thermal module attached to it is shown in Figure 5.6

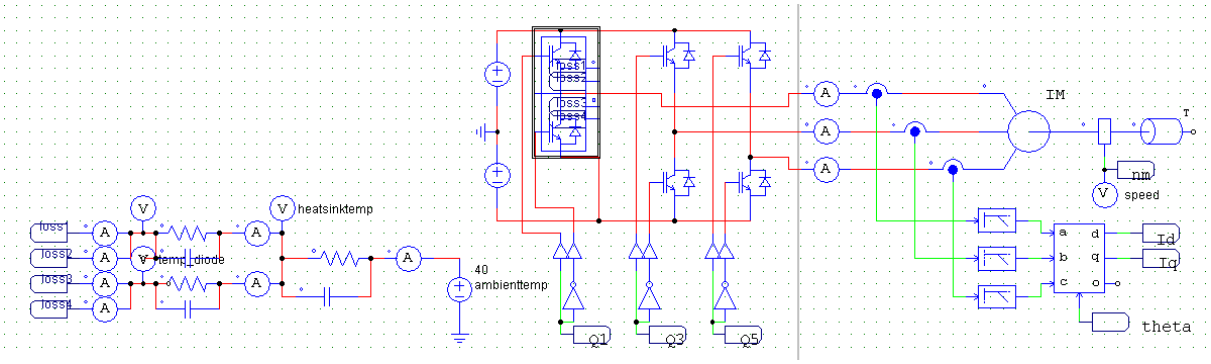

Figure 5.6.The SCIM vector controlled model with the SKM200GB125D dual module (1200 V, 150A)

The conduction and switching losses of the diode and the transistor for 1 module during charging and discharging is presented in Figure 5.7

As discussed in the previous section, it can be seen that the transistor conduction losses are higher during charging than discharging and the diode conduction losses are higher during the discharging cycle. The summary of those losses and the total converter (machine side) losses and efficiency during both the charging and discharging cycles are presented in Table 5.3

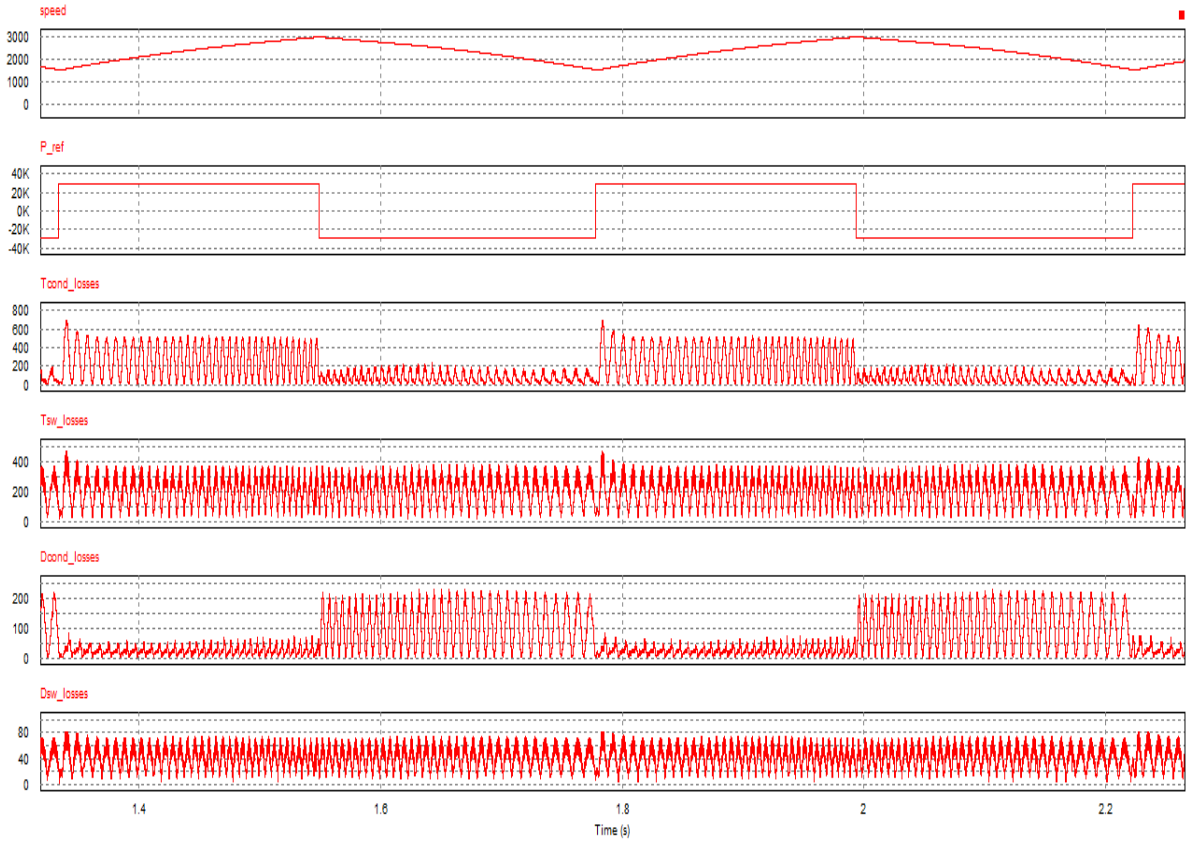

Figure 5.7.The speed range, processed power, IGBT and diode conduction and switching losses during charging and discharging of the SCIM vector controlled model

Table 5.3.Converter losses (IGBT and diode conduction and switching losses) during both charging and discharging cycles for the SCIM system

Charging cycle	**Discharging cycle**
Transistor conduction losses averaged	**Transistor conduction losses averaged**
250 W	100 W
Transistor switching losses averaged	**Transistor switching losses averaged**
190 W	188 W
Diode conduction losses averaged	**Diode conduction losses averaged**
25 W	110 W
Diode switching losses averaged	**Diode switching losses averaged**
42.5 W	43 W
Total losses (summed losses for 3 legs)	**Total losses (summed losses for 3 legs)**
507.5*3 = 1522.5 W	441*3 = 1323 W
Converter losses (percentage)	**Converter losses (percentage)**
$\frac{1522.5}{30000}$ * 100 =5.075%	$\frac{1323}{30000}$ * 100 =4.41%
Converter efficiency (percentage)	**Converter efficiency (percentage)**
100-5.075=94.925 %	100-4.41=95.6%
Round trip efficiency of the machine side converter	
100-5.075-4.41=90.515%	

5.2.2. The Converter thermal stresses for the SCIM based FESS

The temperatures measured at the heat sink as well as the diode and transistor is analyzed in this section to make sure that the devices are not thermally stressed above their limits set by the module data sheet. Those temperatures are shown in Figure 5.8 and it can be seen that for heat sink temperature is within acceptable range (peak 58 ^{o} C*)* and the junction temperature (diode/transistor) peak temperature was 140 ^{o} C experienced by the IGBT during the charging period and these temperatures summery is presented in Table 5.4. The junction temperature limit is set to 150 ^{o} C and this temperature was not exceeded neither during the charging nor thee discharging cycles.

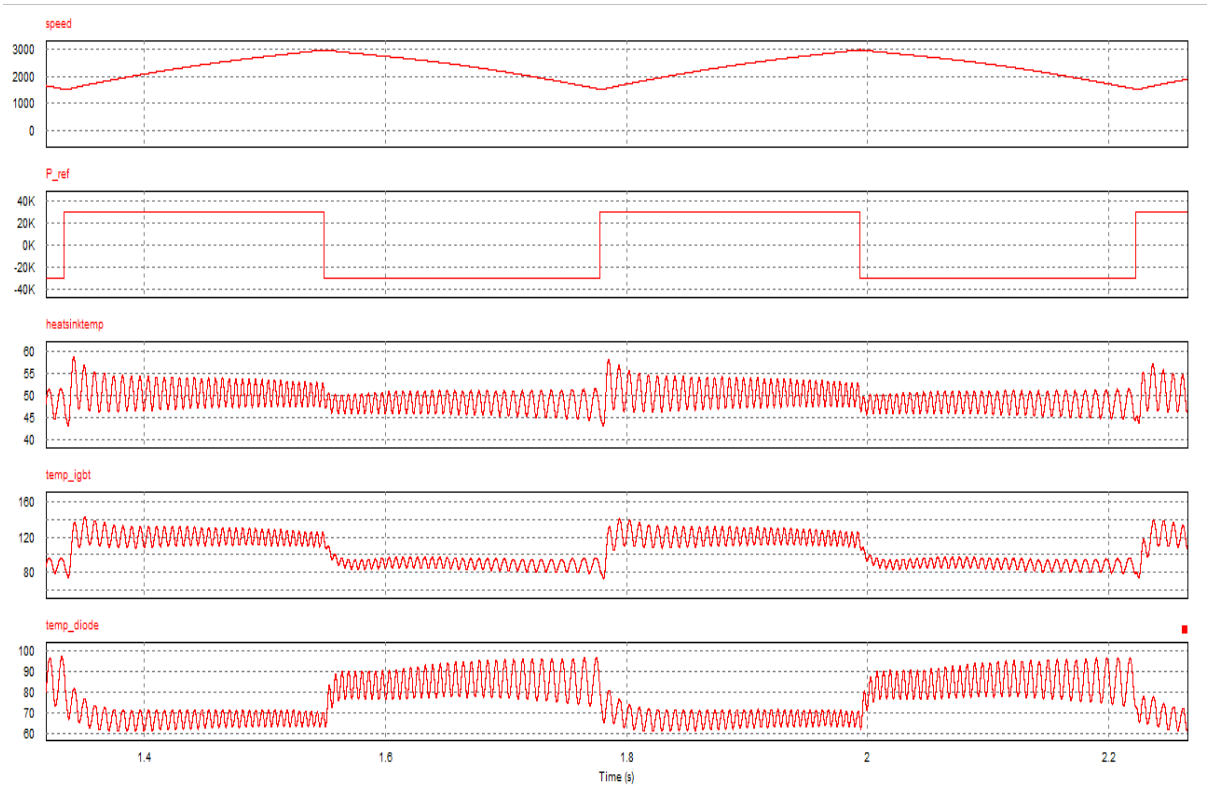

Figure 5.8.Speed, Processed power, heat sink, transistor and diode temperature plots for the SCIM converter thermal module

Table 5.4. The Heat sink, transistor, diode and junction temperature of the SCIM module during charging and discharging

Charging cycle	**Discharging cycle**
Heat sink Temperature (^{o} C)	**Heat sink Temperature (^{o} C)**
58	51
Transistor Temperature (^{o} C)	**Transistor Temperature (^{o} C)**
140	100
Diode Temperature (^{o} C)	**Diode Temperature (^{o} C)**
95	70

5.3. DFIM converter sizing, losses and efficiency analysis using PSIM thermal module.

The DFIM vector controlled model was presented in chapter 4 where its functionality with the FESS application and the control of the system were proven. The speed range that was tested was 1:1.625 from 1200 to 1950 rpm as per the adjustment proposed in chapter 2 for using a smaller speed range rather than a full speed range (1050 rpm to 1950 rpm) in order to reduce the torque peak and thus the rotor current at the lowest speed. The DC link used in the VSI for this analysis is 300 V (peak), but since the machine has a locked rotor voltage of 400 V (L-L) = 700 V (peak) then at the maximum slip (slip =0.3) the maximum peak voltage that can be achieved is 210 V (0.3*700V). So, in order to use a DC link of 300 V, the rotor voltage must be increased. This can be done by increasing the rotor to stator turns ratio by a factor of 1.4285 (300/210) and the turns ratio will be reduced from the one used to obtain 210 V which was 1.7 to 1.2. Having this, a converter of double this DC link voltage (600 V) can be used and the converter voltage rating will be fully utilized. This will result in a reduction of the rotor current by the same factor as the power is constant which will result in reduced converter current rating as well and current was reduced (135.7 A to 95 A). Using the information mentioned above, a converter of voltage rating twice the DC link voltage (600 V) and a current rating of 100A can be used. For this analysis, a Powerex CM100TU-12H six-pack module will be used to calculate the losses of this converter in terms of Transistor conduction and switching losses as well as the diode conduction and switching losses.

5.3.1. The Converter losses for the DFIM based FESS

The Powerex six pack module of 600V/100A ratings will be used in this analysis and the whole system with the thermal module attached to it is shown in Figure 5.9.

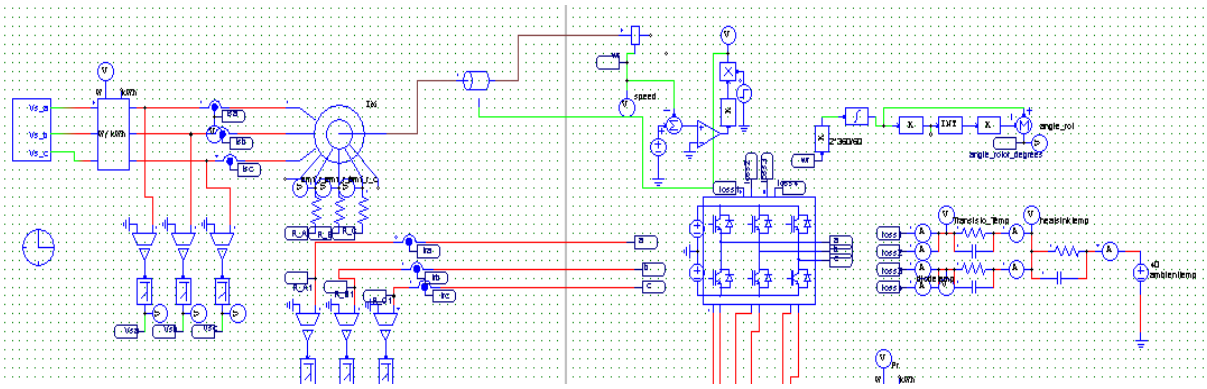

Figure 5.9.The DFIM vector controlled model with the Powerex 6-pack module (600 V, 100A)

The conduction and switching losses of the diode and the transistor for the 6-pack module during charging and discharging are presented in Figure 5.10

As discussed in the previous sections, it can be seen that the transistor conduction losses are higher during charging than discharging and the diode conduction losses are higher during the discharging cycle. It is to be considered that the power processed by the rotor is 30 % of the stator power, this means that the power that which is equivalent to 0.3* 30kW = 90kW but the slip varies and will reach zero during the cycle. For this reason, an average slip of 0.15 can be considered and thus an equivalent power of 0.15* 30 kW= 4.5 kW will be used to calculate the converter efficiency and losses. The summery of those losses and the total converter losses and efficiency during both the charging and discharging cycles are presented in Table 5.5

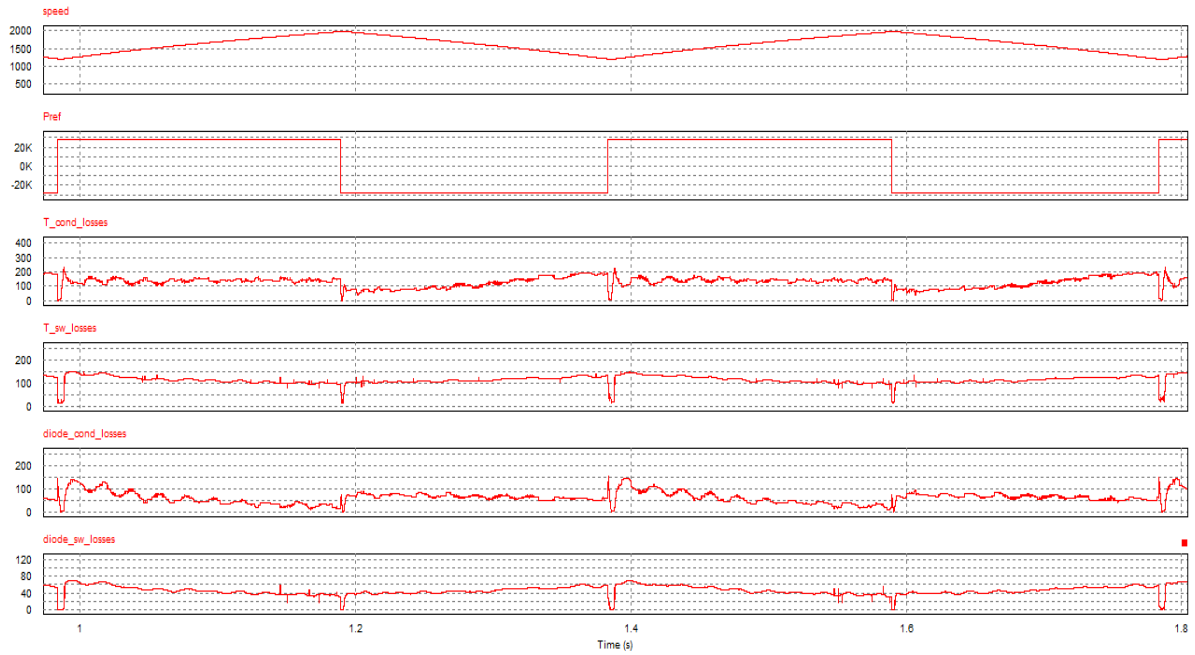

Figure 5.10.The speed range, power, IGBT and diode conduction and switching losses during charging and discharging of the DFIM vector controlled model

Table 5.5.Full (3phase) rotor inverter losses (transistor and diode conduction and switching losses) during both charging and discharging cycles for the DFIM system

Charging cycle	**Discharging cycle**
Transistor conduction losses averaged	**Transistor conduction losses averaged**
151 W	119.5 W
Transistor switching losses averaged	**Transistor switching losses averaged**
148 W	120 W
Diode conduction losses averaged	**Diode conduction losses averaged**
73.5 W	85 W
Diode switching losses averaged	**Diode switching losses averaged**
48.5 W	51.5 W
Total losses (per module)	**Total losses**
421 W	376 W
Converter losses from rotor processed power (percentage)	**Converter losses from rotor processed power (percentage)**
$\frac{421}{4500}$=9.35%	$\frac{376}{4500}$=8.355%
Converter losses from overall power (percentage)	**Converter losses from processed power (percentage)**
$\frac{421}{30000}$=1.4%	$\frac{376}{30000}$=1.25%
Converter efficiency (percentage)	**Converter efficiency (percentage)**
100-9.35 = 90.65%	100-8.355=91.645%
Round trip efficiency of the machine side converter	
100-1.4-1.25=97.35%	

5.3.2. The Converter thermal stresses for the DFIM based FESS

The temperatures measured at the heat sink as well as the diode and transistor is analyzed in this section to make sure that the devices are not thermally stressed above their limits set by the Powerex module data sheet. Same heat sink pattern was used as the one used for the PMSM and SCIM as even though a portion of the stator power is processed via the converter, the converter used for the DFIM analysis is six-pack compared to one leg module used for the previous two drives. Those temperatures are shown in Figure 5.11 and it can be seen that for heat sink temperature is within acceptable range (peak 49.5 ^{o} C) and the peak junction temperature (diode/ transistor) is about 95 ^{o} C and these temperatures summery is presented in Table 5.6. The junction temperature limit is set to 150 ^{o} C and this temperature was not exceeded neither during the charging nor thee discharging cycles.

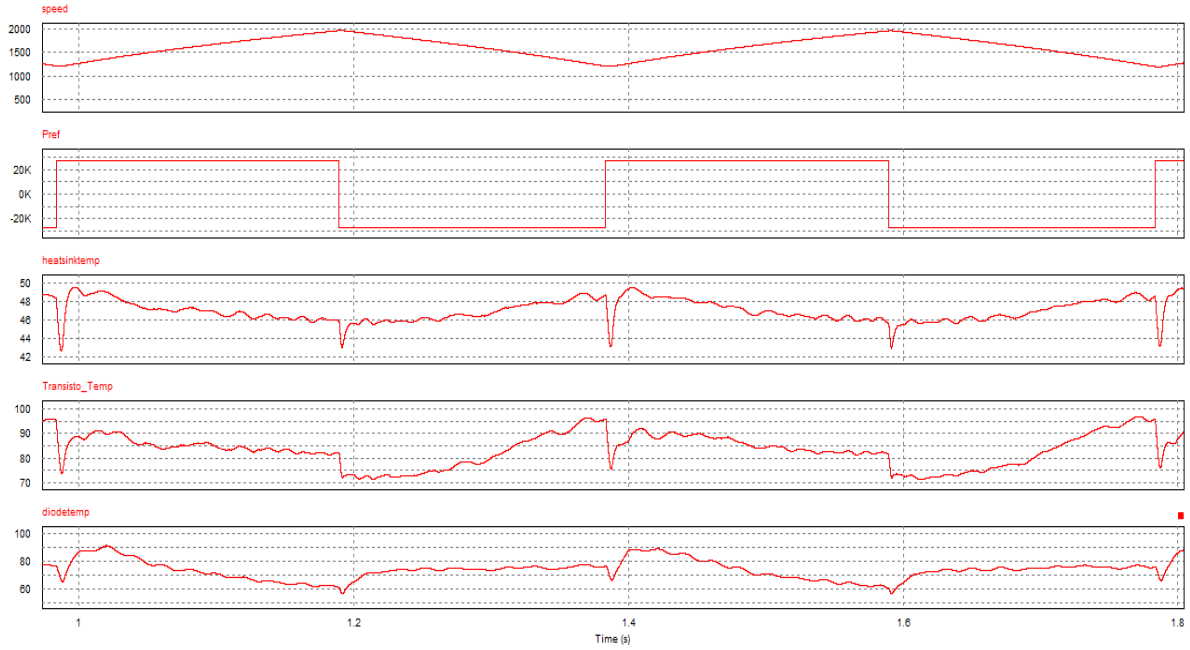

Figure 5.11.The speed range, power, heat sink, transistor and diode temperature plots for the DFIM converter thermal module

Table 5.6.The Heat sink, transistor, diode and junction peak temperature of the DFIM module during charging and discharging

Charging cycle	**Discharging cycle**
Heat sink Temperature (^{o} C)	**Heat sink Temperature (^{o} C)**
49.5	48.5
Transistor Temperature (^{o} C)	**Transistor Temperature (^{o} C)**
95	92
Diode Temperature (^{o} C)	**Diode Temperature (^{o} C)**
90	80

5.4. Discussion on findings:

In this chapter, the machine side converter for the 3 drives used for the FESS application were analyzed in terms of the converter rating, losses, round trip efficiency and thermal stresses and the main points of comparison were as following:

1. It was found that the DFIM can use a converter with rating of (600V/100A) which is only 30% of the converters rating used for the PMSM and SCIM drives (1200V/150 A) to process the same power rating of 30 kW
2. The thermal stresses on the heat sink and the converter junctions were examined for the operation of the three drives, and acceptable stressed were experienced below the limits set by the devices data sheet.
3. The losses and efficiency of the three drives with the converter can be discussed further by including an estimated efficiency percentage for the three machines to estimate the processed power. Assuming that the PMSM has the highest efficiency of 94%, for the SCIM it is about 90% and 88 % can be used for the DFIM. This means that out of the 30 kW the PMSM converter will process 28.2 kW, the SCIM will process 27 kW and the DFIM will process 26.4 kW. Having the total losses per converter of the PMSM to be 1731 W (charging)/1536 W (discharging), for the SCIM to be 1522.5 W (charging) 1323 W (discharging) and for the DFIM to be 421 W (charging) 376W (discharging), the system losses and efficiency can be calculated. So, for the PMSM, the system losses are equal to $\frac{1731}{28200}$*100 = 6.12 % and efficiency is 93.86 %, for the SCIM, the system losses are equal to $\frac{1522.5}{27000}$*100 = 5.64 % and efficiency is 94.36% and for the DFIM, the system efficiency is $\frac{421}{26000}$ = 1.62 % and efficiency is 98.38 %. From the previous calculation it can be seen that the losses in the DFIM are 30 % less than the other two drives and the overall system efficiency of the DFIM is higher as most of the power will go directly from the stator to the grid and only 30 % of the power is processed in the converter were the losses occur.
4. Even though the DFIM offer better system efficiency than the other two drives, the compromise come in terms of less energy storage capability (62%) which is 13% less than that of the SCIM and 23% less than that of the PMSM.

Chapter 6

Conclusion and future development

6.1. Conclusion

The project was done to compare the performance of three types of machines that can be used for the FESS application which are the DFIM, PMSM and the SCIM. The aim of the project was to identify what are the advantages and disadvantages of using each of the machine compared to the others. For this purpose, a vector controlled model for each machine was implemented to prove the functionality of the system for the FESS application by offering a working constant power charge/discharge control, measuring the system currents and voltages required for calculations and comparison and for the converter sizing and losses to be analyzed as well.

Comparing induction machines (DFIM and SCIM), the DFIM has the advantage of rotor windings being separated from the stator windings and they can be accessed via slip rings. This allows the control of the speed of the machine via the slip via a reduced size converter. For this reason, a reduced size converter can be used only on the rotor winding which can process a fraction of the stator power (for a maximum slip of 0.3, only 30 % of stator power only need to be controlled and processed by the converter) and thus smaller/cheaper converter with less losses can be used. Further improvement for reducing the machine torque and thus the rotor current and the converter rating was discussed in chapter 2 by using a smaller speed range 1:1.625 (+30% of rated speed to -20% of rated speed). But the major disadvantage of the DFIM is that the speed range that can be achieved is around (+30% of rated speed to -20% of rated speed) and thus less energy can be stored in the FESS (about 62%) compared to the other machine types and a bigger gearbox is needed to reach the FESS required speed of about 4000 rpm (4000/1200 = 3.31:1).

For the SCIM, since the speed cannot be controlled on the rotor (as the rotor winding cannot be accessed as in case of the DFIM), a full-scale converter is needed which means higher converter rating, losses and costs. But the compromise offered in contrast to the DFIM is that a higher speed range can be reached by applying the field weakening approach allowing the machine to operate at higher speeds above the rated/base speed. This can be done by reducing

the flux in order to keep the back emf voltage constant and thus a constant power can be achieved. Since the main interest is in the FESS application, only constant power region (Speeds above the rated speed) was analyzed and a speed range of 1:2was achieved (1500 to 3000 rpm). This wider speed range allow more energy to be stored (75% of nominal storage capability) compared to the DFIM and also a smaller gear box is needed with a ratio equal 2.66:1 (4000/1500).

Finally, the PMSM which is the commercially used machine for operating the FESS due to its high-power density and a compact design together with a high round trip efficiency was analyzed. A full-scale converter is required to process all the power between the machine and the utility grid which means a larger converter is needed and thus more losses and costs. But on the bright side, a large speed range can be achieved by applying the field weakening approach above the rated speed. The speed range that was achieved was 1:2.67 (from 1500 rpm to 3850 rpm) and thus a higher energy storage capability than the other 2 machines can be achieved (84.8% of nominal storage capability) and a gear box of same ratio as the SCIM can be used (2.66:1). Since the field weakening approach applied for the PMSM will tend to reduce the flux above base speed, the flux, will be reduced and flux current must be injected. But below the base speed, no flux current was existing, this means that above rated speed a lot of negative flux current (reactive current) will need to be injected from zero to keep the back emf and the power constant. The proposed solution was to use smaller magnets and thus a smaller flux will be used in the machine, this means that voltage increment slope will be reduced and the rated back emf will be reached at a speed higher than the rated speed. So, for the speeds above the rated where the back emf has not reached its rated value yet, a positive flux current needs to be injected to increase the back emf voltage till the required constant value. After this point, the flux current reaches zero, and a negative flux current need to be injected to reduce the back emf and keeping it at the constant value. The point at which equal flux ($\frac{L_d * I_d}{\Omega}$) can be achieved is not the mid speed between the base and maximum speed but it is at a point which is equal to $\frac{1}{1+K}$ from the base speed and $\frac{K}{1+K}$ from the maximum speed. Applying this topology, a smaller flux current can be achieved and thus smaller converter current rating.

The converters sizing's were discussed in the previous chapter and it was proven that the DFIM can use a converter rating of (600V, 100A) while PMSM and SCIM require converters of rating (1200V, 150A). This proves that the DFIM can use a converter of 30 % the installed power/size of the converters used for PMSM and SCIM. Also, the thermal stresses of the semiconductors

used for the three drives were discussed to make sure that the temperature experienced by the transistors and diodes (junctions) of the converter does not exceed the temperature limit that was set by the converters datasheets.

A summary of the comparison between the 3 machines that can be used for the FESS application is presented in Table 6.1.

Table 6.1.A comparison between the 3 machines that can be used for the FESS application

	PMSM	DFIM	SCIM
Machine efficiency	+++	+	++
Machine costs	+++	++	+
Speed ranges	1:2.6	1:1.625	1:2
Energy storage capability	84.8 % of the rated FESS energy storage capability	62% of the rated FESS energy storage capability	75% of the rated FESS energy storage capability
Converter rating	(1200 V,15 0A)	(600V, 100A)	(1200V, 150A)
Converter size	Full scale	Reduced scale (slip power)	Full scale
Machine side converter efficiency	94.6%	98.6%	95%
Gear box ratio	2.66:1	3.31:1	2.66:1

6.2. Future development

Some of the key points that can be analyzed in the future to be included in the machines comparison are as following:

1. The impact of using different power rating of the machines (very low or very high) as well as different pole number on the performance of the system.
2. The PI controllers for the vector controlled models can be tuned using some software such as MATLAB for more accurate control results
3. More machine types can be included in the comparison such as self-reluctance or different structure of synchronous machine (axially laminated)

4. Since the losses analysis was based on estimated drive efficiency, the efficiencies of the machine can be tested and some measurement can be obtained for more accurate losses calculations
5. The Grid side converter must be implemented in the system as well to calculate the efficiency of the system as a whole as the current model includes only the machine side converter calculations.

Quality report

The master thesis development at the tower building, lab 617 in the faculty of Electrical and Electronics Engineering at the University of Nottingham-UK was of great academic, technical and personal value. All the needed materials/software to conduct the thesis were provided on time and with good quality. My thesis supervisor provided all the academic guidance and support needed during the 5 months period of my thesis and frequent meetings were conducted to follow up on progress and discuss the problems arose during the software model design phase. The main challenges faced by me were that the topic and the design aspects especially those related to the vector control of the systems were all new for me and only learnt during one course in the master course time so intensive readings, decent discussions with my supervisor and though personal motivation as well.

Moreover, the advantage of conducting the master thesis in the University of Nottingham, is that the technical and IT teams make great effort in providing the software licences and access to laboratories once demanded. They also provide me with a test bench in a massive laboratory provided with a personal computer with all the software required for my simulation work and with a quite environment that helped me focus on my research and progress in a productive way.

The majority of time was spent in performing the required research on the related topics and information needed to conduct the analysis and the simulation together with meetings to clarify the new ideas and discuss them in terms of possibility of implementation and how to approach that. Yet, the research project assigned to me was quite lengthy and I believe more time should be given to perform the master thesis rather than 5 months taking in consideration the time needed by students to obtain their visas before coming to the new institution.

The overall experience was of great benefit to me and I have learnt a lot during my master thesis development in the University of Nottingham, so I would strongly encourage this partnership to continue between the university of Oviedo and the University of Nottingham.

References

[1] P. Medina, A. Bizuayehu , J. Catalao and . J. Contreras, “Electrical Energy storage systems, technologies' state of art, techno economic benefits and application analysis,” in *The 47th Hawaii International Conference on System Sciences*, Waikoloa, 2014.

[2] . I. Hadjipaschalis , A. Poullikkas and . V. Efthimiou, “Overview of current and future energy storage technologies,” *Renew. Sustain. Energy Rev,* vol. 13, p. 1513–1522, 2009.

[3] . P. Del Granado, S. Wallace and Z. Pang, “The value of electricity storage in domestic homes: A smart grid,” *Energy Systems,* vol. 5, p. 211–232, 2014.

[4] P. Parfomak, “Energy Storage for Power Grids and Electric Transportation: A Technology Assessment;,” Congressional Research Services, Washington, DC, 2012.

[5] *Active power: Understanding Flywheel Energy Storage: white paper 112,* 2010.

[6] E. A. Mustafa and R. P. Keith , “A Review of Flywheel Energy Storage System,” Applied sciences, London, 2016.

[7] W. Su , T. Jin and S. Wang, “Modeling and Simulation of Short-term Energy Storage: Flywheel.,” in *International Conference on Advances in Energy Engineering Modeling (ICAEE)*, Bejing, 2010.

[8] . Y. Meng, T. Li and L. Wang , “Simulation of controlling methods to flywheel energy storage on charge section,” in *Third International Conference on Electric Utility Deregulation and Restructuring and*, Nanjing, 2008.

[9] L. Bakay, M. Dubois , P. Viarouge and J. Ruel, “Mass-losses relationship in an optimized 8-pole radial AMB for Long Term Flywheel Energy Storage,” *IEEE AFRICON ,* pp. 1-5, 2009.

[10] . P. Shelke and D. Dighole, “A Review paper on Dual Mass Flywheel system.,” Int. J. Sci. Eng. Technol. Res., 2016.

[11] P. Alzola, . R. Sebastián and J. Quesada, “A Review of Flywheel based Energy Storage Systems.,” in *International Conference on Power Engineering, Energy and Electrical Drives*, Malaga,Spain, 2011.

[12] M. Daoud , A. Abdel-Khalik and A. Massoud, “The Development of Flywheel energy storage systems for power system applications,” in *20th International conference on electrical machines*, Marseille, France, 2012.

[13] Y. Yu , Y. Wang and F. Sun, “The Latest Development of the Motor/Generator for the Flywheel Energy Storage,” in *International Conference on Mechatronic Science, Electric Engineering*, Jilin, 2011.

[14] H. Liu and J. Jiang, “Flywheel energy storage—An upswing technology for energy sustainability,” *Energy Build,* vol. 39, p. 599–604, 2007.

[15] E. Bayoumi, “Power electronics in smart grid distribution power systems: a review,” *International journal of Industrial Electronics and Drives,* vol. 3, 2016.

[16] . E. Carrillo Arroyo, “.Modeling and Simulation of Permanent Magnet Synchronous Motor Drive System.,” University Of Puerto Rico, San Juan, Puerto Rico, 2006.

[17] W. Santiago, “. Inverter Output Filter Effect on PWM Motor Drives of a Flywheel Energy Storage System,” Glenn reserach center, Cleveland, OH, USA, 2004.

[18] S. Faias, P. Santos, J. Sousa and R. JCastro, “An Overview on Short and Long-Term Response Energy Storage for power system applications,” *Renew. Energy Power Qual.,* vol. 1, p. 442–447, 2008.

[19] R. Östergård, “Flywheel energy storage - a conceptual study,” Uppsala universitet, Uppsala, 2011.

[20] I. Gyuk, ““EPRI-DOE Handbook of Energy Storage for Transmission and Distribution Applications”,” U.S department of energy.

[21] *http://www.electricitystorage.org/ 2011-03-01,* 2011.

[22] H. Ibrahim, A. Ilinca and J. Perron, “Energy storage systems--Characteristics and comparisons,” *Renewable and sustainable review,* vol. 12, no. 5, pp. 1221-1250, 2008.

[23] B. Alamri and A. Alamri , “Technical review of energy storage technologies when integrated with intermittent renewable energy,” in *SUPERGEN '09 international conference*, 2009.

[24] R. Hebner, J. Beno and R. Thompson, “Flywheel Batteries for Vehicles,” *scientific research,* pp. 99-101, 2002.

[25] B. Bolund, H. Bernhoff and M. Leijon, “Flywheel energy and power storage systems,” *Renewable and Sustainable Energy Review ,* vol. 11, pp. 235-258, 2007.

[26] S. R. HOLM, “Modelling and optimization,” Technische Universiteit Delft, e Technische Universiteit Delft, 2003.

[27] J. Ochoa, “AFPM Motor/Generator Flywheel for Electric Power Stabilization,” Institutionen för teknikvetenskaper, Uppsala, 2009.

[28] B. E, “Dynamics of the power control of a double fed induction generator connected to the soft power grid,” in *IEEE*, Budapest, 1993.

[29] Y. Zhang and B. T. Ooi, “Adapting DFIGs for doubly-fed induction motors operation,” in *IEEE*, San Diego, 2012.

[30] Z. Wu , C. Zhu and . M. Hu, “Improved Control Strategy for DFIG Wind Turbines for Low Voltage Ride Through,” *energies,* vol. 6(3), pp. 1181-1197, 2013.

[31] B. Hopfensperger, D. Atkinson and R. Lakin, “Stator-flux-oriented control of a doubly-fed induction machine with and without position encoder,” *IEE Proceedings - Electric Power Applications,* vol. 147, pp. 241 - 250, 2000.

[32] R. Pena, J. Clare and G. Asher, “Doubly fed induction generator using back-to-back PWM converters and its application to variable-speed wind-energy generation,” *IEE Proceedings - Electric Power Applications,* vol. 143, pp. 1350-2352, 1996.

[33] G. Joos and C. Abbey, “Integration of energy storage with a doubly-fed induction machine for wind power applications,” in *2004 IEEE 35th Annual Power Electronics Specialists Conference*, Aachen, 2004.

[34] T. Thanh Nguyen, H. Jun Yoo and H. Man Kim, “A Flywheel Energy Storage System Based on a Doubly Fed,” *energies,* vol. 8, pp. 5074-5089, 2015.

[35] N. Kumar , T. Raj Chelliah and S. Prakash Srivastava, “Analysis of doubly-fed induction machine operating at motoring,” *Engineering Science and Technology,* vol. 19, p. 1117–1131, 2016.

[36] L. ZHAI, R. Gao and L.-W. Su, “The reserach on full speed field weakening control method of electric vehicle interior permanent magnet synchtonou motor,” in *ITM web of conferences 11*, 2017.

[37] T. Sebastian and G. Slemon, “Operating limits of inverter-driven permanent magnet motor drives,” in *Electrical machines and drives conference*, 1993.

[38] M. Galea, *Permanent Magnet Machine Drives-Control of PMSM drives slides,* Nottingham: University of Nottingham, 2016.

[39] S. Bolognani, L. Peretti and M. Zigliotto, “Combined speed and current Model Predictive Control with inherent field-weakening features for PMSM Drives,” in *The 14th IEEE Mediterranean Electrotechnical Conference*, Ajaccio, 2008.

[40] W. Soong and N. Ertugrul, “Field-weakening performance of interior permanent-magnet motors,” *IEEE Transactions on Industry Applications,* Vols. vol. 38, no. 5, pp. 1251-1258, 2002.

[41] B. Chalmers and L. Musaba, “Design and field-weakening performance of a synchronous reluctance motor with axially-laminated rotor,” in *ndustry Applications Conference, 1997. Thirty-Second IAS Annual Meeting, IAS '97., Conference Record of the 1997 IEEE*, New Orleans, LA, 1997.

[42] T. Finken, M. Hombitzer and K. Hameyer, “Study and comparison of several permanent-magnet excited rotor types regarding their applicability in electric vehicles,” in *2010 Emobility - Electrical Power Train,*, Leipzig, 2010.

[43] W. L. Soong, D. Staton and T. Miller, “Design of a new axially-laminated interior permanent magnet motor,” *IEEE Transactions on Industry Applications,* Vols. vol. 31, no. 2,, pp. 358-367, 1995.

[44] C. Klumpner, *Doubly-fed Induction Machines (Principles, Vector Control and Ride through operation,* Nottingham: University of Nottingham, 2016.

[45] N. Raju, M. Islam and A. Uddin, “Sinusoidal PWM Signal Generation Technique for Three Phase Voltage Source Inverter with Analog Circuit & Simulation of PWM Inverter for Standalone Load

& Micro-grid System," *INTERNATIONAL JOURNAL of RENEWABLE ENERGY RESEARCH,* vol. 3, pp. 1-12, 2013.

[46] N. Teske, "Sensorless position control of induction machine using high frequency signal injection," Univerity of Nottingham, Nottingham, 2001.

[47] J. D. Park, "Simple flywheel energy storage using squirrel-cage induction machine for DC bus microgrid systems," in *IECON 2010 - 36th Annual Conference on IEEE Industrial Electronics Society*, Glendale, AZ, 2010.

[48] B. Naik, "Comparison of Direct and Indirect Vector," *International Journal of New Technologies in Science and Engineering,* vol. 1, pp. 1-22, 2014.

[49] M. Galea, *Advanced AC Drives induction machines vector control slides,* Nottingham: University of Nottingham, 2016.

[50] C. Xi, H. Shenghua, L. Bingzhang and X. Yangxiao, "Losses and thermal calculation of IGBT and FWD in PWM inverter for electric engineering maintenance rolling stock," in *19th International Conference on Electrical Machines and Systems (ICEMS)*, Chiba, 2016.

[51] *Clean Flywheel Energy Storage Systems, http://www.power-thru.com/,* 2016.

[52] . S. Vazquez, S. Lukic, E. Galvan and L. Franquelo, "Energy Storage Systems for tranport and grid applications," *Industrial Electronics, IEEE Transactions,* vol. 57, pp. 3881-3895, 2010.

[53] M. Guerrero , E. Romero , F. Barrero, M. Milanes and E. Gonzalez, "Overview of medium scale energy storage systems," *Compatibility and Power Electronics,* pp. 93-100, 20-22, 2009.